TECH LIBRARY KAFB, NM
0062263

NASA Contractor Report 3386

The Development of Convective Instability, Wind Shear, and Vertical Motion in Relation to Convective Activity and Synoptic Systems in AVE IV

James G. Davis and James R. Scoggins
Texas A&M University
College Station, Texas

Prepared for
Marshall Space Flight Center
under Contract NAS8-31773

National Aeronautics
and Space Administration

**Scientific and Technical
Information Branch**

1981

FOREWORD

This report contains three parts. The first is on the development of convective instability, the second on the development of wind shear, and the third on the development of vertical motion, each considered in relation to convective activity. Development in the context of this report refers to the local time rate-of-change of the variable. The objective is to explain the conditions/factors that lead to local changes in the variables, and to establish the relative importance of each.

Each part of the report is based on AVE IV data. Discussions of the AVE IV data, synoptic conditions, manually digitized radar data, and the objective approach to data analysis are presented in Part I but apply also to Parts II and III. For those interested in reading Part II and/or Part III before Part I, pages six to the middle of page 16 should be read first. This information applies to all parts but is presented only once. Otherwise, the parts may be read independently.

ACKNOWLEDGEMENTS

The authors thank Dr. Phanindramohan Das, Dr. Norman W. Naugle, and Dr. Kenneth C. Brundidge for reviewing Part I, Mrs. Karen Hood and Mrs. Melinda Culver for typing the manuscript, and Mr. John Rod for drafting the graphs and figures.

The authors gratefully acknowledge support provided under NASA Contract No. NAS 8-31773. This contract is under the auspices of the Atmospheric Sciences Division, Space Sciences Laboratory, National Aeronautics and Space Administration, Marshall Space Flight Center, Alabama.

ABSTRACT

Data from the fourth Atmospheric Variability Experiment (AVE IV) conducted by NASA on 24-25 April 1975 were used to investigate conditions/factors responsible for the development (local time rate-of-change) of convective instability, wind shear, and vertical motion in areas with varying degrees of convective activity (none to MDR Code 9). AVE IV sounding data were taken at 3- or 6-h intervals during a 36-h period on 24-25 April 1975 over approximately the eastern half of the United States. An error analysis was performed for each variable studied.

The development of convective instability was analyzed for the layers from the surface-850 mb, 850-700 mb, 700-500 mb, and 500-300 mb. The 3- and 6-h sounding intervals allowed time changes in convective stability to be studied in areas of convective storms. A stability development equation was derived and each term was examined to determine when and where it made a significant contribution to the development process. The usefulness of satellite data in describing stability development and the processes effecting its change also was evaluated. Of the terms in the stability development equation, the residual, representing subsynoptic-scale processes, had the largest average magnitude in all the layers considered. The terms describing the vertical advection of convective stability and divergence on an isobaric surface revealed processes whereby the stability is increased in the boundary layer in the region of thunderstorms. Most stability development resulted from moisture-related processes but stability development due to changes in the temperature profile could not be neglected. Satellite data could depict with reasonable accuracy only the extreme values of stability change and differential advection of equivalent potential temperature.

The development of wind shear was investigated for geostrophic and ageostrophic components over 3-, 6-, and 12-h periods. The shear at any given time is given primarily by the geostrophic component, while the ageostrophic component is primarily responsible for development of wind shear. However, the importance of the ageostrophic component diminished as the time interval increased. While some development of wind shear occurred over longer periods, most of the development occurred over a period of 3 to 6 h. Layers considered were surface-850, 850-700, 700-500, and

500-300 mb with 500-300 mb layer showing the best agreement between measured and geostrophic shear development. Shear development did not correspond consistently with convective activity, but measured shear was greater in the lower and middle troposphere in convective areas than in nonconvective areas, and greater in the upper troposphere in nonconvective areas as well as areas with severe thunderstorms.

The development of divergence and vertical motion showed definite relationships to convective activity. At the time of convection, convergence at low levels and divergence aloft with positive vertical motion were observed. Development of vertical motion preceded the convective activity by 3 to 6 h. Coincident fields of vertical motion development at 850 mb and convective activity showed no clear relationship.

TABLE OF CONTENTS

TABLE OF CONTENTS (CONTINUED)

TABLE OF CONTENTS (CONTINUED)

LIST OF TABLES

LIST OF FIGURES

LIST OF FIGURES (CONTINUED)

1. INTRODUCTION

a. Statement of problem

Instability is a necessary though not sufficient condition for the development of convective storms. Miller (1967) stated that few, if any, severe thunderstorms developed in regions of negligible convective instability. Some of the most important predictors used by the National Weather Service in the forecasting of thunderstorms and severe weather are indices involving the magnitude of the instability. The underlying assumption in the prediction of areas containing convective storms is that the actual triggering of the storms are due to small scale processes, while the large scale flow patterns are responsible for creating areas with conditions favorable for storm development. Once the thunderstorms have developed, they interact with the synoptic scale processes so as to modify their immediate environment, including its stability. This modification would then be a factor, along with the changing large-scale processes, in determining the further growth and development of convective activity.

Although both the conditions controlling instability development and evidence of stability modification by convective storms can be seen on the synoptic scale, important temporal variations in the meteorological parameters are often not revealed in the operational 12-h rawinsonde data. Poor results by House (1958) in determining air mass modification by upper-level divergence were attributed to possible reversals of vertical motion or horizontal advection occurring closely in space or time. One possible explanation for this is that the duration of the convective storm systems can be less than the interval between successive rawinsonde soundings. Thus the 12-h soundings cannot accurately resolve the interaction between synoptic- and convective-scale systems and their influence on the variation in stability.

In this study, the large-scale processes relating to the development of instability and the modification of stability by convective storms will be investigated using the fourth Atmospheric Variability Experiment (AVE IV) data. This rawinsonde data set has the advantage of being taken over 3- and 6-h sounding intervals. This greater time resolution provides an opportunity to better determine both the temporal changes in stability, and the processes causing the change than would the standard 12-h soundings.

b. Objectives

The main objective of this research is to describe the development of convective instability in various atmospheric layers as seen by rawinsonde data taken at 3-h intervals.

Specific objectives include:

1) Investigate the relative importance of the various processes influencing the development of convective instability.
2) Study the interrelationships between synoptic and small-scale systems in the development process, and relate the development to radar-observed convection.
3) Determine if satellites can measure typical stability changes and the important factors in the development process such as differential advection of equivalent potential temperature or vertical advection of convective instability.

2. REVIEW OF PREVIOUS STUDIES

Three basic conditions generally accepted as necessary for thunderstorm development are: an adequate moisture supply, the existence of potential convective instability in the lower troposphere, and a mechanism to release this instability (Newton, 1963). Interrelationships between convective processes and synoptic-scale features have been established enabling Scoggins and Wood (1971) to study the factors responsible for the development and prediction of convection from synoptic-scale data. They found instability and vertical motion to be the two most important synoptic-scale parameters responsible for convection. It is clear that the accuracy of a forecast for convective activity depends in part on our ability to describe the variation of convective instability in space and time. A clear understanding is needed of the processes effecting these changes.

Lloyd (1942) was among the first to point out the characteristics of a sounding that was convectively unstable. Along with previous investigators, he attributed the development and release of instability to the movement from the west of cold air aloft over a warm, moist layer at the surface. Crawford (1950) found the instability line to develop along the axis of a warm tongue at 850 mb after cold advection at 700 mb had reached the fore part of an associated trough and began overtaking the warm tongue. He recognized that the horizontal processes may not be the primary or even most important causes of instability development but that they could be readily identified on constant pressure surfaces. He therefore gave rules for the forecasting of the development of instability lines based on horizontal advection. Appleby (1954) advected temperature and moisture by trajectories for a period of 6 h and found the combined effects of the resulting horizontal Laplacian of the advection, dew point temperature, and stability, as shown by the Showalter index, to fit well with the observed rainfall pattern. Admitting that factors other than advection might be important, Fulks (1951) postulated the differential cooling

with height due to differential horizontal advection to be the most important factor in destroying the capping inversion of typical severe weather soundings and thereby releasing convective instability.

However, Beebe and Bates (1955) showed that vertical lifting alone could develop and release instability if the vertical displacement of the air column was large enough. They hypothesized that vertical motion and the resulting severe weather were due to upper tropospheric divergence superimposed over low level moisture, instability, and convergence. In an explanation of the occurrence of nocturnal thunderstorms in one area and the dissipation of convection in another, Bonner (1966) found the vertical velocity field to be a mechanism for prolonging the lives of squall lines and that temperature or moisture advection by the low-level jet was not a sufficient condition for the development or persistence of thunderstorms.

House (1959) studied upper-level wind fields and temperature soundings typically preceding instability line formation. He computed temperature changes due to both horizontal and vertical advection, thereby demonstrating a physical process which could decrease thermal stability in the same area where increases in positive vertical motion were observed. Ninomiya (1971) included moisture in his study and found strong convergence of water vapor in the lower layer of the atmosphere in areas of thunderstorm development. The combination of a cold vortex aloft and warm moist airflow in the lower troposphere enhanced the production of potential convective instability prior to thunderstorm development. In an objective analysis of environmental conditions associated with severe thunderstorms and tornadoes, Endlich and Mancuso (1968) were able to rate the performance of selected quantities as indicators of instability development and the resulting severe storm activity. Of basic physical importance were vertical motion, divergence of sensible heat and moisture fluxes, advection, and frontogenetical factors.

Lewis et al. (1974) looked at the conservation of potential temperature and specific humidity to describe the development of a shallow unstable layer between 850 and 700 mb in the NSSL network.

They were able to examine the relative importance of the various processes involved in generating mesoscale disturbances. Synoptic features considered important in the stability change were strong horizontal moisture gradients and wind shears between the surface and 700 mb, with advective cooling causing insignificant destabilization. The large-scale circulation also was seen to be responsible for creating an extensive area favorable for convection in which the most probable areas could be isolated by examining mesoscale features.

Fritsch et al. (1976) showed that the synoptic-scale processes act over a period of 6 to 12 h to prepare the atmosphere for deep moist convection by boundary layer heating and moisture convergence. However, since the rate of mesoscale consumption of water vapor and the mass transport by squall lines was found to be significantly larger than synoptic-scale budgets, they concluded that additional vertical circulations must exist on a smaller scale. These subsynoptic-scale flows, and the interaction between different scales, have received considerable study lately. They have been shown to have a variety of effects such as triggering instability release through the local enhancement of horizontal moisture convergence and suppression of further thunderstorm development by modifying the large-scale environment (Kreitzberg and Perkey, 1976; Doswell, 1977; Feteris, 1977). Interaction between thunderstorm systems and the synoptic-scale environment was also observed by Read and Scoggins (1977) who found the instability to be greater 3 h prior to thunderstorm development than at the actual time of development. They also observed that instability in the surface- to 850-mb layer and 850- to 700-mb layer was important for the initial convective development, while additional instability in the 700- to 500-mb layer determined further intensification of the thunderstorm activity.

3. DATA

a. AVE IV experiment

The data used in this study consists of rawinsonde soundings taken during the fourth Atmospheric Variability Experiment (AVE IV) conducted by the National Aeronautics and Space Administration (NASA) and summarized in a data report by Fucik and Turner (1975). These soundings were taken at forty-two stations over the United States east of approximately 105° west longitude (Fig. 1) for a period of 36 h on 24-25 April 1975 at 3- or 6-h intervals instead of the conventional 12-h interval.

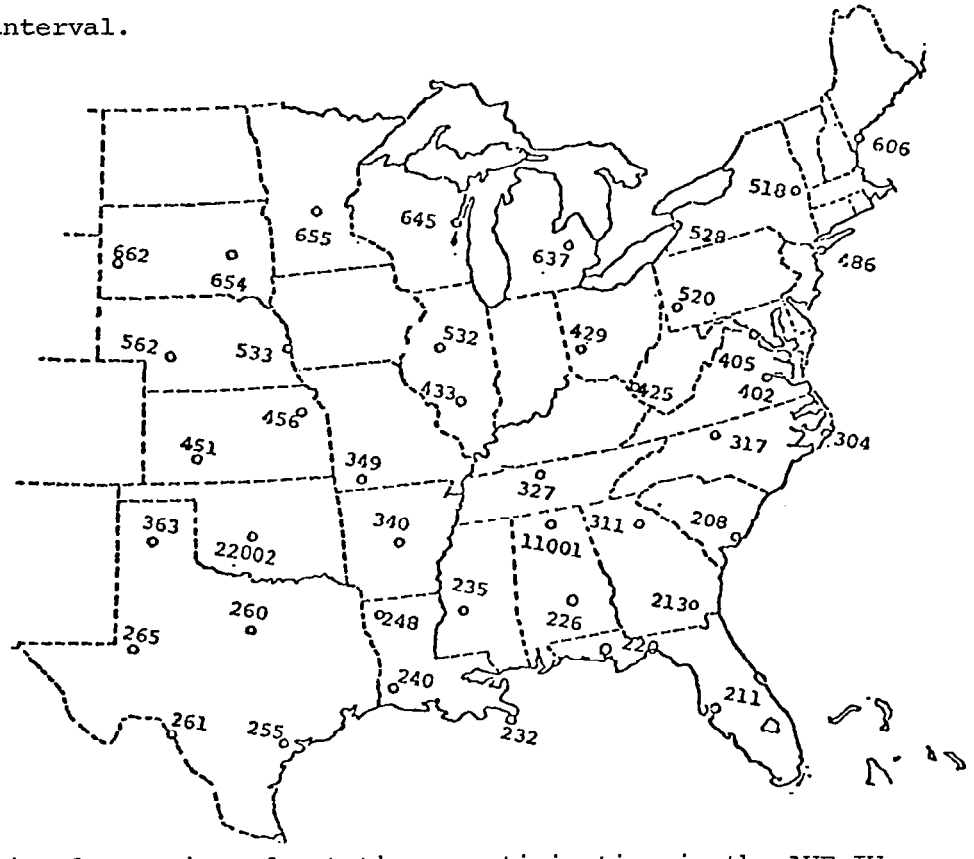

Fig. 1. Rawinsonde stations participating in the AVE IV experiment.

The data were reduced by a method described by Fuelberg (1974) giving the best possible accuracy from the available rawinsonde data. Thermodynamic data were computed at each pressure contact. Azimuth and elevation angles measured at 30-s intervals were used to compute

the wind by means of centered finite differences and subsequently smoothed and interpolated to each pressure contact. These detailed soundings were then interpolated to give 25-mb interval soundings. Standard error estimates of the rawinsonde data as computed by Fuelberg (1974) are given in Table 1.

Table 1. Standard error estimates of the rawinsonde data (from Fuelberg, 1974).

a. Thermodynamic

Parameter	Approximate RMS error
Temperature	1°C
Pressure	1.3 mb from surface to 400 mb 1.1 mb from 400 to 100 mb 0.7 mb from 100 to 10 mb
Humidity	10 percent
Pressure Altitude	10 gpm at 500 mb 20 gpm at 300 mb 50 gpm at 50 mb

b. Wind

	Elevation Angle		Elevation Angle	
	40°	20°	40°	20°
Level	RMS Direction Error		RMS Speed Error	
700 mb	1.8°	3.8°	0.5 m s^{-1}	1.0 m s^{-1}
500 mb	2.5°	5.6°	0.8 m s^{-1}	2.0 m s^{-1}
300 mb	3.1°	7.5°	1.0 m s^{-1}	3.8 m s^{-1}
100 mb	6.2°	15.0°	2.0 m s^{-1}	5.7 m s^{-1}

The rawinsonde data were supplemented by hourly surface data obtained from the National Climatic Center for the duration of the AVE IV experiment. Due to the smaller spacing between stations, they provided better resolution of detail in the thermodynamic and wind data than did the rawinsonde network.

b. Manually Digitized Radar (MDR) data

In order to determine areas and intensity of convection during AVE IV, manually digitized radar (MDR) data were obtained from the Techniques Development Laboratory of the National Oceanic and Atmospheric Administration (NOAA). The MDR network is shown in Fig. 2. Echo intensity and areal coverage of rainfall within each block for each hour determined the MDR code value assigned to that block as shown in Table 2 (Foster and Reap, 1975). The maximum reported MDR values for each block over a 3-h period centered at the rawinsonde observation time were compiled to give a composite MDR data field. By this method, composite MDR data fields were constructed for each observation time enabling comparisons between computed quantities in areas with the same intensity of precipitation. MDR values greater than or equal to 4 were considered to indicate general convective activity while values greater than or equal to 8 represented severe thunderstorms.

Table 2. Explanation of manually digitized radar (MDR) data.

Code No.	Maximum Observed VIP[1] Values	Coverage In Box	Maximum Rainfall Rate (in./hr)	Intensity Category
0	No Echoes			
1	1	Any VIP1	<.1	Weak
2	2	≤ 50% of VIP2	.1- .5	Moderate
3	2	> 50% of VIP2	.5-1.0	Moderate
4	3	≤ 50% of VIP3	1.0-2.0	Strong
5	3	> 50% of VIP3	1.0-2.0	Strong
6	4	≤ 50% of VIP3 and 4	1.0-2.0	Very Strong
7	4	> 50% of VIP3 and 4	1.0-2.0	Very Strong
8	5 or 6	≤ 50% or VIP3, 4, 5, and 6	>2.0	Intense or Extreme
9	5 or 6	> 50% or VIP3, 4, 5, and 6	>2.0	Intense or Extreme

[1]Video Integrator Processor

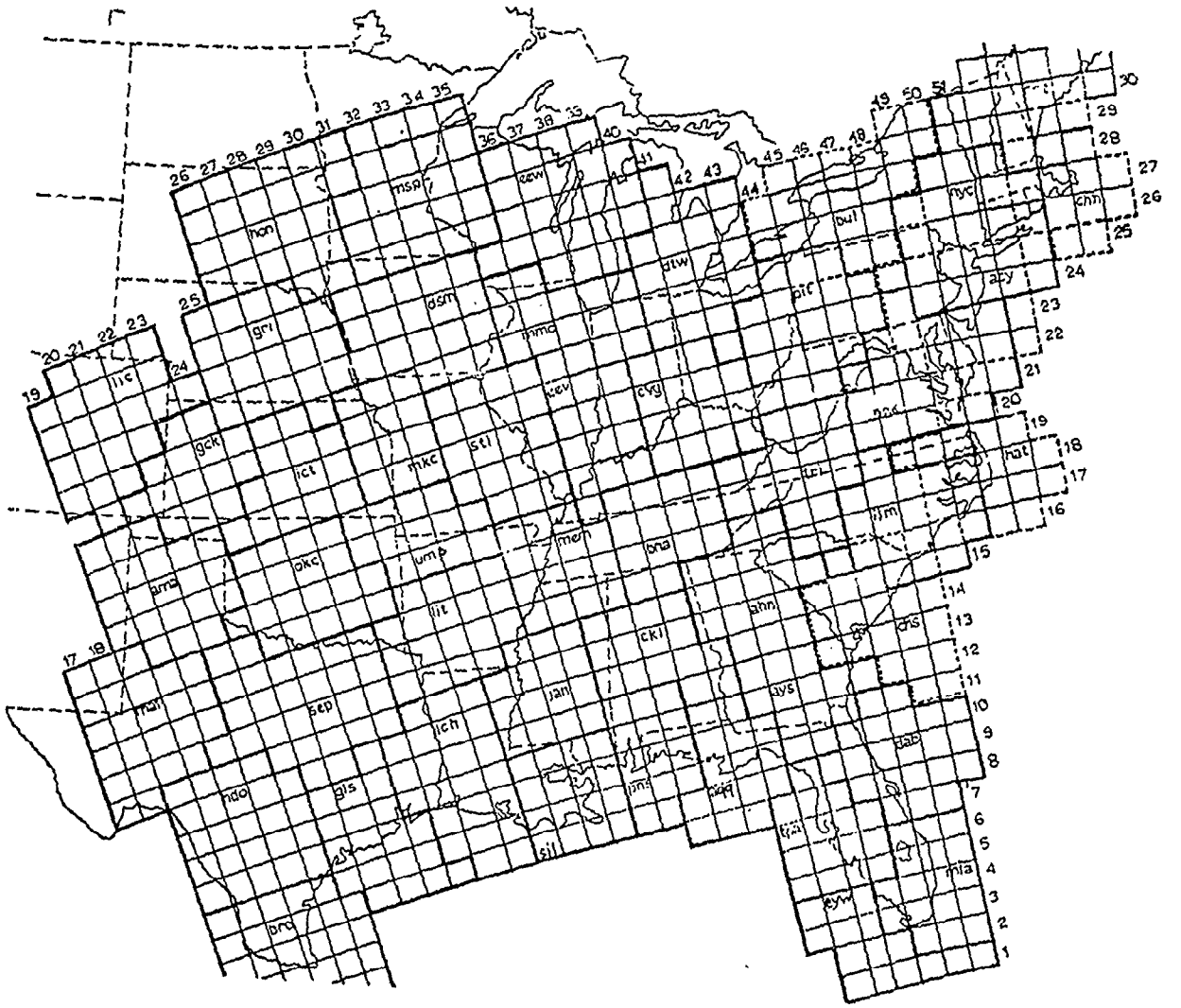

Fig. 2. Manually Digitized Radar (MDR) network.

4. SYNOPTIC CONDITIONS

In general, the AVE IV synoptic situation represented a typical low wind speed springtime situation in the lower levels with mostly zonal flow in the upper levels. Two relatively weak short wave pertubations in the middle and upper troposphere moved across the AVE IV network during the course of the experiment causing the development of widespread convection along the surface front. Figures 3 and 4 give the surface, 500-mb, and 300-mb maps for 0000 GMT on 24 April 1975, and 1200 GMT on 25 April 1975, the beginning and ending times of the experiment, respectively. Surface maps show frontal positions and the surface pressure field, while the 500- and 300-mb maps give height contours and the temperature pattern for these levels.

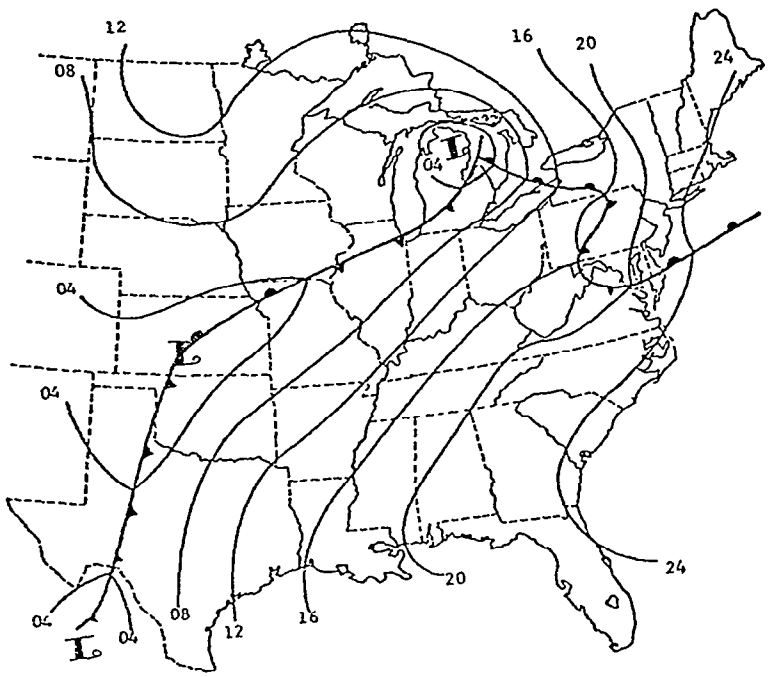

Surface

Fig. 3. Synoptic charts for 0000 GMT on 24 April 1975.

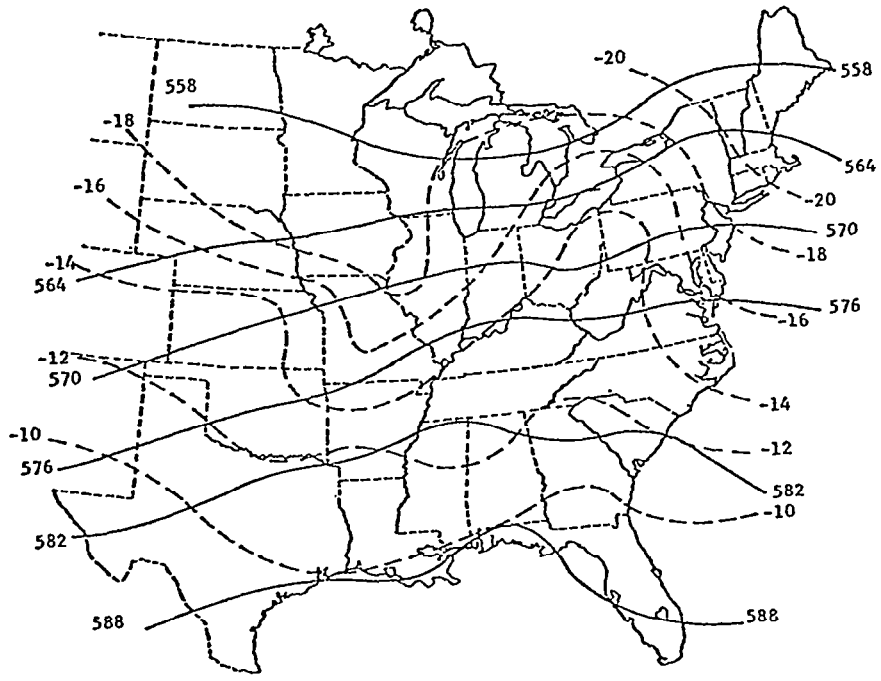

500 mb

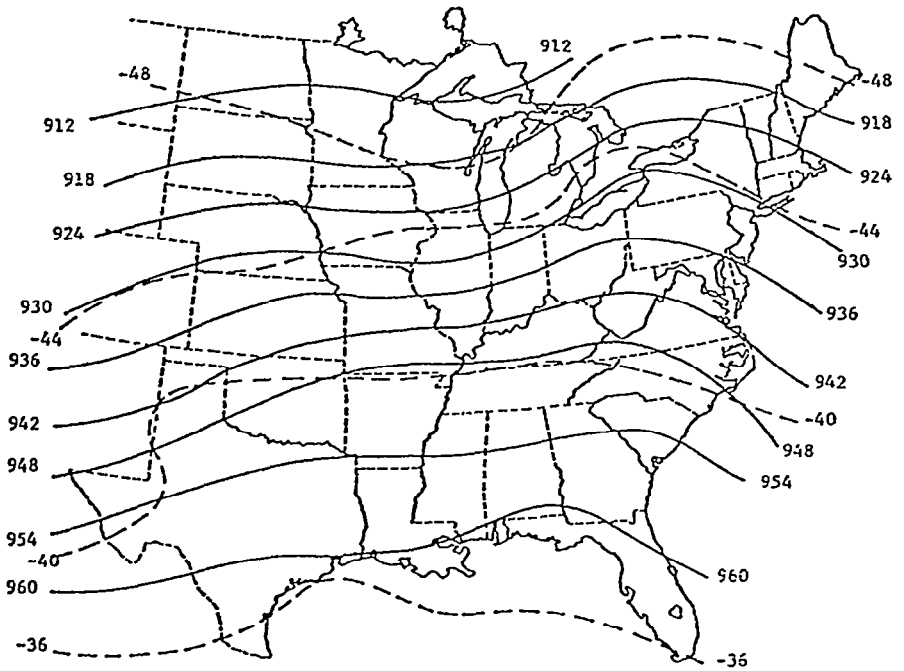

300 mb

Fig. 3. (Continued)

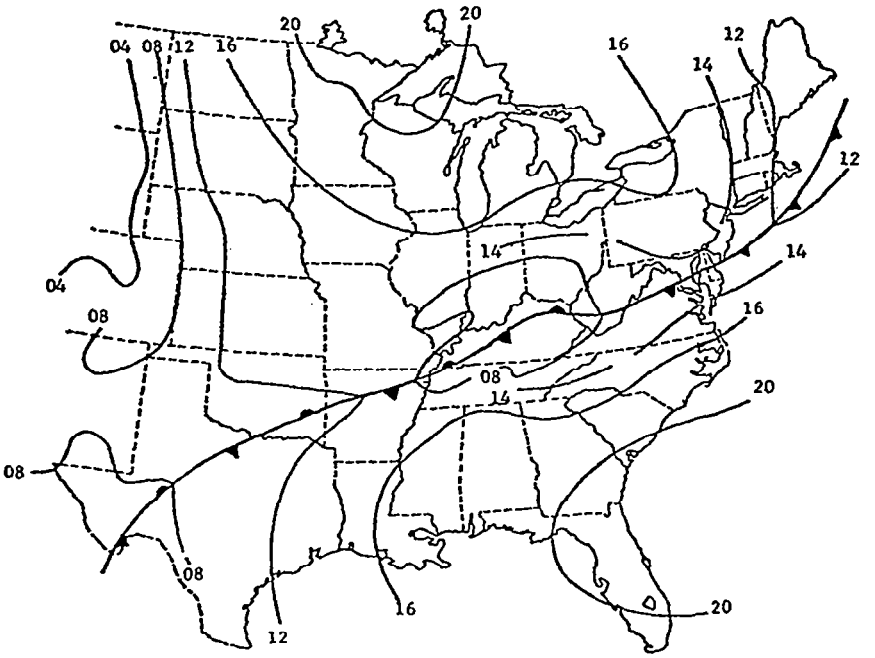

Surface

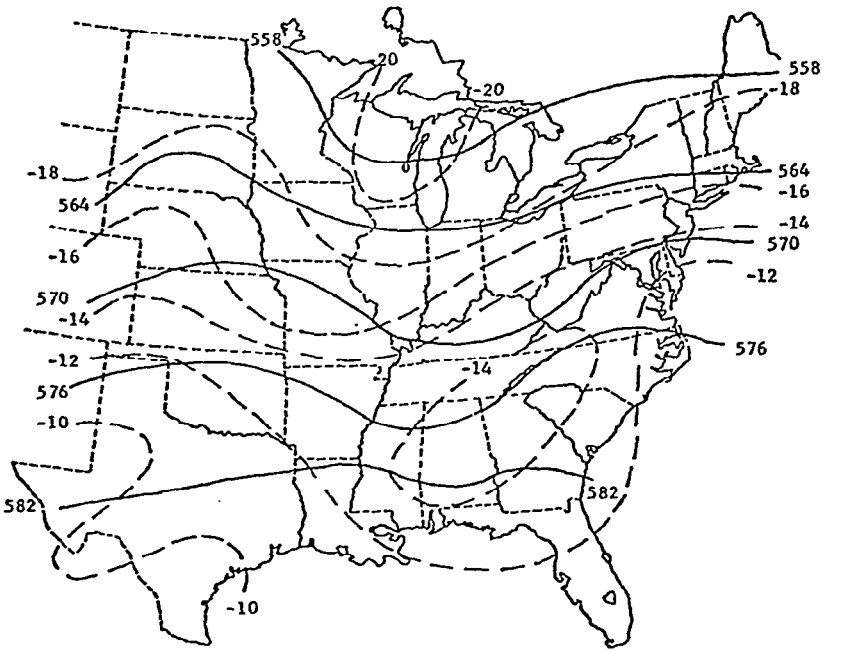

500 mb

Fig. 4. Synoptic charts for 1200 GMT on 25 April 1975.

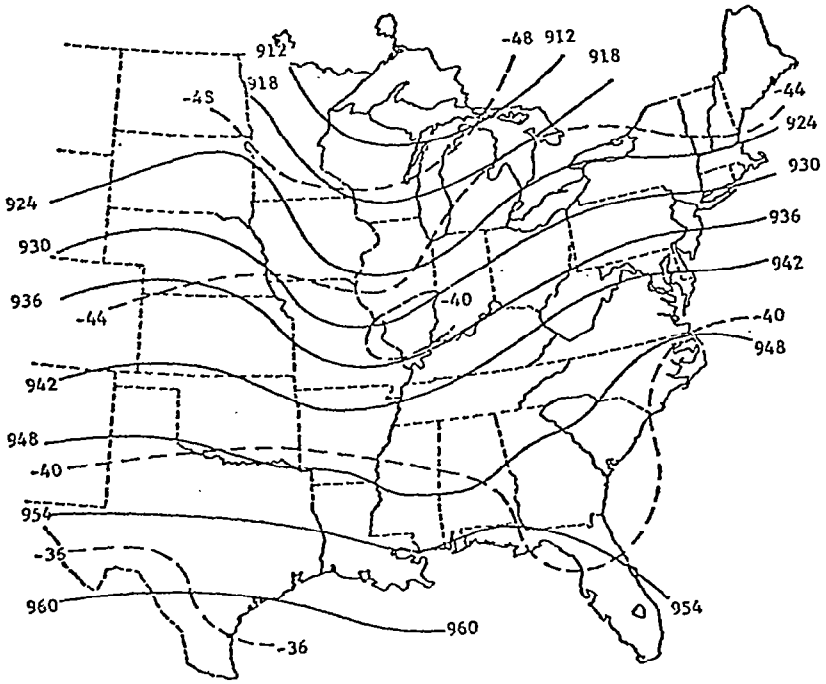

300 mb

Fig. 4. (Continued)

At the beginning of AVE IV, the primary synoptic features consisted of a moderately strong cyclone located over northern Michigan with a cold front extending southwestward into Kansas behind which continental polar air was moving southeastward over the north central states. Ahead of the front, maritime tropical air was flowing through the Gulf coast and middle Atlantic states northeastward into the Ohio valley. This flow was around an anticyclone centered about 550 km off the coast of the Carolinas. A warm front extended southeastward from the cyclone in northern Michigan through Pennsylvania and moved northeastward ahead of the warm moist Gulf air flowing through the eastern United States. By the end of the experiment, the cyclone had moved into the Gulf of St. Lawrence and the cold front, while making little progress southward, had advanced slowly eastward through the northern United States.

A second cyclone was centered over Kansas at the beginning of AVE IV with a cold front extending into west Texas separating

relatively dry maritime polar air from the moist maritime tropical air ahead of it. This front was relatively inactive and remained nearly stationary throughout the experiment.

Two squall lines moved across the AVE IV network during the course of the experiment associated with the short waves located in the middle and upper troposphere. At 0000 GMT on 24 April, the beginning of the experiment, the first squall line extended from northern Missouri into central Illinois. The squall line moved eastward ahead of the cold front associated with the first short wave and intensified. By 2100 GMT on 24 April the highest radar echo tops of 16,000 m were measured as the storms extended from central Tennessee into West Virginia. At the end of the experiment, 1200 GMT on 25 April, the line had dissipated with only scattered thunderstorms located in the Atlantic off the Virginia coast.

The second short wave resulted in two areas of severe convective activity. The first area had developed behind the surface cold front by 1200 GMT on 24 April in western Nebraska and South Dakota. These storms moved slowly eastward while dissipating until only weak thunderstorms were reported in eastern Iowa at the end of the experiment. As the short wave moved southeastward, a second squall line formed just after 2100 GMT on 24 April stretching from northern Arkansas into Oklahoma. Severe thunderstorms developed along the line with echo heights exceeding 20,000 m and both hail and tornadoes were reported. The thunderstorms reached maximum intensity at 0600 GMT on 25 April but at the end of the experiment, 1200 GMT on the 25th, the line was still strong and extended from West Virginia through eastern Tennessee and northern Mississippi into southeastern Arkansas.

5. ANALYTICAL METHODS

a. Objective analysis technique

To facilitate use of the observed data in numerical computations, a technique developed by Barnes (1964) was used to interpolate data from the irregularly arranged rawinsonde stations onto a symmetric grid. An 18 x 18 grid point array was placed over the region of the United States included in the AVE IV network. The array had a spacing of approximately 158 km between grid points and is shown in Fig. 5. Barr et al. (1971) have shown that this spacing gives the best possible horizontal resolution for data taken over the standard rawinsonde network while a smaller grid point separation does not give any greater detail of subsynoptic-scale systems. The Barnes

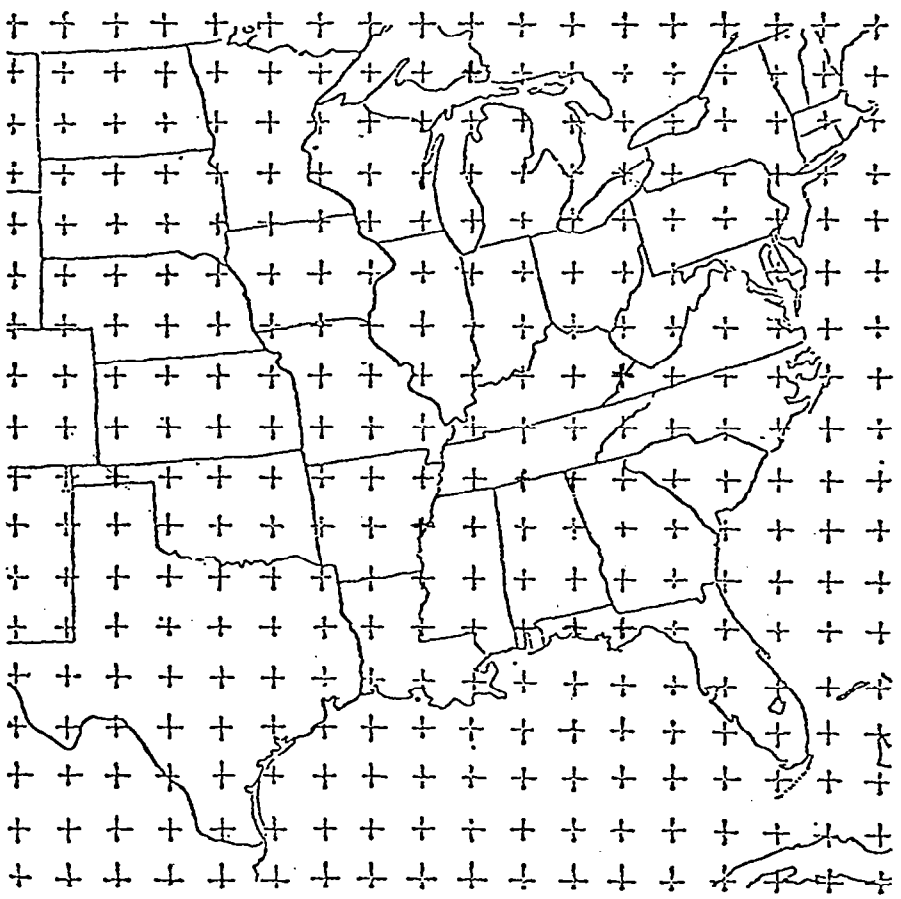

Fig. 5. Grid used for numerical computations.

technique is a Fourier analysis method. The first guess to the field was obtained by interpolating values of meteorological variables from the original data to the grid points. Successive corrections are then made by four iterations of the interpolating scheme. A scan radius of three grid distances was used for the interpolation to each point. The resulting fields were then smoothed by a process described by Schuman (1957) to remove any spurious high frequency variations in the gridded fields. Computations in this study used gridded fields of wind, temperature, dew point temperature, and humidity analyzed at 50-mb intervals from 900 mb to 200 mb.

The Barnes technique also was applied to surface data but the scan radius was reduced to only two grid distances. This was possible since the initial surface data with its smaller average distance between stations contained better horizontal resolution than the initial rawinsonde data.

The MDR data were gridded by assigning to each grid point the maximum MDR value from the composite MDR charts within a scan radius of one grid distance for the appropriate time.

b. Stability development equation

The stability of the atmosphere refers to the tendency of a parcel of air to be accelerated away from its initial position if given a vertical displacement. Stability is proportional to the difference between the existing lapse rate of the atmosphere and the dry-adiabatic lapse rate if the parcel remains unsaturated, or the moist-adiabatic lapse rate if the displacement is sufficient to cause the parcel to reach the condensation level and become saturated. The stability concept is not as simple when considering layers of finite thickness in the atmosphere but becomes a function of the temperature and moisture distribution with height.

Convective stability, σ_e, is defined by $-\frac{\partial \theta_e}{\partial p}$, where θ_e is the equivalent potential temperature. Grid point values of θ_e were computed using the gridded fields of temperature and dew point temperature. Finite differencing of the grid point values of θ_e at

the top and bottom of each layer gave σ_e with Δp equal to the pressure difference. The equivalent potential temperature is conserved during both dry and saturated adiabatic processes.

A development equation for convective instability can be derived analogous to the stability change equation given by Panofsky (1958). Beginning with the assumption that atmospheric motions are adiabatic, conservation of equivalent potential temperature is given as

$$\frac{d\theta_e}{dt} = 0. \tag{1}$$

Expanding the total derivative into its local rate-of-change, and horizontal and vertical advection terms in an x, y, p coordinate system, one has

$$\left(\frac{\partial\theta_e}{\partial t}\right)_p = -\vec{V}\cdot\vec{\nabla}_p\theta_e - \omega\frac{\partial\theta_e}{\partial p} \tag{2}$$

where $\vec{V}$ is the velocity of the wind on a constant pressure surface and ω is the vertical velocity in pressure coordinates.

The data used in this study were obtained from a synoptic-scale network and represent large scale processes. Therefore, the variables in (2) should be divided according to $A = \overline{A} + A'$ where the bar symbol, $\overline{A}$, is used to denote the synoptic-scale processes. The primed term, A', denotes subgrid-scale convective processes and eddy transport. If (2) is separated into synoptic-scale and small-scale processes and then averaged over an area corresponding to the grid size, one obtains

$$\left(\frac{\partial\overline{\theta_e}}{\partial t}\right)_p = -\vec{\overline{V}}\cdot\vec{\nabla}_p\overline{\theta_e} - \overline{\omega}\frac{\partial\overline{\theta_e}}{\partial p} - \overline{\vec{V}'\cdot\vec{\nabla}_p\theta_e'} - \overline{\omega'\frac{\partial\theta_e'}{\partial p}}. \tag{3}$$

Since the measured values of wind and equivalent potential temperature usually vary only a small amount over one grid distance, terms containing the product of a barred and primed quantity have been neglected.

By differentiating with respect to pressure at constant x, y, and t, one has (4)

$$\frac{\partial^2\bar{\theta}_e}{\partial p\partial t} = -\frac{\partial}{\partial p}(\bar{\vec{V}}\cdot\bar{\vec{\nabla}}_p\bar{\theta}_e) - \frac{\partial\bar{\omega}}{\partial p}\frac{\partial\bar{\theta}_e}{\partial p} - \bar{\omega}\frac{\partial^2\bar{\theta}_e}{\partial p^2} - [\frac{\partial}{\partial p}(\overline{\vec{V}'\cdot\vec{\nabla}_p\theta_e'}) - \overline{\frac{\partial\omega'}{\partial p}\frac{\partial\theta_e'}{\partial p}} - \overline{\omega'\frac{\partial^2\theta_e'}{\partial p^2}}].$$

Recalling that $\sigma_e \equiv -\frac{\partial\theta_e}{\partial p}$ and that by the equation of continuity $-\frac{\partial\omega}{\partial p} = \mathrm{div}_p\vec{V}$, one obtains (5)

$$\frac{\partial\bar{\sigma}_e}{\partial t} = \frac{\partial}{\partial p}(\bar{\vec{V}}\cdot\bar{\vec{\nabla}}_p\bar{\theta}_e) + \bar{\sigma}_e\mathrm{div}_p\bar{\vec{V}} - \bar{\omega}\frac{\partial\bar{\sigma}_e}{\partial p} + [\frac{\partial}{\partial p}(\overline{\vec{V}'\cdot\vec{\nabla}_p\theta_e'}) + \overline{\sigma_e'\mathrm{div}\,\vec{V}'} - \overline{\omega'\frac{\partial\sigma_e'}{\partial p}}].$$

For purely synoptic-scale motion, the terms in the bracket would be equal to zero. However, smaller scale processes are always present and must be accounted for. A residual term, R, will represent the subgrid-scale processes which the large-scale data cannot depict, giving as a final form

$$\frac{\partial\bar{\sigma}_e}{\partial t} = \frac{\partial}{\partial p}(\bar{\vec{V}}\cdot\bar{\vec{\nabla}}_p\bar{\theta}_e) + \bar{\sigma}_e\mathrm{div}_p\bar{\vec{V}} - \bar{\omega}\frac{\partial\bar{\sigma}_e}{\partial p} + R. \qquad (6)$$

The terms in (6) are the local rate-of-change of convective stability, differential horizontal advection of equivalent potential temperature, divergence on an isobaric surface, vertical advection of convective stability, and the residual, respectively.

c. Interpretation and computation of the terms

1) Layers and times considered

Computation of the terms in (6) were made for the layers: surface-850 mb, 850-700 mb, 700-500 mb, and 500-300 mb. Layers of 100-mb thickness from 900 mb to 300 mb were also considered but most of the results presented in this study are those found in the deeper layers. This decision was made for two reasons. First, the results from the deeper layers better defined major trends in the terms seen both in average vertical profiles and in individual constant pressure charts. There is much more variability in the layers of 100-mb thickness and the major trends are not as clear. Secondly, the deeper layers include levels commonly used in regular operational work today, and thus the results considering the layers between these levels are much more practical to the synoptician. The RMS errors were also slightly smaller if the terms were calculated over a thicker layer.

Constant pressure charts of the five terms in (6) were computed for 1500 GMT, 1800 GMT, and 2100 GMT on 24 April. These were the observational times during the experiment for which the data allowed the use of a 6-h centered difference to compute the local rate-of-change of convective stability and the resulting residual term. However all observational times were used to compute average vertical profiles of the development of convective instability by the large-scale processes.

2) Local changes

The local rate-of-change of convective stability is given by $\frac{\partial \sigma_e}{\partial t}$. Grid point values of θ_e at the top and bottom of a layer computed from the gridded fields of temperature and dew point temperature were first used to compute fields of convective stability using the definition $\sigma_e \equiv -\frac{\partial \theta_e}{\partial p}$. The evaluation of $\frac{\partial \sigma_e}{\partial t}$ for each grid point was then performed by a centered finite difference using values of the convective instability at times adjacent to the one being considered.

Positive development, defined by $\frac{\partial \sigma_e}{\partial t} > 0$, can either represent increasing stability if the air at that grid point was initially stable and the stability is becoming greater with time, or it can

represent decreasing instability if the air was initially unstable but is becoming less unstable with time. Likewise, negative development, given by $\frac{\partial \sigma_e}{\partial t} < 0$, can either represent increasing instability if the air was initially unstable, or it can represent decreasing stability if the air was initially stable. In this report, positive development will indicate simply $\frac{\partial \sigma_e}{\partial t} > 0$ and negative development will indicate $\frac{\partial \sigma_e}{\partial t} < 0$. When possible, the exact process will be further defined.

3) Differential advection of equivalent potential temperature

Differential horizontal advection of equivalent potential temperature is given by $\frac{\partial}{\partial p}(\vec{V} \cdot \vec{\nabla}_p \theta_e)$. Horizontal advection of θ_e at each grid point was evaluated by first computing values for the components of $\vec{\nabla}\theta_e$ using centered finite differences and then summing the values of $u\frac{\partial \theta_e}{\partial x}$ and $v\frac{\partial \theta_e}{\partial y}$. Taking the difference in the advection between corresponding grid points at the top and bottom of the layer and dividing by the pressure interval completed the evaluation of this term.

Cold advection above warm advection contributes to negative development ($\frac{\partial \sigma_e}{\partial t} < 0$), usually expressed as decreasing stability, while warm advection over cold advection contributes to positive development ($\frac{\partial \sigma_e}{\partial t} > 0$), usually expressed as increasing stability. However, since equivalent potential temperature is a function of moisture as well as temperature, moisture advection affects the local change of stability also. The advection of moist air over dry air may cause positive development ($\frac{\partial \sigma_e}{\partial t} > 0$) while dry air advected over moist air may result in negative development ($\frac{\partial \sigma_e}{\partial t} < 0$).

4) Divergence on an isobaric surface

The effect of divergence on an isobaric surface on the development of convective instability is given by $\sigma_e \text{div}_p \vec{V}$. Centered finite differencing of the wind components at the center level in each layer was used to calculate the divergence defined by $\frac{\partial u}{\partial x} + \frac{\partial v}{\partial y}$. Multiplication by the convective stability at each grid point completed the evaluation of this term.

Isobaric divergence ($\text{div}_p \vec{V} > 0$) results in vertical shrinking causing the equivalent potential temperature surfaces to become

closer together. Whether the air becomes more or less stable depends on its initial state. If it were initially stable ($\sigma_e > 0$), then divergence leads to greater stability ($\frac{\partial \sigma_e}{\partial t} > 0$), but if the air were initially unstable ($\sigma_e < 0$), divergence results in greater instability ($\frac{\partial \sigma_e}{\partial t} < 0$). Isobaric convergence ($\text{div}_p \vec{V} < 0$) causes vertical expansion and the separation of equivalent potential temperature surfaces with time. Initially stable air ($\sigma_e > 0$) will become less stable ($\frac{\partial \sigma_e}{\partial t} < 0$) as a result of convergence and initially unstable air ($\sigma_e < 0$) will become less unstable ($\frac{\partial \sigma_e}{\partial t} > 0$). Simply stated, divergence causes the initial state of stability of the air, whatever it happens to be, to increase in magnitude and convergence results in the decrease in magnitude of the initial state.

5) Vertical advection of convective stability

Vertical advection of convective stability is given by $-\omega \frac{\partial \sigma_e}{\partial p}$. Vertical motion for this study was computed using the kinematic method presented by O'Brien (1970). In this method, the vertical motion is calculated from the vertical summation of the horizontal wind divergence and adjusted so as to equal the adiabatic vertical motion at the top of the air column (100 mb). This term was evaluated by taking the difference at each grid point between values of σ_e at the top and bottom of the layer, multiplying by the vertical motion, dividing by the pressure difference and changing the sign.

Like the other terms in the stability change equation, the effect of this term depended on the initial state of the atmosphere, namely, whether it is increasingly stable (decreasingly unstable) with height or decreasingly stable (increasingly unstable) with height. In the first case, $\frac{\partial \sigma_e}{\partial p} < 0$ and upward motion results in negative development ($\frac{\partial \sigma_e}{\partial t} < 0$) since lower values of stability are being advected vertically to the point. However, downward motion results in the advection of higher values of stability and the development is positive ($\frac{\partial \sigma_e}{\partial t} > 0$). In the second situation, when the initial state is decreasingly stable with height ($\frac{\partial \sigma_e}{\partial p} > 0$), upward vertical motion results in positive development ($\frac{\partial \sigma_e}{\partial t} > 0$) but downward motion results in negative development ($\frac{\partial \sigma_e}{\partial t} < 0$).

6) Residual

The residual term represents an imbalance between the large-scale physical processes and the local rate-of-change of convective instability. In general, these terms do not sum to zero, resulting in the residual. This imbalance is attributed to subgrid-scale processes and their interaction with the synoptic-scale systems. These small-scale processes are described by the terms containing primed variables in (5). Sanders and Paine (1975) found that the equivalent potential temperature was not conserved in many places following the mesoscale flow. Included in the imbalancing small-scale processes are convection and eddy transport. House (1959) reported that areas of convection are characterized by the small-scale upward motion of warm moist air and downward motion of rain-cooled air. These transports would be seen as sources and sinks of heat and moisture not depicted by the large-scale processes on the synoptic scale. Wilson (1977) reported that eddies on the order of 100 km and with characteristic velocities of up to 5 m s^{-1} are not detected by the AVE data. Their influence would be included in the residual term. Since horizontal eddy fluxes are often negligible compared to vertical eddy fluxes, and the vertical velocity in convective regions is frequently two orders of magnitude greater than the synoptic-scale vertical motion, the term representing subgrid-scale vertical advection of stability pertubations, $-\overline{\omega' \frac{\partial \sigma_e}{\partial p}'}$, is probably the dominant term in the residual. The residual also represents data measurement error and errors introduced by finite difference approximations of the partial derivatives found in (6).

d. Error analysis

An error analysis of the terms in the stability development equation was done to determine the reliability of the computed fields and to see which terms are more sensitive to errors in the basic rawinsonde data. A propagation of error method described by Deming (1943) was used to calculate the effect of random errors in the measured wind, temperature, and specific humidity. The general form of the propagation of error equation is

$$\delta_Q = [(\frac{\partial Q}{\partial a})^2 \delta_a^2 + (\frac{\partial Q}{\partial b})^2 \delta_b^2 + (\frac{\partial Q}{\partial c})^2 \delta_c^2]^{\frac{1}{2}}$$

where δ_Q is the root mean square (RMS) of the errors in the derived quantity, Q, which is a function of the observations of a, b, and c, and δ_a, δ_b, and δ_c are the known RMS errors of a, b, and c. It was assumed that the errors were independent of one another and that the partial derivatives of Q could be accurately approximated by linear relationships.

RMS errors for temperature, moisture, and the wind measured at an elevation angle of 20° were obtained from Fuelberg (1974). The resulting error estimates along with the average magnitude and extreme value for each term in the stability development equation are given in Table 3. These errors are for the original rawinsonde data and do not reflect the errect of the gridding and smoothing which took place in the objective analysis technique. Although the exact effect of the analysis method on the errors is not known, work by Vincent and Chang (1975) implies that the errors are smaller than that calculated by a propagation of error if the data are smoothed in the analysis.

Table 3 shows that errors of the individual terms are generally the same order of magnitude as the term's absolute mean value but usually an order of magnitude smaller than the extreme values. Mean and extreme values of the terms generally decrease with height. The errors in the local rate-of-change of convective stability and differential advection of equivalent potential temperature also decrease with height due to the decrease in moisture content of the air in the

Table 3. Estimated rawinsonde RMS errors of terms in the stability development equation (10^{-7}°C mb^{-1}s^{-1}).

Quantity	Sfc - 850 mb			850 - 700 mb			700 - 500 mb			500 - 300 mb		
	Average Magnitude	Extreme Value	RMS Error	Average Magnitude	Extreme Value	RMS Error	Average Magnitude	Extreme Value	RMS Error	Average Magnitude	Extreme Value	RMS Error
$\frac{\partial \sigma_e}{\partial t}$	19.0	51.0	9.3	13.0	48.0	5.9	7.1	23.0	2.8	5.0	16.0	1.9
$\frac{\partial}{\partial p}(\vec{V}\cdot\hat{\nabla}\theta_e)$	9.3	39.0	4.6	9.5	40.0	4.7	6.1	29.0	3.2	4.8	18.0	3.1
$\sigma_e \, \mathrm{div}_p \vec{V}$	6.8	20.0	1.8	3.1	16.0	2.7	2.5	9.8	3.5	3.7	18.0	3.7
$\omega\frac{\partial \sigma_e}{\partial p}$	7.9	40.0	1.6	13.0	89.0	2.8	7.1	32.0	4.9	4.1	22.0	7.9
Residual	26.0			23.0			12.0			8.8		

upper atmosphere and therefore its effect on the error. The rate of decrease in the value of the error was approximately the same as that in the values of the terms. However the errors in the divergence on an isobaric surface and the vertical advection of convective stability increased with height due to increasing error in wind measurement. The largest error was found in the vertical advection term since ω is computed by vertically integrating the continuity equation and thus is very sensitive to wind errors. The errors in these terms in the upper levels became as large or larger than the term's absolute mean value, although the extreme values were still larger by at least a factor of three.

6. RESULTS

a. Relationships between terms in the stability change equation

All terms in (6) were computed using the procedures outlined above at 1500 GMT, 1800 GMT, and 2100 GMT on 24 April for the surface-850 mb, 850-700 mb, 700-500 mb, and 500-300 mb layers. Table 4 gives the mean and average magnitude of each of the terms for the times and layers considered. The average magnitude is found by averaging the absolute values of the term in each layer. It represents a typical magnitude which the term can be expected to have in the layer even if its mean is near zero. All terms generally had their largest average magnitude in the boundary layer (surface-850 mb) and decreased with height, except the divergence term which had a secondary maximum in the 500-300 mb layer and the vertical advection which was largest in the 850-700 mb layer instead of the boundary layer. The divergence term usually was found to have the smallest contribution to stability change in all layers at all times. However, it could not be neglected, especially in the boundary layer and the 500-300 mb layer where the divergence term was sometimes as large or larger than the advective terms. In the boundary layer, the local tendency and residual terms had the largest average magnitudes, while the advective terms were smaller by a factor of two or three. The tendency term decreased in value faster with height than did the residual so that by the 700-500 mb layer, the tendency and advective terms had about the same average magnitude. The average value of the residual was still sometimes a factor of two larger than the advective terms.

Neither the magnitudes of the means nor their signs showed a characteristic vertical trend that was consistent between every time period considered. House (1958) found that there were important changes in vertical motion and horizontal advection of temperature with possible reversals in their sign occurring quickly in space and time behind an instability line. These rapid changes could cause the inconsistencies in the various terms found in this study.

An example of the stability change fields is given in Fig. 6 for the 850-700 mb layer at 1500 GMT on 24 April 1975. Figure 6(a) is

Table 4. Means and average magnitudes of the terms in the stability development equation (10^{-7}°C $mb^{-1}s^{-1}$).

		$\frac{\partial \sigma_e}{\partial t}$		$\frac{\partial}{\partial p}(\vec{v}\cdot\vec{\nabla}\theta_e)$		$\sigma_e \, \mathrm{div}_p \vec{v}$		$-\omega \frac{\partial \sigma_e}{\partial p}$		Residual	
Time	Layer	Mean	AAM*	Mean	AAM	Mean	AAM	Mean	AAM	Mean	AAM
1500 GMT	Surface-850 mb	-20.0	26.0	-1.6	12.0	2.3	7.2	-0.4	4.9	-20.0	30.0
	850-700 mb	-3.6	12.0	0.8	11.0	1.4	3.8	-3.6	15.0	-2.2	23.0
	700-500 mb	-2.6	7.8	0.3	4.2	0.7	2.5	1.6	7.1	-5.2	13.0
	500-300 mb	0.3	4.5	-0.3	4.8	-1.0	4.1	0.3	4.1	1.2	8.8
1800 GMT	Surface-850 mb	-13.0	19.0	0.8	9.3	3.5	6.8	0.5	4.8	-17.0	26.0
	850-700 mb	-7.7	16.0	-0.9	8.5	-0.2	3.1	-7.4	13.0	0.9	23.0
	700-500 mb	1.9	7.1	-0.1	6.2	1.1	2.3	0.8	7.1	0.1	12.0
	500-300 mb	-2.2	5.0	0.7	4.4	-0.6	3.7	-0.1	2.8	-2.2	7.9
2100 GMT	Surface-850 mb	2.8	15.0	-1.4	8.4	3.3	6.8	0.1	4.6	0.8	20.0
	850-700 mb	-3.5	13.0	0.3	9.5	0.6	3.1	-2.2	11.0	-2.2	21.0
	700-500 mb	-0.3	7.0	1.2	6.1	0.7	2.7	1.6	7.6	-3.7	12.0
	500-300 mb	-1.4	5.3	-1.3	5.2	0.2	3.2	-0.8	4.1	0.5	9.6

* Average Absolute Magnitude

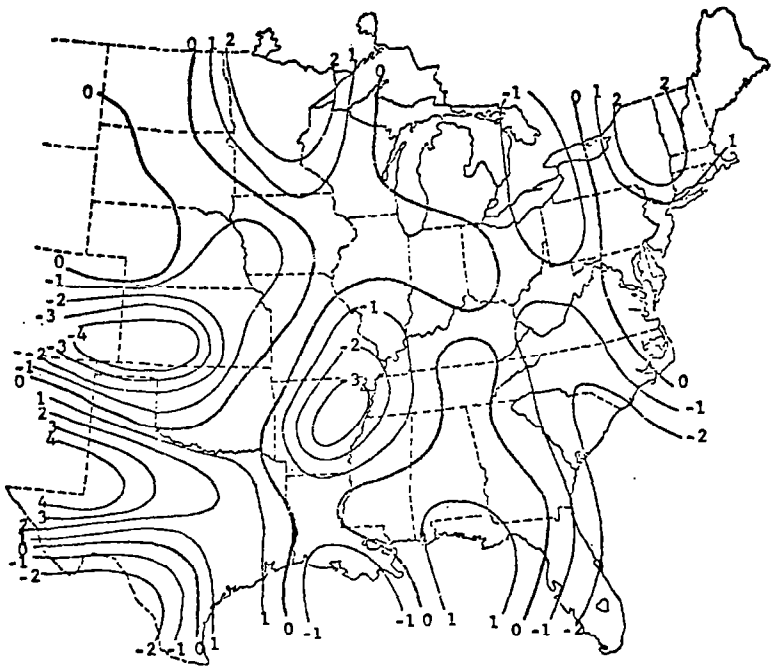

(a) $\partial\sigma_e/\partial t$

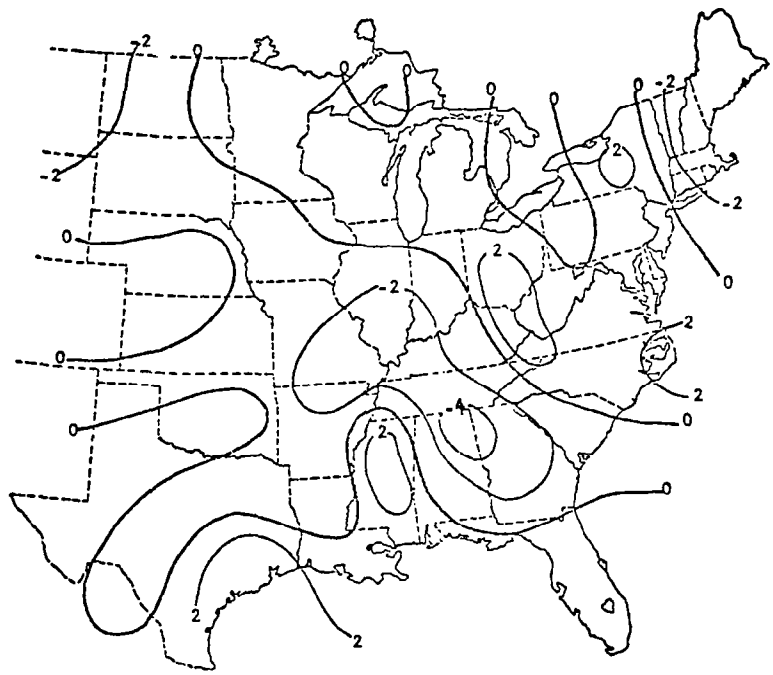

(b) $\frac{\partial}{\partial p}(\vec{V}\cdot\vec{\nabla}\theta_e)$

Fig. 6. Analysis of terms in the stability development equation in the layer from 850-700 mb at 1500 GMT on 24 April 1975 (10^{-7}°C $mb^{-1}s^{-1}$).

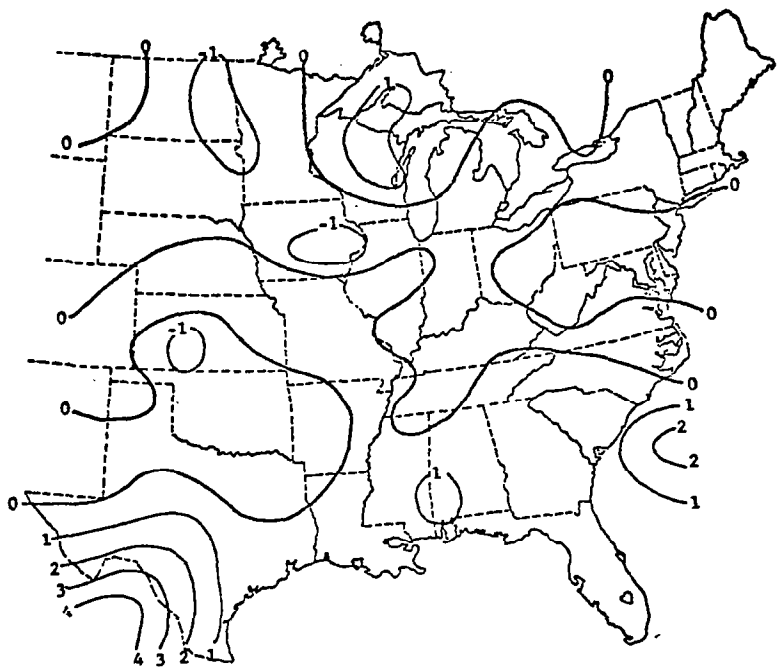

(c) $\sigma_e \, \mathrm{div}_p \vec{V}$

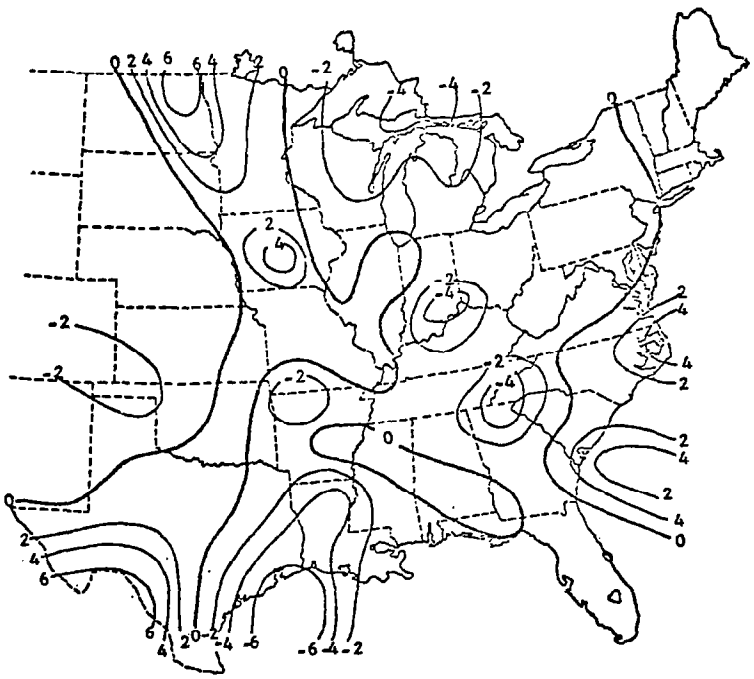

(d) $-\omega \frac{\partial \sigma_e}{\partial p}$

Fig. 6. (Continued)

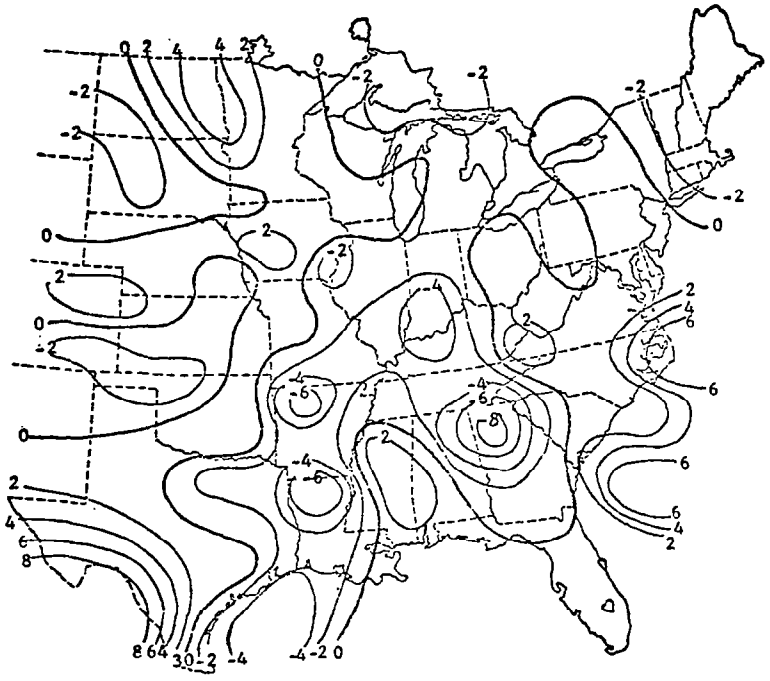

(e) $\frac{\partial}{\partial p}(\vec{v}\cdot\vec{\nabla}\theta_e) + \sigma_e \text{div}\,\vec{v} - \omega\frac{\partial\sigma_e}{\partial p}$

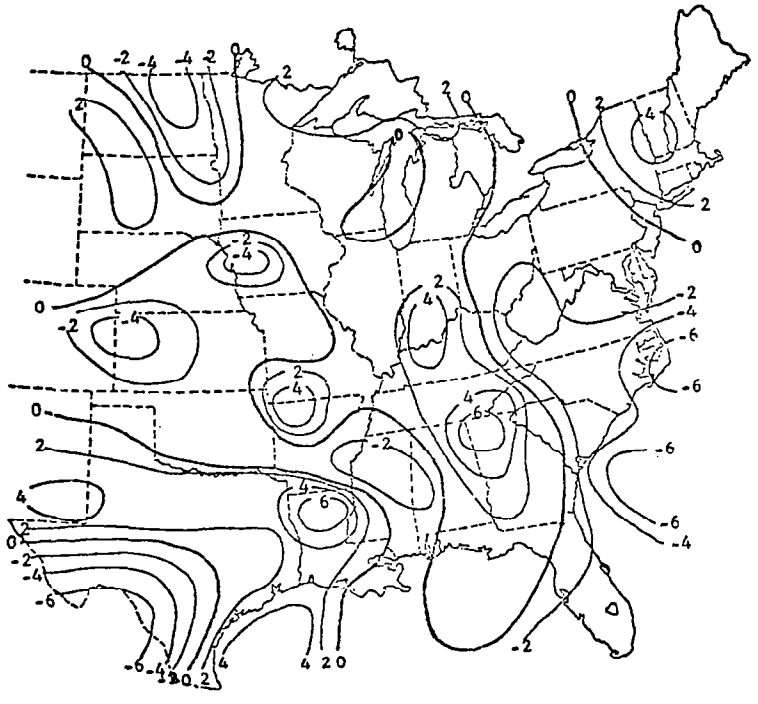

(f) Residual

Fig. 6. (Continued)

the local change of stability at this time showing negative development centers in western Kansas, eastern Arkansas, and off the Louisiana Gulf Coast with a tongue of negative tendencies from the eastern Great Lakes region to the southeastern Atlantic coast. Positive development was centered in southern Arizona, northern Minnesota, off the Gulf Coast of the Florida Panhandle and in the New England area. Figures 6(b), 6(c), and 6(d) show the stability change contribution from the differential advection, divergence, and vertical advection terms of the stability development equation, respectively. The summation of these three terms is shown in Fig. 6(e) which can be considered a field of the calculated stability development due to large-scale processes. The imbalance between the calculated stability development and actual stability development results in the residual field shown in Fig. 6(f). Although the computed change of stability tended to show centers of stability development with larger magnitudes than the actual local change of stability, areas of stability tendency are in fair agreement between the two maps. The calculated stability development showed an area of negative tendencies in the Oklahoma panhandle-western Kansas region stretching northward into North and South Dakota as did the actual local change of convective instability. A band of negative development also stretched from the Texas and Louisiana Gulf Coast up through Arkansas, Indiana, and into the Great Lakes region. The negative center found off the coast of South Carolina in the local change appears to have been displaced westward into northern Georgia in the calculated field of stability change. The positive stability development in west Texas, Minnesota, and the Gulf Coast show general agreement between the two maps, although the centers are usually too large and displaced eastward in the calculated field.

Although both actual and calculated stability change fields showed centers of positive and negative stability development on either side of the front, the terms combined to give calculated instability development areas of largest magnitude ahead of the front. This instability development was within the moist Gulf air flowing in the lower levels across the eastern half of the United States.

However, two regions of positive stability development were calculated in the moist low level flow. They were in Mississippi and the Virginias where the stabilizing influence of differential temperature advection, with stronger warm advection at 700 mb than at 850 mb, was larger in magnitude than the destabilizing influence of the moist low level flow.

The large discrepancies between actual and calculated stability change in southwest Texas, New England, and the Southeast Atlantic Seaboard occur in the corners or along the edges of the grid and should be regarded with suspicion. This time (1500 GMT) showed the best agreement between calculated and actual stability changes of the times considered. Overall convective activity was also at a minimum during this time. The lack of thunderstorm interaction and subgrid-scale modification of the atmospheric structure might account for the better agreement of the stability change fields at this time than at later times when the thunderstorms were more severe and widespread.

b. Relationships between stability development and convection

Average vertical profiles based on categories of convective severity were determined in order to reduce the effect of random errors and show general relationships between terms in the stability development equation and convection. The relative magnitude of the terms and their importance in various layers for the different categories of convection also can be observed from the average vertical profiles. The profiles were calculated by taking an average of each term computed for each category of convection determined from the gridded MDR data. Four categories of MDR values showing an increasing severity of convection were selected for the purpose of making comparisons. They were MDR$\leq$1 representing no convection, MDR$\geq$2 representing all convection, MDR$\geq$4 representing thunderstorms and MDR$\geq$8 representing severe thunderstorms. All observational times were used to compute average vertical profiles of the development of convective instability by differential advection of θ_e, divergence and vertical advection of convective stability. However, only 1500 GMT, 1800 GMT, and 2100 GMT allowed the use of a 6-h centered

difference to compute average vertical profiles of the local rate-of-change of convective stability and the resulting residual term.

The average vertical profiles for the local rate-of-change of convective stability are shown in Fig. 7. Except in the surface boundary layer, profiles of the local change show little difference between convective and nonconvective areas or between the different categories of convective intensity. All show negative local stability change above 850 mb with nonconvective areas having equal or larger average magnitudes of negative development as convective areas. However, below 850 mb increasing severity of convection shows an increasingly positive local stability change. This possibly is due to thunderstorm subgrid-scale processes, especially since the positive development increases with increasing MDR value. Other studies have shown that thunderstorms interact with the boundary layer structure so as to increase the low-level stability. Read and Scoggins (1977) found the stability in the surface-850 mb layer to be smaller prior to than during convection.

Figure 8 shows analyzed fields of the local tendency of convective stability in the boundary layer for 1500 GMT, 1800 GMT, and 2100 GMT on 24 April 1975. Although the variability between adjacent observation times is great, definite centers of stability change and trends in their movement can be observed. Most noticable is the center of negative tendency which is located in western Missouri at 1500 GMT which expands to include Iowa at 1800 GMT with some movement eastward by 2100 GMT. Negative centers located over northern Minnesota and Lake Huron are generally stationary in time with the negative tendencies on the eastern seaboard and southeastern United States showing a tendency to weaken and be replaced with positive stability development by 2100 GMT. Positive tendencies located initially in northeastern Arkansas also show a trend to move into north Texas. Convection usually occurs in areas of positive tendency at the time of occurrence with the more severe storms often coinciding with centers of positive stability development.

The center of negative development located in western Missouri at 1500 GMT moved ahead of the front to a position in northern

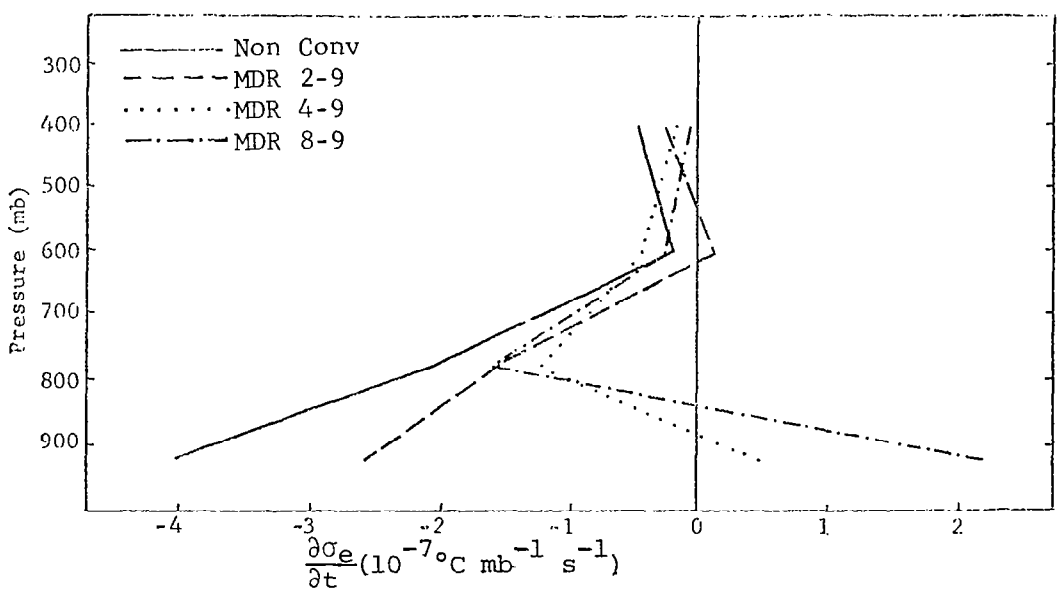

Fig. 7. Average vertical profiles for the local derivative of convective stability.

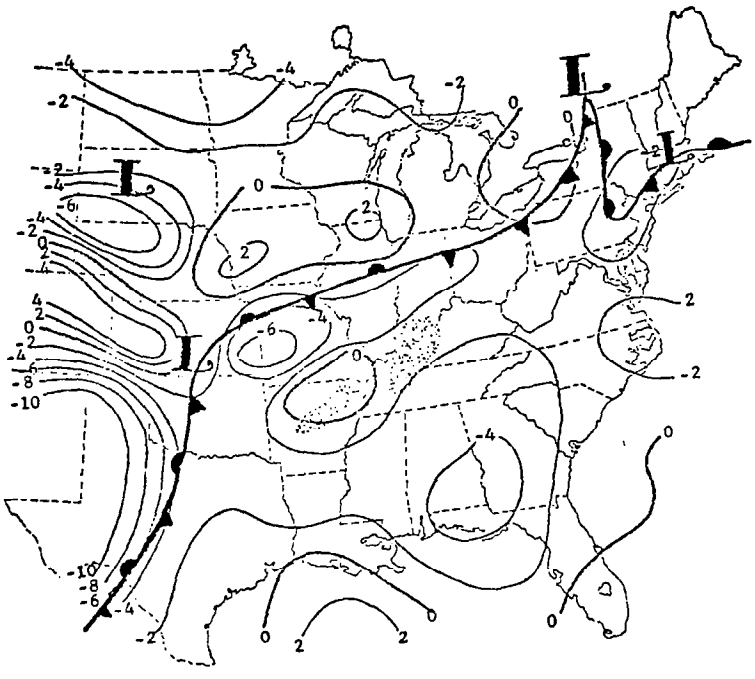

(a) 1500 GMT

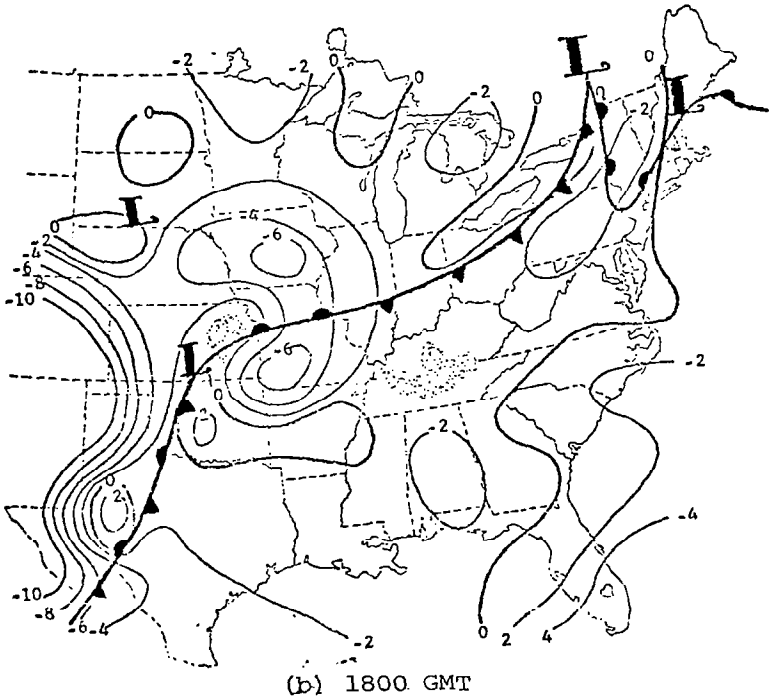

(b) 1800 GMT

Fig. 8. Analysis of the local tendency of convective stability (10^{-7}°C mb^{-1} s^{-1}) in the layer from the surface-850 mb (surface front and thunderstorm areas shown for reference).

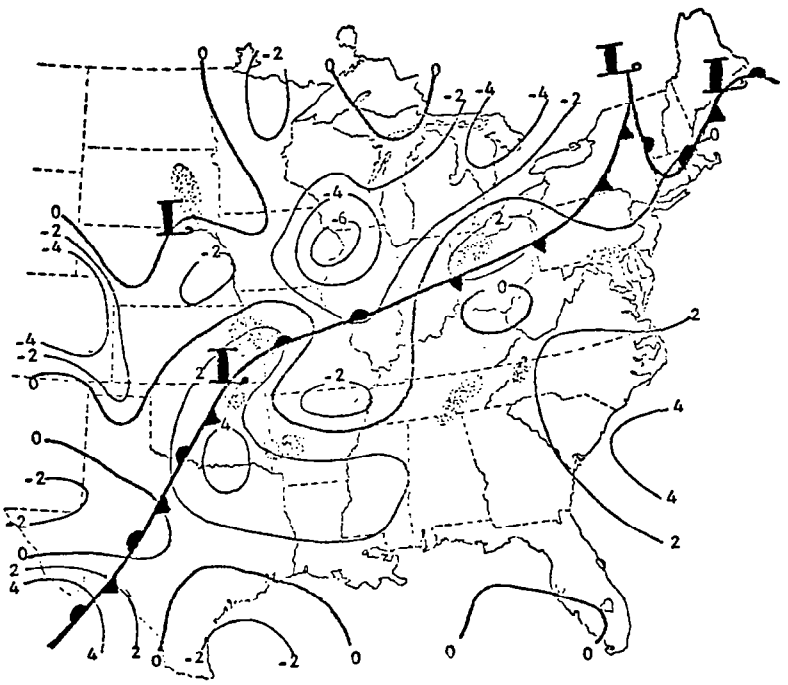

(c) 2100 GMT

Fig. 8. (Continued)

Arkansas 6 h later, and a negative center formed in Iowa behind the front at 1800 GMT replacing positive tendencies located in that area just 3 h earlier. Therefore, at 1800 GMT and 2100 GMT, negative development centers were located on either side of the front in the central United States but in the immediate area of the front the negative tendencies were diminished. Although the relationship between the frontal position and the sign of centers of stability change was not consistent along the entire length of the front, in the boundary layer the front was often in areas of positive stability development or diminished negative tendencies.

Figure 9 shows fields of local tendency for the 850-700 mb layer. As the vertical profiles implied, there is often a reversal in the sign of centers with height especially evident at 2100 GMT. Time continuity is still evident with the positive center located initially over Minnesota expanding and moving south to overlie the negative tendency centers in the boundary layer located in western Illinois and northern Arkansas. Regions of precipitation were located generally in areas of negative stability development.

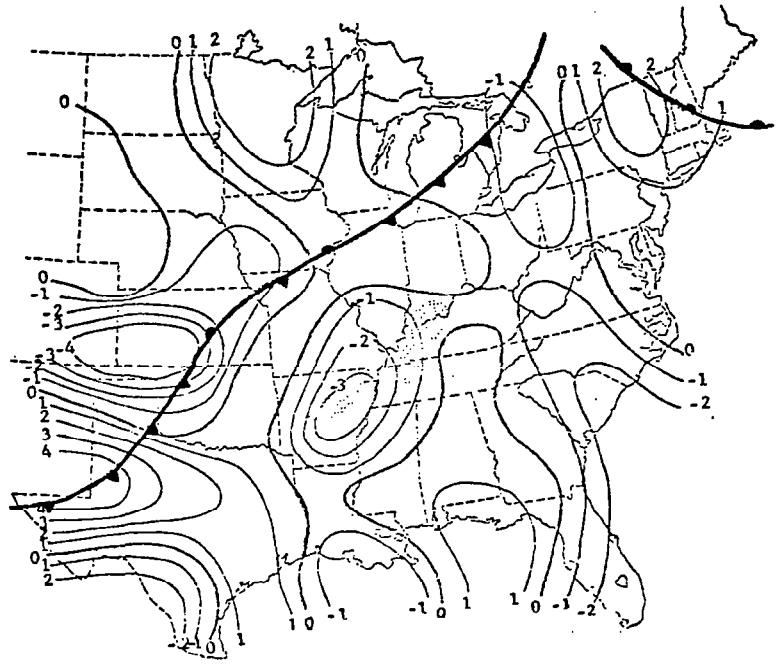

(a) 1500 GMT

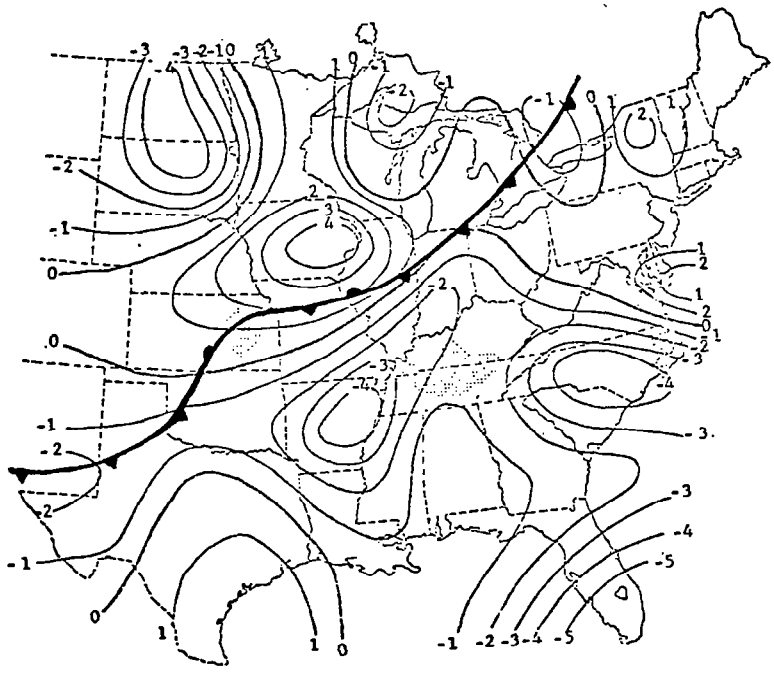

(b) 1800 GMT

Fig. 9. Analysis of the local tendency of convective stability (10^{-7}°C mb^{-1} s^{-1}) in the layer from 850-700 mb (850-mb front and thunderstorm areas shown for reference).

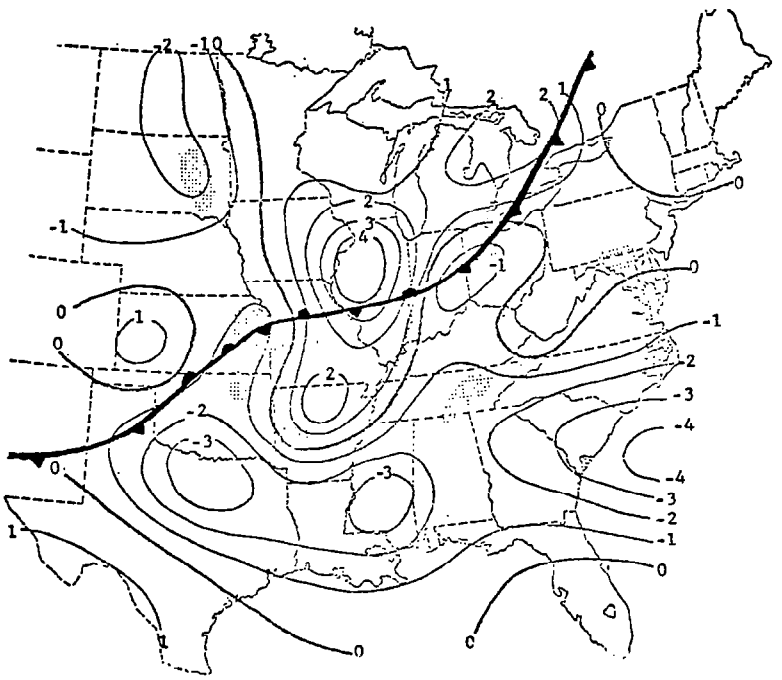

(c) 2100 GMT

Fig. 9. (Continued)

The only area where the front showed significant movement from 1500 GMT to 2100 GMT was the region from northern Missouri to Lake Erie. The fields in Fig. 9 show positive stability tendencies increasing in Iowa and Illinois during this time as the front moved through. Negative tendencies could still be found in the south and southeastern United States within the moist Gulf flow ahead of the front in this layer. At 1800 GMT and 2100 GMT the front was located in areas of positive stability development, but the relationship between the front and positive tendency centers was not as good at 1500 GMT. Significant changes in the sign and magnitude of the stability tendency also took place away from the front.

Centers of tendency continued to show temporal continuity in the 700-500 mb and 500-300 mb layers (not shown) although the values are smaller and variability somewhat greater. Nonconvective and convective areas showed little preference to lie within centers of local stability change in these layers.

Profiles of average magnitudes of the differential advection of equivalent potential temperature are shown in Fig. 10. Convective and nonconvective areas are generally opposite in sign with the surface-850 mb layer and 700-500 mb layer showing increasing positive stability development with increasing severity of the convection. Nonconvective areas showed small negative development on the average. In the 850-700 mb layer the signs were reversed with the more severe thunderstorms showing a trend toward increasing negative stability development, while nonconvective areas showed positive stability development. During the AVE IV experiment, much of the convective activity occurred as a result of the intrusion of dry southwest air into Missouri and Kansas at the 700-mb level. This would correspond well with the maximum instability development indicated in the vertical profiles to occur between 850 and 700 mb since the advection of dry air over moist air can result in a layer becoming convectively unstable. Decreasing stability in the 850-700 mb layer would also tend to destroy any capping inversion which could suppress convective activity whereas the warm-over-cold advection associated with the nonconvective areas would strengthen the inversion and so prevent the occurrence of deep convective overturning.

Analyzed fields of stability change due to differential advection at 1500 GMT, 1800 GMT, and 2100 GMT in the 850-700 mb layer are shown in Figure 11. Convection generally occurs in regions of destabilizing differential advection although the strongest centers of instability development do not overlie the areas of severest thunderstorms. The differential advection term is generally continuous in time with centers showing a general eastward progression in the synoptic scale flow.

The synoptic condition during AVE IV was a low wind speed situation with predominately zonal flow at all levels. This may account for the lack of dominance in calculated stability change by the term describing differential advection of equivalent potential temperature. However, differential advection associated with the second short wave moving across the network during the experiment did cause instability to develop in the Mississippi River Basin as

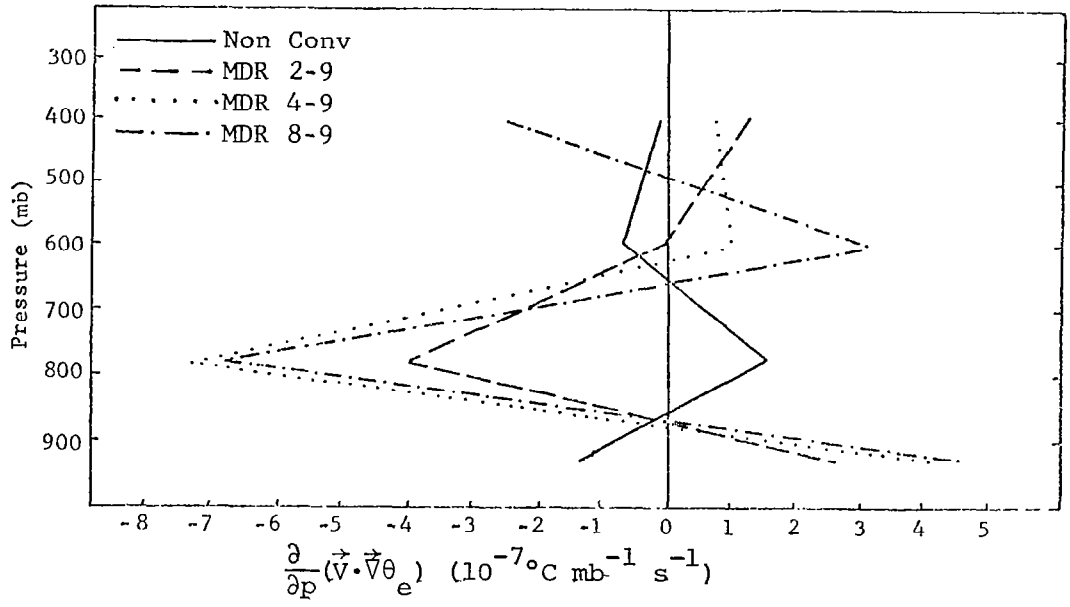

Fig. 10. Average vertical profiles for the differential advection of equivalent potential temperature.

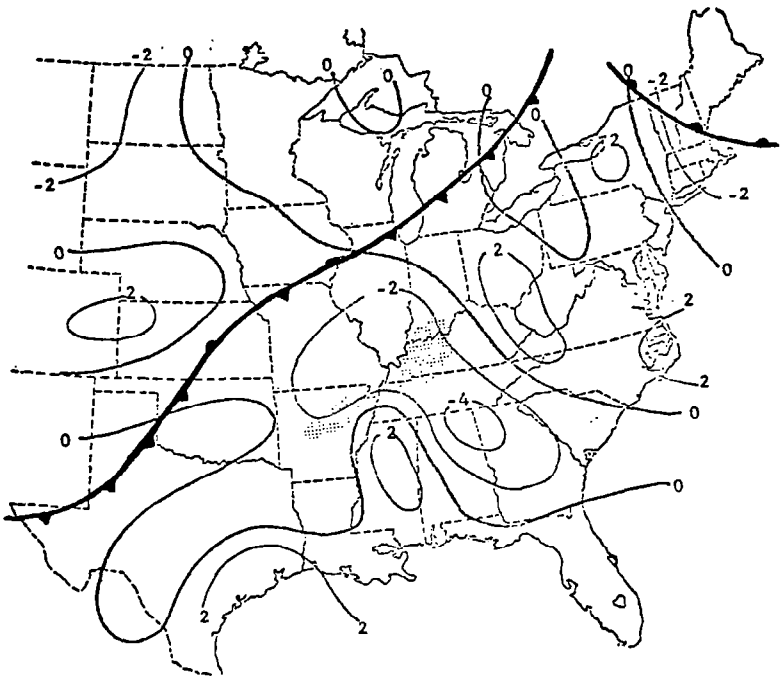

(a) 1500 GMT

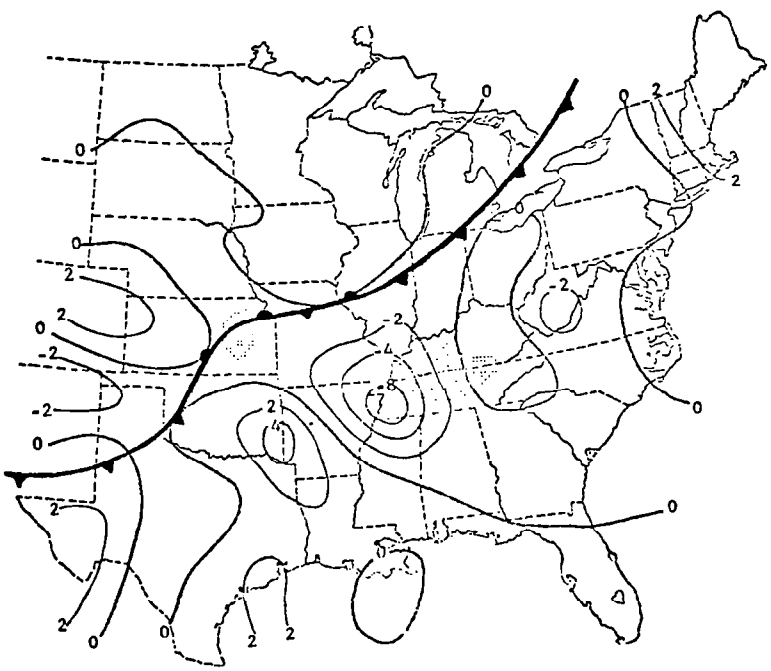

(b) 1800 GMT

Fig. 11. Analysis of the differential advection of equivalent potential temperature (10^{-7}°C mb^{-1} s^{-1}) in the layer from 850-700 mb (850-mb front and thunderstorm areas shown for reference).

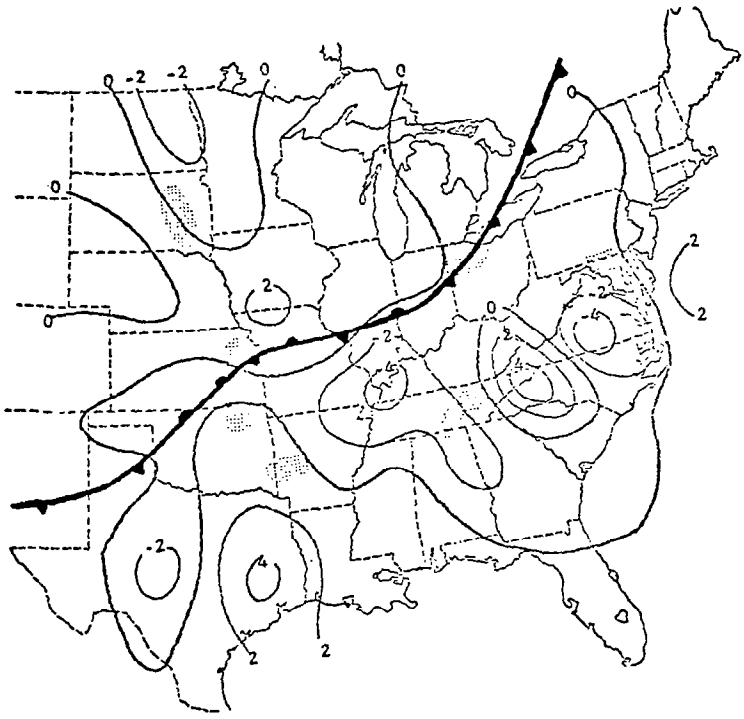

(c) 2100 GMT

Fig. 11. (Continued)

seen in Fig. 11. A squall line formed in northern Arkansas and Oklahoma and moved northeastward through this unstable area.

Scott and Scoggins (1977) found regions of precipitation to have a characteristic maximum in positive moisture advection in the 700-500 mb layer. This would explain the presence of an average stabilizing influence due to the differential advection term for convective areas in the 700-500 mb layer since moist advection over dry advection results in stabilization of the atmosphere. Above 500 mb, differential advection distinguishes poorly between convection of varying intensity.

Although analyzed fields for the other layers showed the general characteristics described by the average vertical profile and were continuous in time, there was poor correlation between the areas of convection and centers of maximum differential advection.

The average vertical profile of the divergence term in the stability development equation, shown in Fig. 12, shows non-convective areas generally to have a small positive contribution to stability development from this term up through 500 mb. It also shows the contribution to positive stability development increasing in average value with increasing MDR value and reaching a maximum in the 850-700 mb layer, and a secondary maximum in the 500-300 mb layer. However, in the 700-500 mb layer, increasing severity of the convection was found to be associated with increasing instability development. Nonconvective areas still showed positive stability development in this layer.

To interpret the vertical profiles of the divergence term we note that Wilson and Scoggins (1976) found surface wind convergence strongly correlated with convective activity, and that convection was seldom found in the field of divergent wind at the surface. At 850 mb, convective activity, and particularly thunderstorms, consistently occurred in areas of convergence, and stronger areas of convergence corresponded to stronger convective activity. At 700 mb, no consistent correlation was found between convective activity and the convergence or divergence of wind fields, but at 500 and 300 mb the wind field was generally divergent over areas of

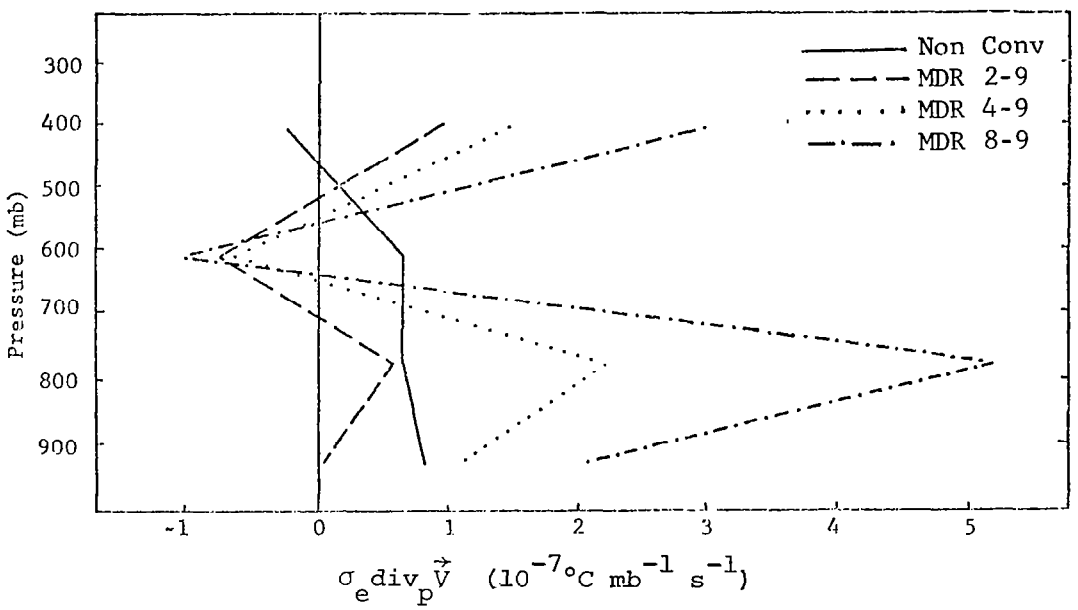

Fig. 12. Average vertical profiles for the divergence term.

convection. Similar relationships between convective activity and convergent or divergent wind fields were found for AVE IV.

Therefore, for the surface-850 mb layer in convective areas, wind fields are convergent and σ_e is less than zero. Areas with MDR$\geq$2 are unstable, as we would expect. However, the divergence term is acting so as to make the air less unstable. Similarly, since nonconvective areas generally have divergence in the surface-850 mb layer and σ_e is positive, the air is stable and the divergence term is acting to increase that stability. Although the 700-mb level did not show consistent correlation between convective activity and convergence or divergence, the 850-mb level did. Therefore, the same general results just described for the boundary layer would also apply to the 850-700 mb layer.

The vertical profiles showed convective areas (MDR≥2) in the 700-500 mb layer to have a negative stability contribution by the divergence term. Since the middle levels over convection generally had divergence and the air was unstable in this region, the divergence term was creating greater instability. Read and Scoggins (1977) found instability in the 700-500 mb layer was related to further intensification of convective activity, and that instability present in this layer was important in maintaining thunderstorm systems. The divergence term explains the process whereby crucial instability may be formed. For the 500-300 mb layer all values for the convection categories shift back to positive development in the average vertical profile, but Wilson and Scoggins' study showed the wind field in this layer to remain divergent over convective regions. Therefore, σ_e is positive and divergence on an isobaric surface is causing greater stability to develop. The average value of the divergence term for nonconvective areas in this layer is very small, and thus no conclusions can be made from it.

The importance in examining the average vertical profiles of the divergence term in relation to commonly observed trends in the divergence field is that it explains how thunderstorms act to increase the stability in their environment. Evidence of the process was observed by Read and Scoggins (1977) who found instability in the lower levels to be greater three to six h prior to thunderstorm development than during the time which the thunderstorms were developing. They attributed this to thunderstorm interaction with the environment. The divergence term in the stability change equation explains how thunderstorms and their associated convergence in the lower levels act to decrease instability, and divergence in the upper levels acts to increase the stability.

As Fig. 13 shows, the divergence term on individually analyzed fields correlated poorly with areas of convection or, by comparing to Fig. 8, to areas of actual stability development. The term shows great variability but was generally continuous in time. Instability development in the boundary layer due to divergence on an isobaric surface expanded in the northern plains states from 1500 GMT to 2100

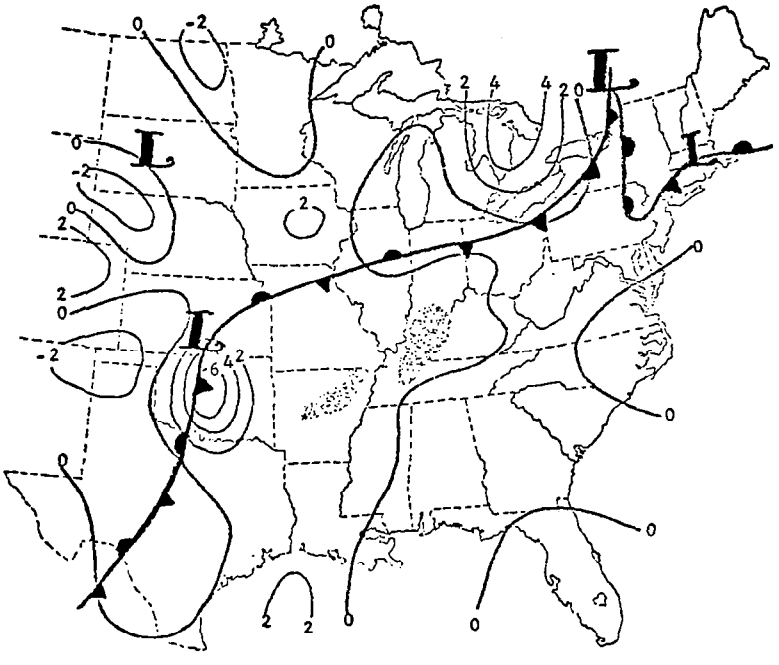

(a) 1500 GMT

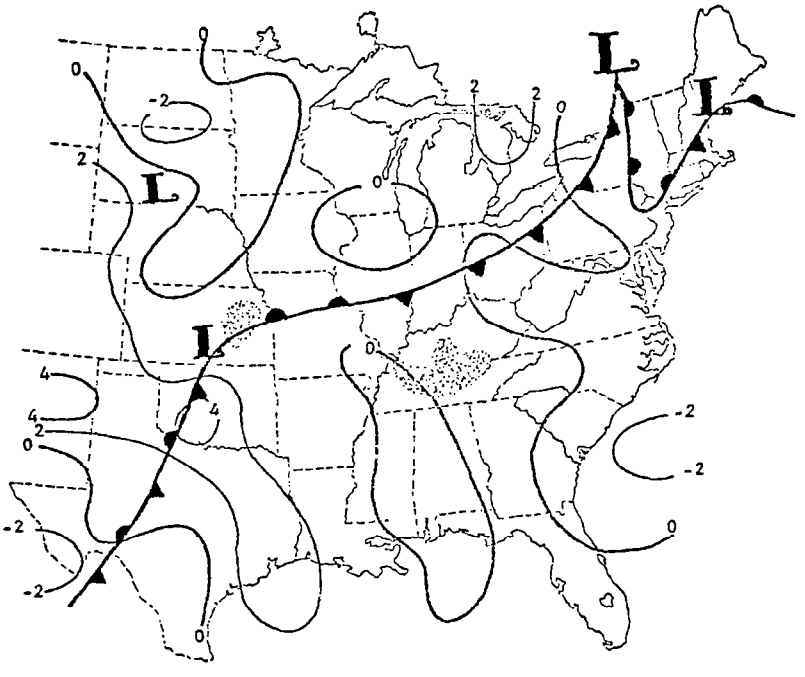

(b) 1800 GMT

Fig. 13. Analysis of the divergence term (10^{-7}°C mb^{-1} s^{-1}) for the layer from the surface-850 mb (surface front and thunderstorm areas shown for reference).

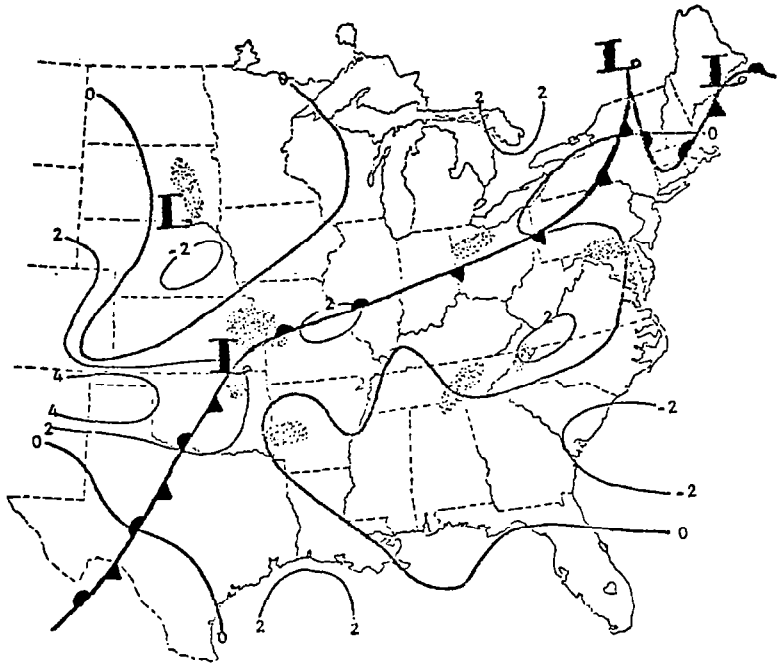

(c) 2100 GMT

Fig. 13. (Continued)

GMT, while positive development was present from Oklahoma to the Texas Gulf Coast and over the Lake Huron area. The zonal nature of the flow during the AVE IV experiment may account for the small influence of the divergence term on the actual stability change.

Average profiles for the vertical advection of convective instability are shown in Fig. 14. Values for nonconvective areas are generally small with negative stability development below 650 mb and positive stability development above that level. For convective areas below the 650-mb level, increasing positive stability development was associated with increasing storm severity. A maximum in the stability development occurred in the 850-700 mb layer. Above 650 mb, instability development increased with increasing severity of the storms and maximum instability development was found in the 700-500 mb layer. The fact that vertical motion is observed to correlate well with convection allows further description of the effects of this term to be made.

Wilson and Scoggins (1976) found that fields of vertical motion near the surface were almost perfectly correlated with convective

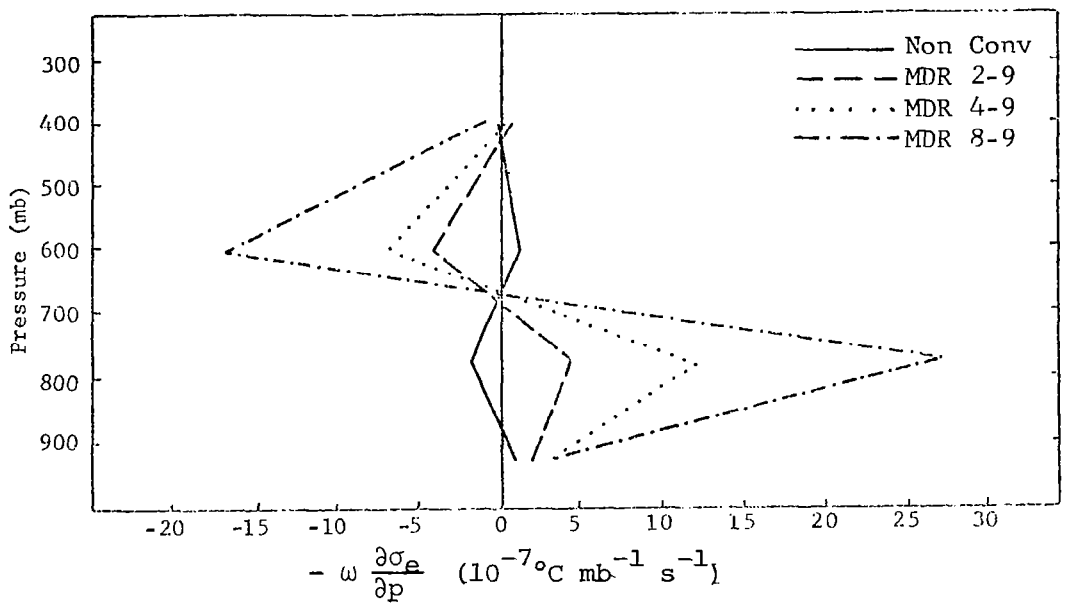

Fig. 14. Average vertical profiles for the vertical advection of convective stability.

activity, and stronger vertical motion usually corresponded to stronger convection. Areas of thunderstorms (MDR≥4) were seldom located within subsidence close to the surface. At the top of the boundary layer (850 mb), convection was usually present within areas of upward motion although some occurred in areas of subsidence. At least the areas of severe convection correlated well in space with centers of positive vertical motion. Endlich and Mancuso (1968) reported that upward motion in the boundary layer seemed to be a necessary condition for the formation of convection. At 700 mb and 500 mb, thunderstorms generally occurred in regions of upward motion but positive vertical velocities at these levels were not necessary for storm development. Generally, strong convection occurred in areas where strong vertical motion extended from the surface up through the entire lower and middle troposphere.

Convective areas show positive stability development due to vertical advection in the vertical profiles up to approximately 700 mb, the region where convection and positive vertical motion

correlated well. The stability was also found to decrease with height in this layer for convective areas. Referring to the term for the vertical advection of convective instability in (6) positive stability development and upward motion also imply decreasing stability with height ($\frac{\partial \sigma_e}{\partial p} > 0$) since higher values of stability are being transported upward. In this situation of decreasing stability with height, once a parcel of air has begun to rise, there would be nothing to inhibit further motion and release of potential instability creating deep convection. The increasing value of this effect for increasing MDR values, as seen in the vertical profiles below 700 mb, could be due to stronger vertical motion associated with the more severe thunderstorms or a sharper decrease in stability with height. However, both of these are characteristic of regions containing thunderstorms. The vertical advection term also indicates a process whereby the fields of strong upward motion associated with thunderstorms can actually increase the stability in the lower atmospheric layers. As was mentioned earlier, this was observed to occur by Read and Scoggins (1977).

Above approximately 700 mb, the contribution of vertical advection to increasing instability development was associated with increasing storm severity. Thus the vertical advection term, as well as the divergence term, provides a process for creating instability in the 700-500 mb layer that is important to the maintenance and further intensification of the thunderstorm systems.

The vertical advection term showed the greatest variability in time of all the terms due to the highly variable nature of the vertical motion field. However, some continuity of the term could be found. Figure 15 shows the development of stability due to vertical advection of convective instability in the 700-500 mb layer. Positive contributions occurred in a band from the Texas Gulf Coast generally northeastward to a center in northern Illinois with the negative centers in North Dakota, the Texas Panhandle, and over Lake Ontario being more or less continuous. The extreme variability of this term can be observed in the Virginia-Kentucky area which switched from strong negative development by vertical advection at 1500 GMT to

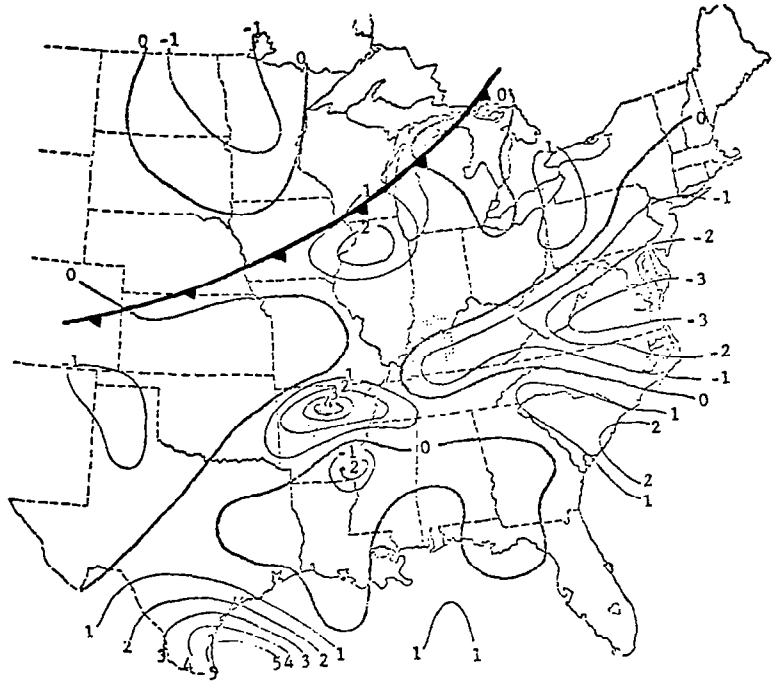

(a) 1500 GMT

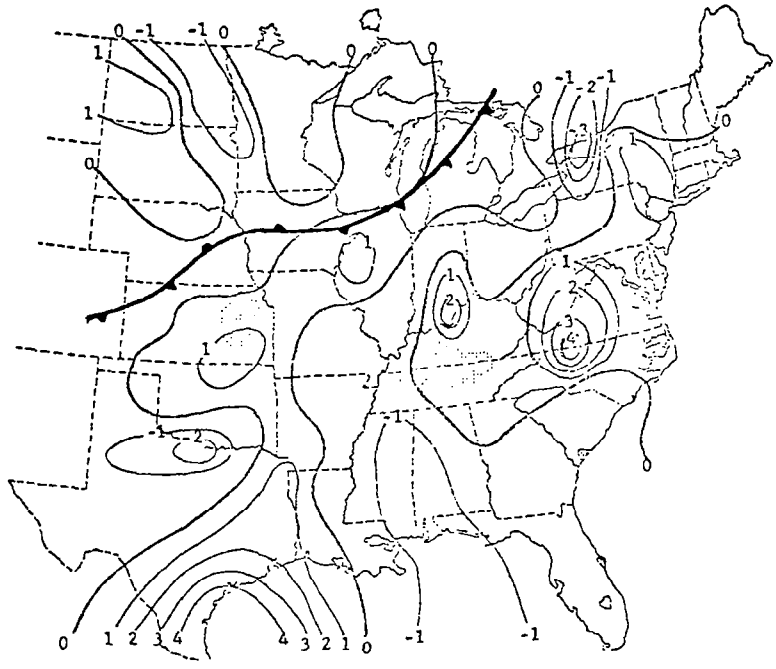

(b) 1800 GMT

Fig. 15. Analysis of the vertical advection of convective stability (10^{-7}°C mb^{-1} s^{-1}) for the layer 700–500 mb (700-mb front and thunderstorm areas shown for reference).

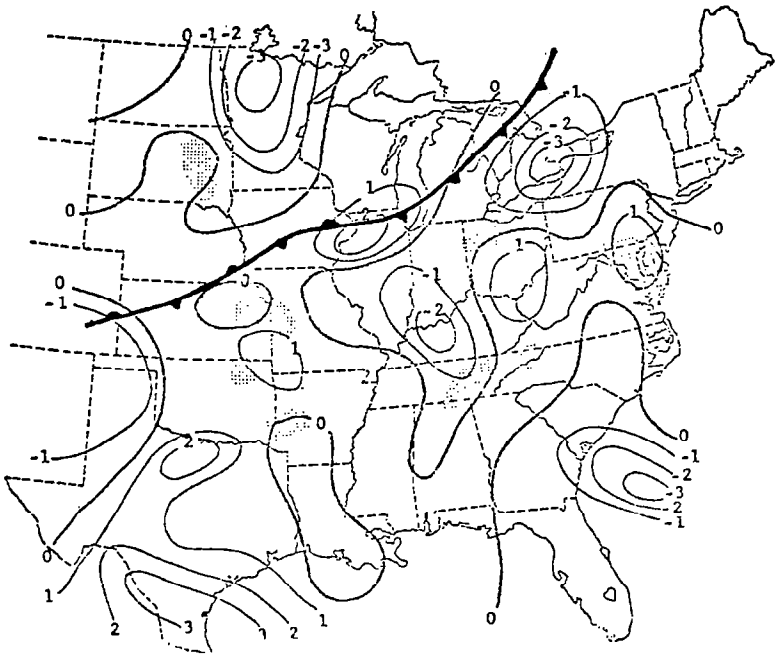

(c) 2100 GMT

Fig. 15. (Continued)

strong positive development at 1800 GMT. Positive contributions to stability development by vertical motion ahead of the front are seen in Fig. 15. Positive stability development resulted in northern Illinois and southern Kansas indicating that the stability decreases with height in these regions. There were also significant changes in stability development by the vertical advection term away from the front.

The average vertical profiles for the residual term in the stability development equation, shown in Fig. 16, indicate a systematic imbalance in the mean values of the terms in the stability change equation, especially in the lower layers. In the boundary layer, nonconvective areas show large negative stability development by the residual. This was due to a large negative local tendency not reflected in any of the individual terms describing the large-scale processes or their sum. With increasing MDR value, the magnitude of the negative stability development decreased until positive stability development by the residual term was observed for areas

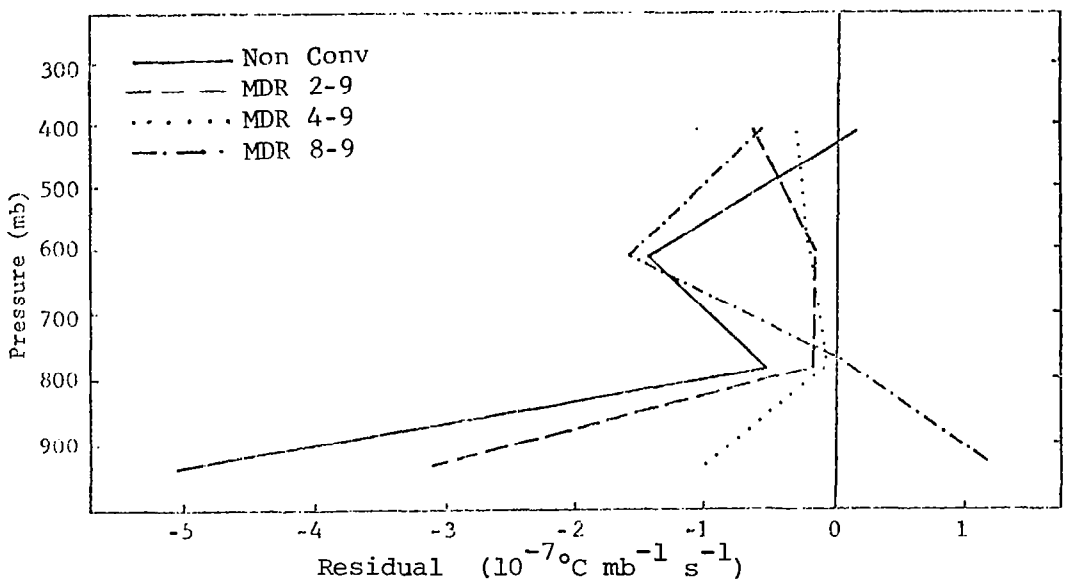

Fig. 16. Average vertical profiles for the residual term.

containing severe thunderstorms (MDR≥8). This positive residual corresponds to the effect of thunderstorms, mentioned earlier, in increasing the stability in the boundary layer. Stability development due to the residual was generally small in the 850-700 mb layer, but the signs and magnitudes of the different categories of convection showed the same trend as observed in the surface-850 mb layer.

At the upper levels, the vertical profiles indicate that non-convective areas were likely to have the same magnitude of negative residual as were areas containing severe storms.

Wilson (1977) used a 3-dimensional subsynoptic-scale trajectory model to determine relationships between convective storms and their environment in AVE IV including the diabatic effects within the mean flow such as condensation, evaporation, radiation, and the turbulent eddy flux of heat. Average profiles of the diabatic effects related to MDR values were plotted. Areas of precipitation were found to exhibit, on the average, diabatic warming from 800 mb to 250 mb with cooling above 250 mb and below 800 mb. The more intense precipitation areas showed larger diabatic values especially above 500 mb with larger vertical differences in diabatic effects for all

precipitation cases. These vertical differences would result in changes of the stability since they provide subgrid-scale sources and sinks of heat and moisture. These small-scale processes would cause deviations from the mean value of the equivalent potential temperature, signified by the primed quantities in the derivation of the stability development equation. The low level cooling was attributed to the evaporation of precipitation and surface radiation effects, and the cooling in the upper layers to radiative cooling from thunderstorm cirrus shields. The warming in the middle troposphere was thought to be due to turbulent interaction and thunderstorm condensation. This mid-level warming could also be due to compensating subsidence in the distant environment of the clouds. Low-level cooling topped by mid-level warming would result in the positive stability development in the boundary and 850-700 mb layers seen in the average vertical profile of the residual for areas containing severe thunderstorms. However, the increasing diabatic warming to a maximum at the 400 mb level in areas of severe thunderstorms contradicts the instability development found in the middle and upper tropospheric layers in the residual term.

In a study of the interaction between squall lines and their environment in a mesoscale network, Lewis (1975) found similar profiles of combined latent and sensible heat transport by small-scale motions to those of Wilson except evaporative cooling thought to be due to detrainment resulted in an area of net cooling near 600 mb. This cooling above the net heating at 700 mb would produce the average destabilization found in the 700-500 mb layer in the vertical profiles of the residual term.

Figures 17 and 18 show analyzed fields of the residual term for 1500 GMT, 1800 GMT, and 2100 GMT in the surface-850 mb layer, and the 700-500 mb layer, respectively. As noted earlier in the discussion of the average magnitudes of the terms in the stability change equation, most of the stability development is due to the residual. This can be seen in the boundary layer by comparing Fig. 17 with Fig. 8. At 1500 GMT and 1800 GMT, while the severe thunderstorms were still developing, convection showed no distinct tendency to

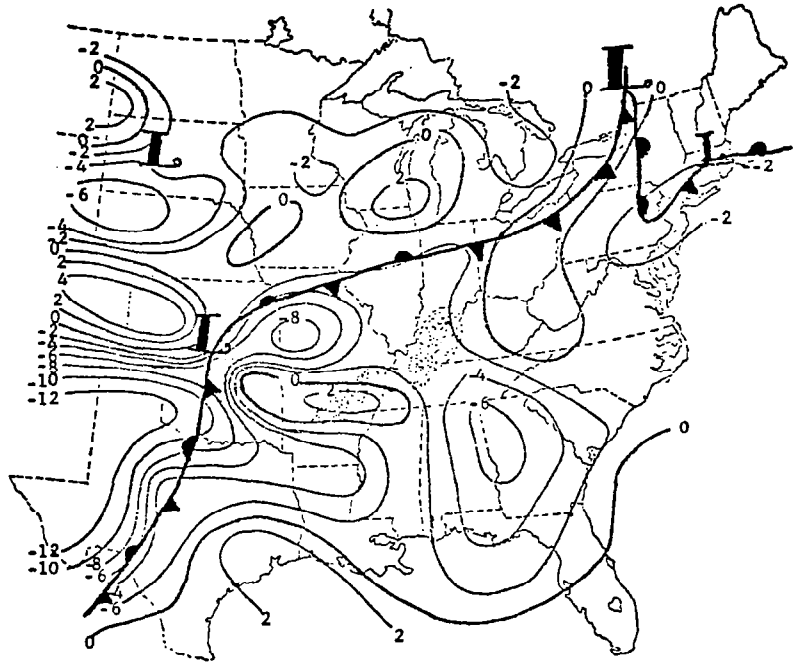

(a) 1500 GMT

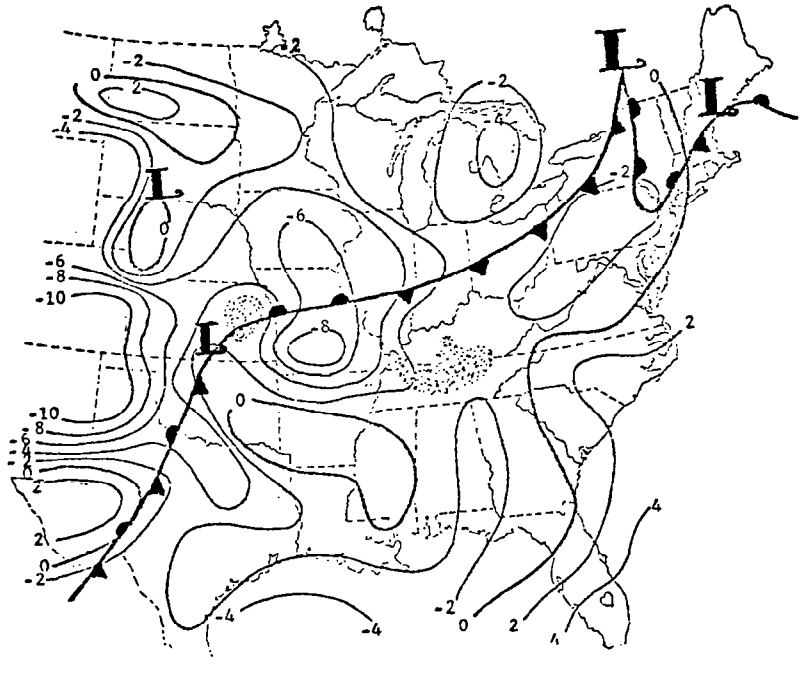

(b) 1800 GMT

Fig. 17. Analysis of the residual (10^{-7}°C mb^{-1} s^{-1}) for the layer from the surface-850 mb (surface front and thunderstorm areas shown for reference).

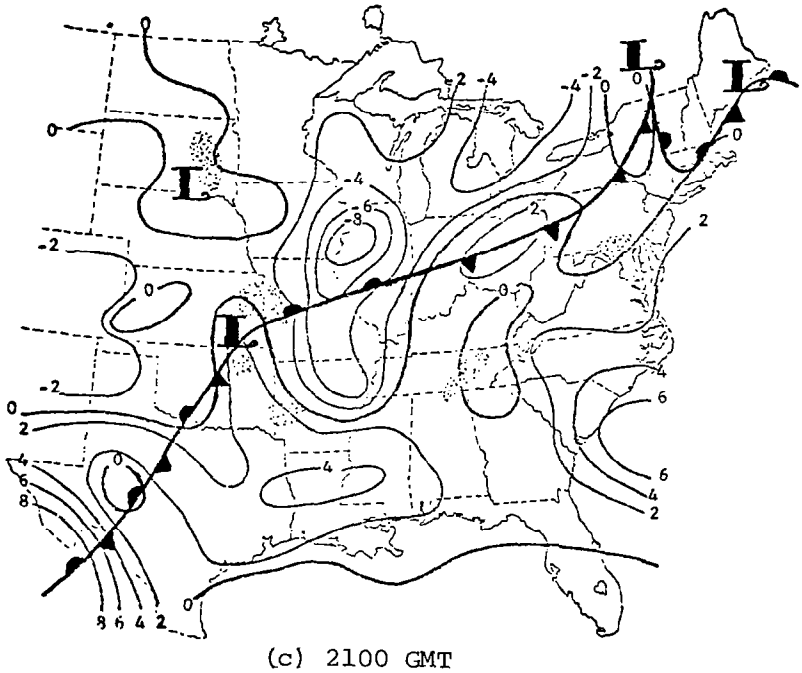

(c) 2100 GMT

Fig. 17. (Continued)

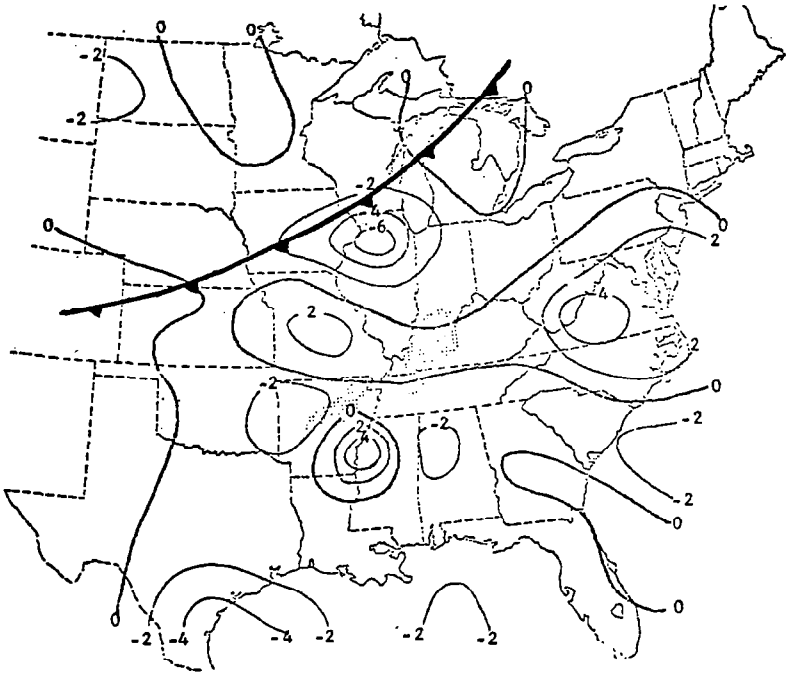

(a) 1500 GMT

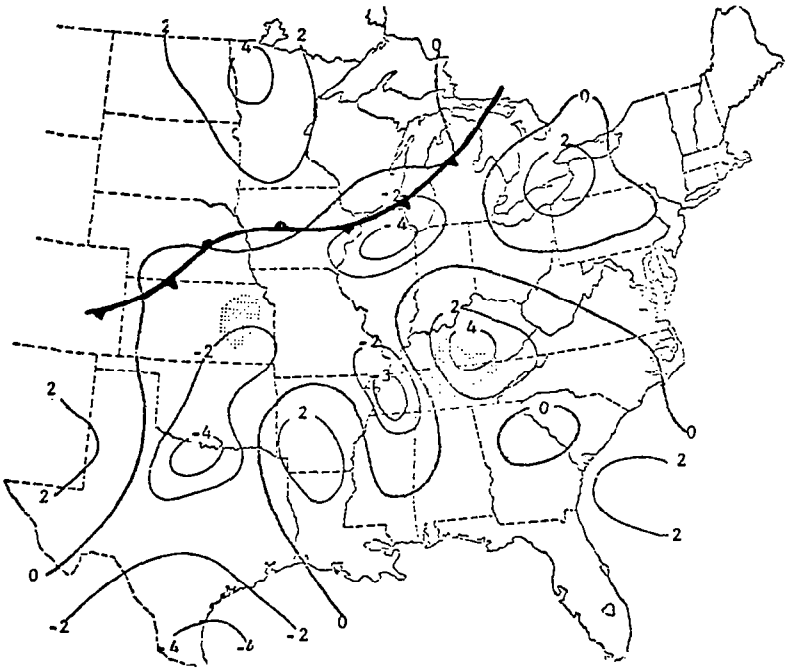

(b) 1800 GMT

Fig. 18. Analysis of the residual (10^{-7}°C mb^{-1} s^{-1}) for the layer from 700-500 mb (700-mb front and thunderstorm areas shown for reference).

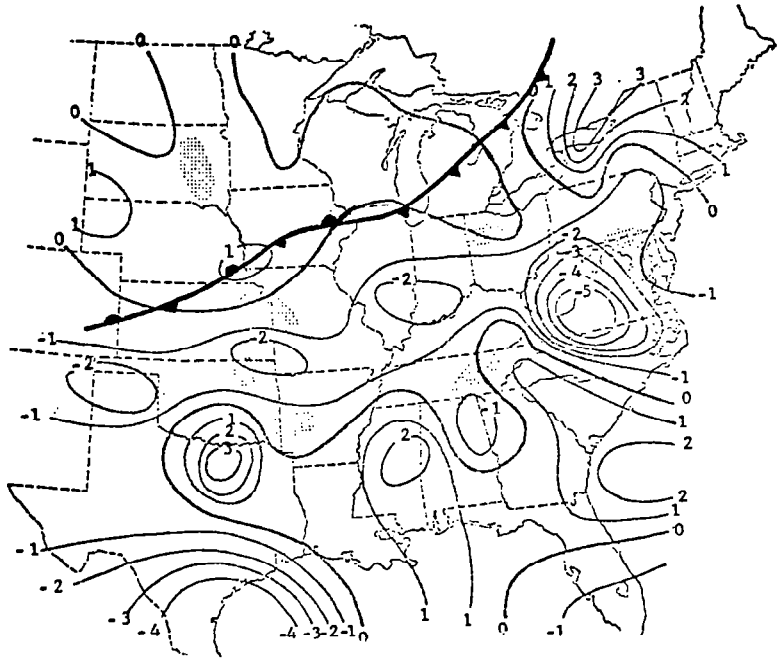

(c) 2100 GMT

Fig. 18. (Continued)

lie in areas of positive or negative development indicated by the residual in either the surface-850 mb layer or the 700-500 mb layer. But at 2100 GMT as the second squall line formed, most severe convection occurred in regions with a positive residual effect in the surface-850 mb layer, and negative development in the 700-500 mb layer as implied by the average vertical profiles.

Much of the imbalance represented in the residual term in layers other than the boundary layer was due to centers of strong vertical advection of convective instability. These centers were not reflected in equally strong local tendencies of convective instability or balanced by the other processes causing stability changes. This can be seen for the 700-500 mb layer by a comparison of Fig. 18 with Fig. 15 which show fields of vertical advection and the residual to be similar in pattern but opposite in sign. For example, at 1500 GMT the centers of positive stability development by vertical advection in northern Arkansas and off the coast of South Carolina correlate well with negative centers of stability change due to the residual term, while the areas of negative stability development due to vertical advection in southern Arkansas and in the Virginia-Kentucky region are areas of positive stability residuals. Centers of stability change due to the residual also sometimes overlay centers of differential advection. There was no consistent relationship between the front and the sign or centers of the residual term. There also were significant changes in the magnitude and sign of the residual away from the front.

Table 5 summarizes the results of the stability change equation related to observed MDR values. The budgets presented in this table do not balance because different amounts of data were used to evaluate the terms. This procedure was followed to take advantage of all available data. The processes described in the first four terms exhibit an excess source of positive stability development causing the residual representing subgrid-scale processes to be usually negative. This is especially true in the boundary layer with moderate or no convection.

Table 5. Averages for terms in the stability development equation related to values of MDR (10^{-7}°C $mb^{-1}s^{-1}$).

MDR Category	Layer	$\frac{\partial \sigma_e}{\partial t}$ [1]	$\frac{\partial}{\partial p}(\vec{V}\cdot\vec{\nabla}\theta_e)$ [2]	$\sigma_e \text{div}\ \vec{V}$ [2]	$-\omega \frac{\partial \sigma_e}{\partial p}$ [2]	Residual [1]
MDR ≤ 1 (No Conv.)	Surface-850 mb	-4.0	-1.4	0.8	0.8	-5.0
	850-700 mb	-2.0	1.5	0.7	-1.8	-0.5
	700-500 mb	-0.2	-0.7	0.7	0.9	-1.4
	500-300 mb	-0.5	-0.2	-0.2	-0.2	0.1
MDR ≥ 2 (All Conv.)	Surface-850 mb	-2.6	2.5	0.1	2.1	-3.1
	850-700 mb	-1.5	-4.0	0.6	4.3	-0.2
	700-500 mb	0.1	-0.1	-0.7	-3.9	-0.1
	500-300 mb	-0.3	1.2	0.9	0.4	-0.6
MDR ≥ 4 (Thunderstorms)	Surface-850 mb	0.5	3.9	1.1	3.6	-1.0
	850-700 mb	-1.8	-7.3	2.2	12.0	-0.1
	700-500 mb	-0.4	1.0	-0.7	-7.1	-0.2
	500-300 mb	-0.2	0.7	1.4	0.2	-0.3
MDR ≥ 8 (Severe Thunderstorms)	Surface-850 mb	2.2	4.4	2.1	3.6	1.2
	850-700 mb	-1.6	-6.9	5.2	27.0	0.2
	700-500 mb	-0.2	3.1	-1.0	-17.0	-1.6
	500-300 mb	-0.1	-2.5	3.0	-1.3	-0.6

1 - Computed over three 6-h time intervals
2 - Computed for nine times

The unique 3- and 6-h data of AVE IV also allow one to study conditions prior to the occurrence of convection. Figure 19 shows the average vertical profiles for the local rate-of-change of convective instability computed over a 6-h period by centered finite differencing

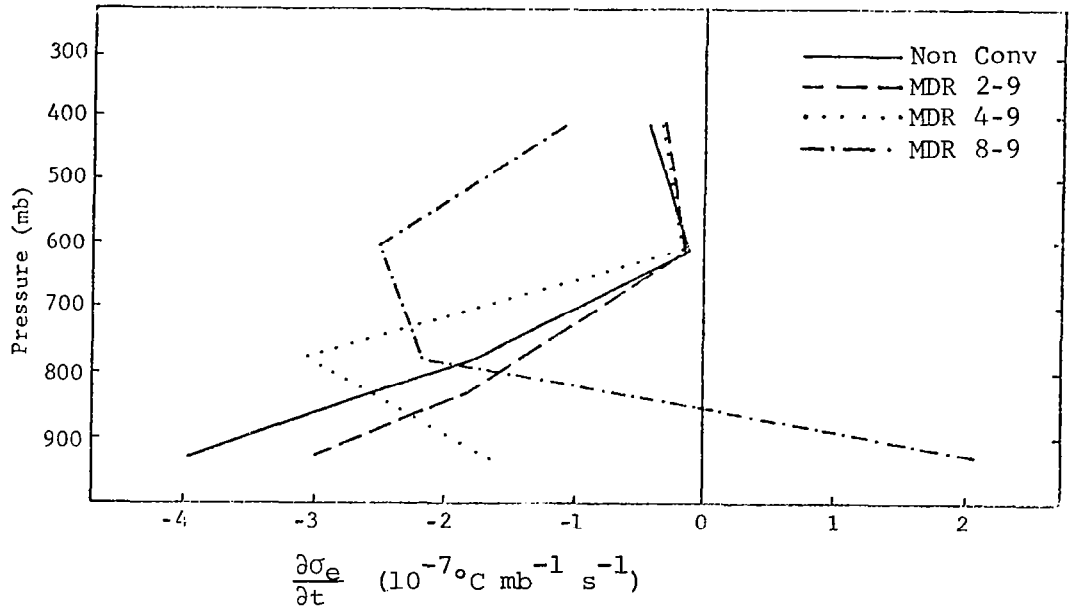

Fig. 19. Average vertical profiles for the local tendency of convective stability with MDR data lagged 3 h.

and related to the MDR values at the end of the time interval (3-h lag in MDR values). Profiles of areas containing no convection (MDR≤1) or including all convection (MDR≥2) are almost identical to the profiles in Fig. 7 without a 3-h lag in the MDR data. Average profiles of areas containing thunderstorms (MDR≥4) are similar to profiles without the lag in the upper layers, but have more instability development in the lower layers 3 h prior to the thunderstorms than after their development. This again supports the observation that thunderstorms interact with the environment in such a way so as to increase the boundary layer stability. Areas of severe thunderstorms (MDR≥8), however, still showed positive stability development in the

lowest layer, even with a 3-h lag in the MDR data. This is probably because the thunderstorms were present 3 h prior to their reaching the severe state, and their influence on boundary layer stability still overshadowed any existence of instability prior to development. Areas of severe thunderstorms were observed to have much more instability development in the middle and upper levels 3 h prior to their reaching the severe state than at the time they were classified severe. This supports the hypothesis that instability in the 700-500 mb layer is important in the maintenance and intensification of thunderstorms.

Figure 20 shows the average profiles of differential advection of equivalent potential temperature with a 3-h lag in the MDR data. The profiles are very similar to those without lag in the MDR data with the differential advection term not distinguishing in the upper levels between nonconvective or convective areas either prior to or after thunderstorm development. Positive stability development in the boundary layer and negative development in the 850-700 mb layer exist 3 h prior to as well as at the time of development.

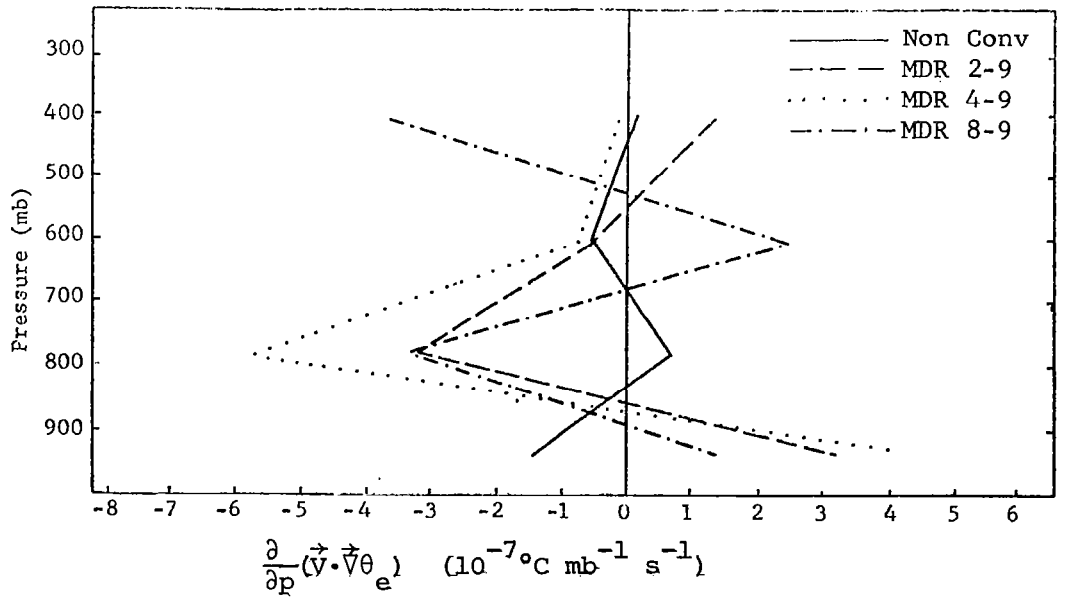

Fig. 20. Average vertical profiles for the differential advection of equivalent potential temperature with MDR data lagged 3 h.

Averages of the divergence term with a 3-h lag in MDR data, shown in Fig. 21, reveal significant differences in the boundary layer processes 3 h prior to the occurrence of severe thunderstorms. The divergence term exhibits greater positive stability development in areas containing thunderstorms 3 h prior to their development than at the time of their development. As described earlier, this positive development represents a decrease in the instability already present in the layer, and occurs in the boundary layer through the influence of the divergence term at least 3 h prior to the classification of the storms as strong or severe. Areas of no convection or in which all the storms did not become severe, showed little difference in their profiles from those without the 3-h lag in MDR data. The instability development present in the 700-500 mb layer for the profiles without lag was not present 3 h prior to the convective activity.

Average vertical profiles of the vertical advection of convective instability with 3-h lag in MDR data are shown in Fig. 22. The values are smaller 3 h prior to the development of the storms but the relation-

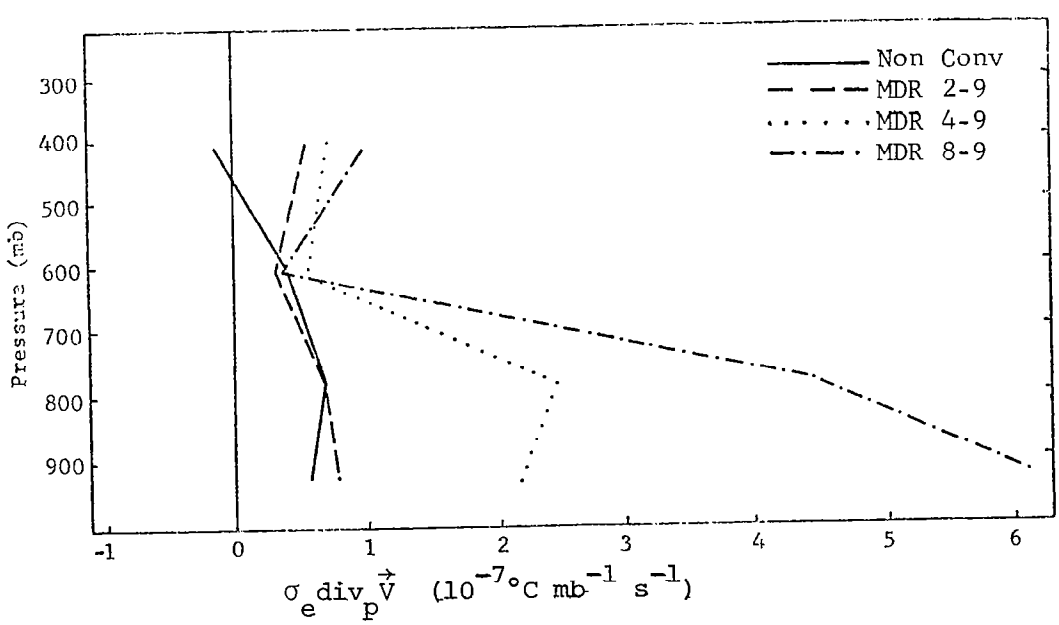

Fig. 21. Average vertical profiles for the divergence term with MDR data lagged 3 h.

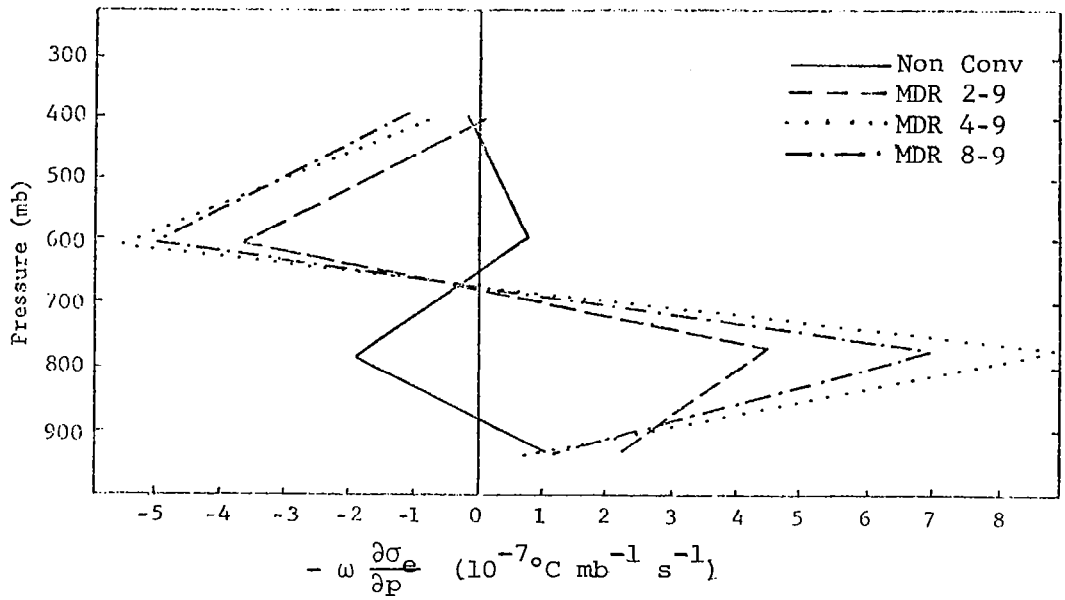

Fig. 22. Average vertical profiles for the vertical advection of convective stability with MDR data lagged 3 h.

ships between categories of convective activity are almost exactly the same. The development of stability in the lower layers and instability in the higher layers by the vertical advection term is greater at the time of the observed convective activity than 3 h prior to it.

The average vertical profiles of the residual term with 3-h lag in MDR data are shown in Fig. 23. A comparison with the residual profiles without a lag in the MDR data shows the two to be very similar except for thunderstorm profiles below about 850 mb. Prior to the storms, the residual term for all categories of convection showed negative stability development in the lower layer. A large negative local tendency in the nonconvective areas was not reflected in any of the individual terms or their sum, and the positive local tendency in areas containing severe storms was overcalculated by the terms in the stability change equation, especially the divergence term. Both resulted in a negative residual term. However, at the time of the severe thunderstorms, the residual term switched to positive stability development in the boundary layer on the average.

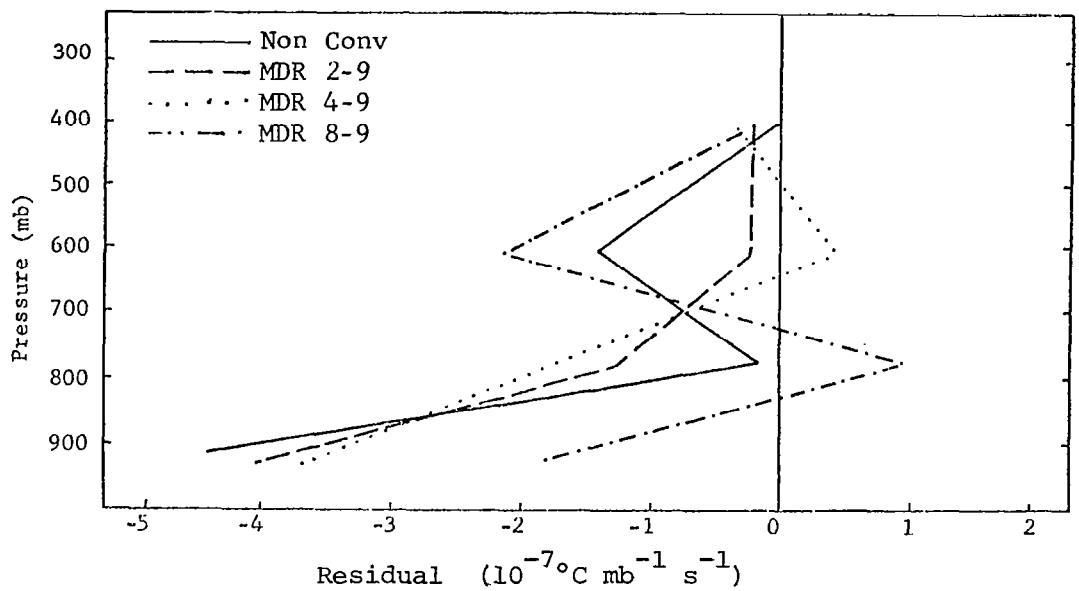

Fig. 23. Average vertical profiles for the residual with MDR data lagged 3 h.

c. Relative influence of moisture and temperature change

Equivalent potential temperature is defined by

$$\theta_e = \theta \exp\left(\frac{Lq}{c_p T_c}\right) \tag{7}$$

where θ is the potential temperature, L is the latent heat of evaporation, c_p is the specific heat at constant pressure, q is the mixing ratio, and T_c is the temperature of the level at which condensation would occur. Taking the derivative of (7) with respect to time gives

$$\frac{\partial \theta_e}{\partial t} = \exp\left(\frac{Lq}{c_p T_c}\right) \frac{\partial \theta}{\partial t} + \frac{L\theta_e}{c_p T_c} \frac{\partial q}{\partial t} - \frac{L\theta_e q}{c_p T_c^2} \frac{\partial T_c}{\partial t} . \tag{8}$$

The last term on the right-hand side is several orders of magnitude smaller than the other two terms and can be neglected giving

$$\frac{\partial \theta_e}{\partial t} = \exp\left(\frac{Lq}{c_p T_c}\right) \frac{\partial \theta}{\partial t} + \frac{L\theta_e}{c_p T_c} \frac{\partial q}{\partial t} \tag{9}$$

which describes the local rate-of-change of equivalent potential temperature at a given level as a function of the local rate-of-change of potential temperature and moisture. The local rate-of-change of temperature in (9) can be substituted for by

$$\frac{\partial \theta}{\partial t} = -\vec{V} \cdot \vec{\nabla}\theta - \omega \frac{\partial \theta}{\partial p} + R_\theta \tag{10}$$

where the terms on the right-hand side are the horizontal advection of potential temperature, the vertical advection of potential temperature and a residual term, respectively. Similarly, the local rate-of-change of mixing ratio can be replaced by

$$\frac{\partial q}{\partial t} = -\vec{V} \cdot \vec{\nabla} q - \omega \frac{\partial q}{\partial p} + S \tag{11}$$

where S represents sources or sinks of moisture and eddy processes.

By making these substitutions and determining the difference between the value of each term at the top of the layer from its value at the bottom of the layer, it is possible to determine the relative effect of the various temperature and moisture processes in the development of convective instability.

Table 6 gives the average absolute magnitudes at 1500 GMT on 24 April 1975 of the total stability development and residual, the stability development due to differential moisture change and its component processes, and the stability development due to differential temperature change and its component processes for various layers of 100-mb thickness. Most of the stability development results from the processes causing differential moisture change in each layer, while stability development due to differential temperature change has an average value a factor of two smaller than that of total stability development and development due to differential moisture change. The moisture terms are dominant in all of the processes causing stability change. The difference between potential temperature residuals and sources and sinks of moisture at the top and bottom of each layer were the dominant terms for their respective processes, while differential horizontal and vertical advective terms were smaller and about equal in magnitude. Most terms show a general decrease in magnitude with height.

Not only did the moisture-related processes show dominance in their average magnitudes over temperature-related processes, but they also showed a greater correlation with the actual stability change fields. Figure 24 shows the development of convective instability in the 800-700 mb layer at 1500 GMT, and the development of instability in that layer due to the difference between moisture changes and the difference between temperature changes at the top and bottom of the layer. The actual stability development fields and the development due to the difference between moisture changes at the top and bottom of the layer are similar. Development due to the difference between temperature changes at the top and bottom of the layer, however, cannot be neglected. It is usually of opposite sign to that of the moisture field.

The residual term of stability development is predominately due to the difference between sources and sinks of moisture at the top and bottom of the layer as seen in Fig. 25. However, the effect of differential residuals of potential temperature again cannot be neglected, but modify the general patterns of stability change set by

Table 6. Average magnitudes of differential moisture and temperature changes causing a change in the stability at 1500 GMT on 24 April 1975 (10^{-7}°C $mb^{-1}s^{-1}$).

Quantity	Layers			
	800-700 mb	700-600 mb	600-500 mb	500-400 mb
Total Stability Development	15.0	14.0	9.6	7.1
Total Stability Residual	30.0	26.0	28.0	21.0
Development due to:				
Differential Moisture Change	17.0	14.0	9.2	7.6
Differential Horizontal Moisture Advection	15.0	7.4	6.9	7.1
Differential Vertical Moisture Advection	12.0	11.0	9.5	6.6
Differential Moisture Residuals	19.0	22.0	18.0	14.0
Development due to:				
Differential Temperature Change	5.8	4.9	5.1	5.9
Differential Horizontal Temperature Advection	4.2	5.4	4.5	6.3
Differential Vertical Temperature Advection	6.0	5.6	6.3	5.8
Differential Temperature Residuals	9.9	7.9	8.7	9.1

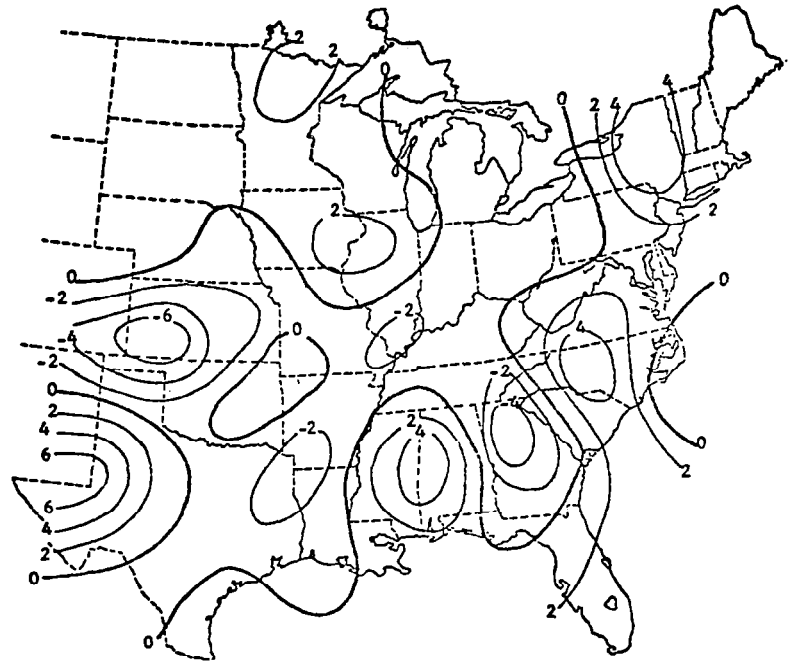

(a) Total stability change

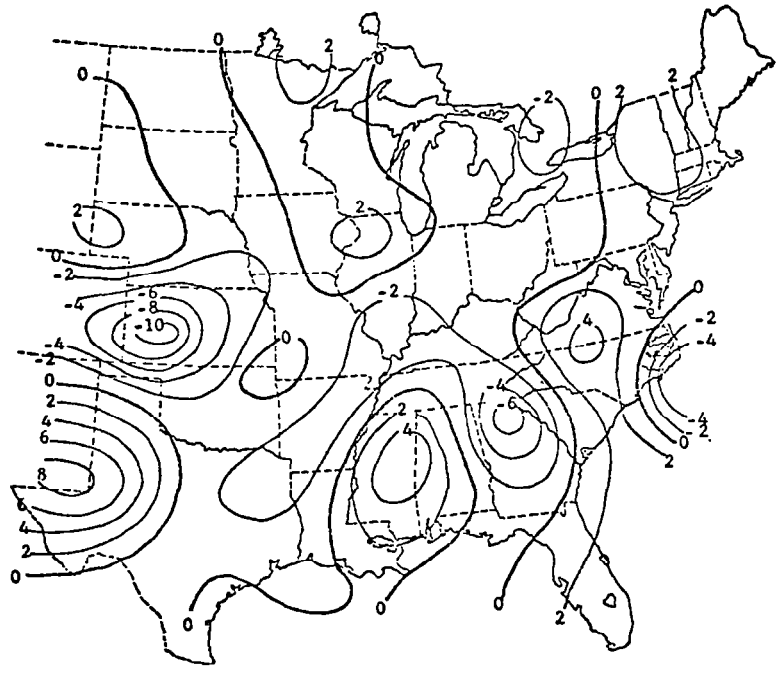

(b) Stability change due to differential moisture change

Fig. 24. Analysis of stability change due to differential moisture and temperature change in the layer from 800-700 mb at 1500 GMT on 24 April 1975 (10^{-7}°C mb^{-1} s^{-1}).

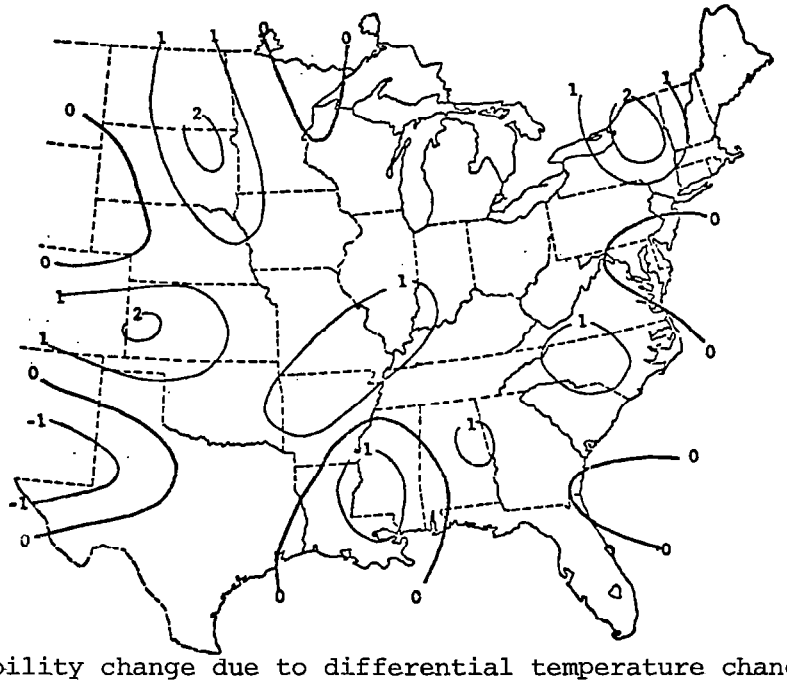

(c) Stability change due to differential temperature change

Fig. 24. (Continued)

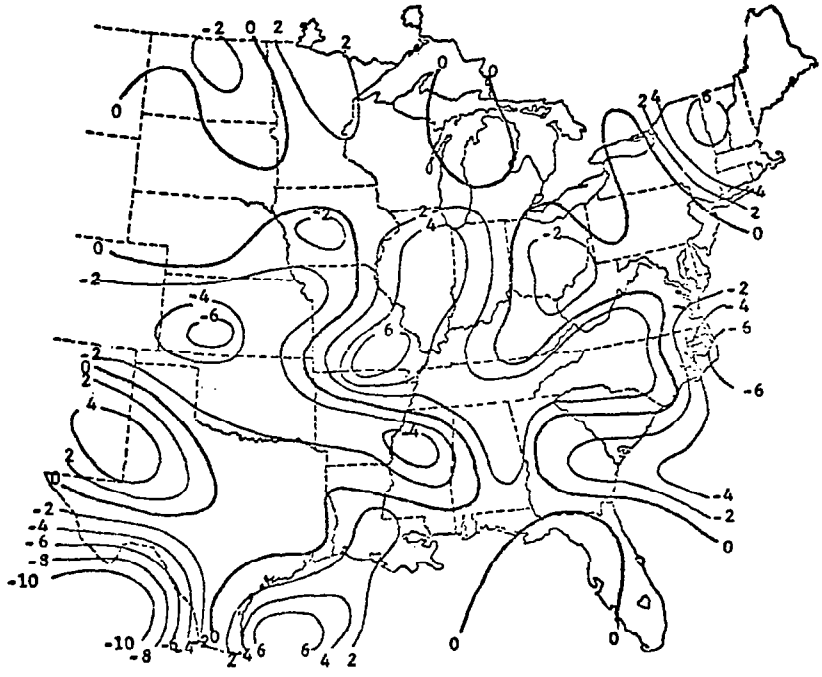

(a) Total stability residual

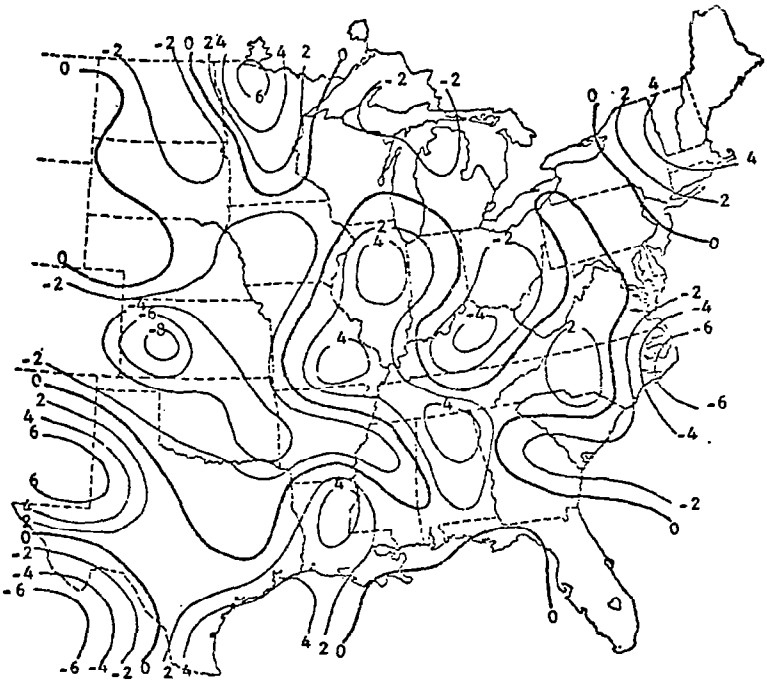

(b) Stability change due to differential moisture residuals

Fig. 25. Analysis of stability change due to differential moisture and temperature residuals in the layer from 800-700 mb at 1500 GMT on 24 April 1975 (10^{-7}°C mb^{-1} s^{-1}).

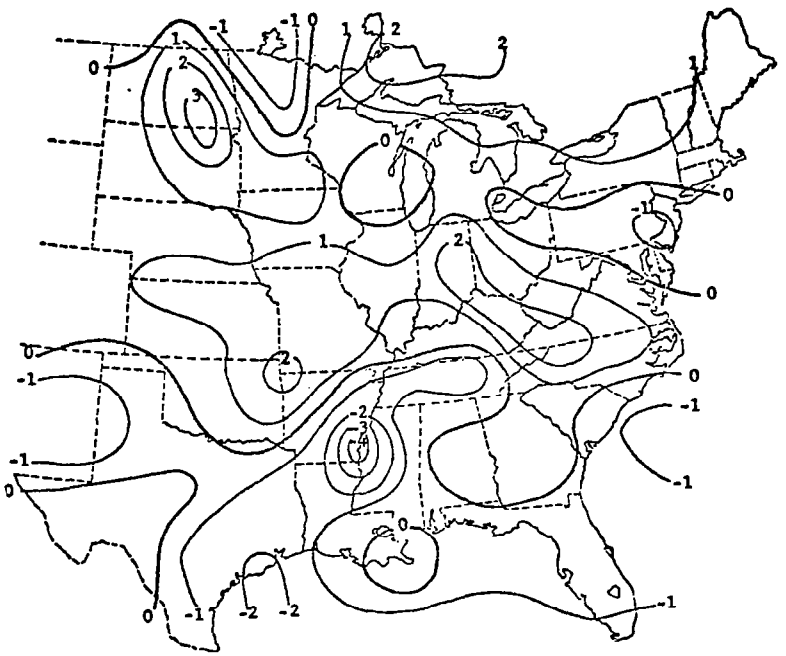

(c) Stability change due to differential temperature residuals

Fig. 25. (Continued)

the moisture term. The development due to the difference between moisture and temperature residuals at the top and bottom of the layer are again of opposite sign. This would be expected since a sink of moisture is usually associated with a source of heat and vice versa.

d. Satellite capabilities

In order to determine the ability of satellites to measure stability development and the processes effecting its change, an error analysis was made of the terms in (6) using RMS errors of routine Nimbus 6 satellite data and the propagation of error method described earlier. Moyer et al. (1978) found that satellites could determine the stability fairly well in regions of marked stability but less dependably in unstable areas. The purpose of this part of the study was to determine how well satellites could indicate changes in the stability with time.

The results are summarized in Table 7 and compared to average magnitudes and extreme values of the terms for various layers. For the local rate-of-change and differential horizontal advection terms, the satellite error was usually as large or larger than the average magnitudes of these terms but smaller than the extreme values. While satellites could not determine the general pattern of the fields of these two terms, it could indicate the centers of strongest change. However, for the divergence and vertical advection terms the satellite RMS errors were not only usually larger than the average magnitudes of these terms, but also larger than the extreme values. Satellite data could not be used to depict these terms. The only exception was the 850-700 mb layer where the satellite RMS error of the vertical advection of stability was smaller in value than the extreme values of this term found in that layer. The errors were predominantly a result of the large errors in divergence determined from satellite-derived geostrophic winds. Summation of the divergence is also used to calculate values for vertical motion making it very sensitive to wind errors.

Table 7. Estimated RMS errors for terms in the stability development equation evaluated from satellite data (10^{-7}°C mb^{-1}s^{-1}).

Quantity	850 - 700 mb			700 - 500 mb			500 - 300 mb		
	Avg. Abs. Magnitude	Extreme Value	RMS Error	Avg. Abs. Magnitude	Extreme Value	RMS Error	Avg. Abs. Magnitude	Extreme Value	RMS Error
$\frac{\partial \sigma_e}{\partial t}$	13.0	48.0	11.8	7.1	23.0	8.5	5.0	16.0	8.5
$\frac{\partial}{\partial p}(\vec{v}\cdot\vec{\nabla}\theta_e)$	9.5	40.0	12.5	6.1	29.0	10.0	4.8	18.0	13.0
$\sigma_e \mathrm{div}_p \vec{v}$	3.1	16.0	14.2	2.5	9.8	12.5	3.7	18.0	15.2
$\omega \frac{\partial \sigma_e}{\partial p}$	13.0	89.0	24.1	7.1	32.0	25.4	4.1	22.0	39.0

7. SUMMARY AND CONCLUSIONS

The development of convective instability has been studied using the 3- and 6-h AVE IV rawinsonde data and a derived stability development equation. Analyzed fields of the terms in the equation and average vertical profiles related to categories of radar-observed convection were studied to establish relationships between the terms in the stability change equation, the actual observed stability change, and convective systems. Processes causing a change in the moisture distribution with height were compared to those changing the temperature profile to determine their relative importance in stability development. Finally, the ability of satellites to measure typical changes in the stability and the terms in the stability development equation was evaluated.

The following conclusions were reached on the the basis of the results presented above:

1. Of the terms in the stability development equation, the residual, representing subsynoptic-scale processes, had the largest average magnitude. The term describing the effect of divergence on an isobaric surface usually had the smallest value although it could not be neglected, especially in the boundary layer and the layer from 500-300 mb. Most terms had their largest average magnitude in the surface-850 mb layer and decreased with height except the vertical advection term which had its maximum in the layer from 850-700 mb.

2. All terms were found to have temporal continuity. The term describing vertical advection of convective stability was the most variable in time due to the greater variability of the vertical motion field. A decrease in the thickness of the layer over which the computations were made increased the calculated variability of the terms.

3. The average vertical profiles of the terms describing the vertical advection of convective stability and divergence on an isobaric surface revealed processes whereby the stability would be increased in the boundary layer in the region of thunderstorms, as was observed to occur in other studies. These processes also were shown to

have in areas of thunderstorms a net destabilizing effect in the layer from 700-500 mb which is important to the maintenance and intensification of convective systems.

4. The largest centers of instability development were ahead of the front in the moist Gulf air flowing over the eastern half of the United States. However, centers of positive and negative stability change were on either side of the front with all terms in the stability development equation showing significant changes in their magnitude and sign away from the front. Centers of the term describing the differential advection of θ_e showed a general eastward progression within the synoptic flow.

5. Most stability development resulted from processes that cause differential moisture change with height. Among these processes, stability change due to differential sources and sinks of moisture at the top and bottom of each layer was predominate. Although stability development due to changes in the temperature profile was half of that due to differential moisture change, it could not be neglected.

6. Satellites could measure with reasonable accuracy the extreme values of stability change and the differential advection of equivalent potential temperature. Due to errors mainly in satellite-derived geostrophic winds, satellites could not determine fields of the vertical advection of convective instability or divergence on an isobaric surface.

PART II: WIND SHEAR

1. INTRODUCTION

a. Statement of problem

The structure of the wind field, its variability, and the effect on other meteorological phenomena has received much study throughout the years. Vertical wind shear is of great interest in meteorology and other disciplines that are affected by the weather. Wind shear is important in generating turbulence and in energy production. Fulks (1951) stated that the significance of vertical wind shear is that kinetic energy drawn from the wind field may provide an important energy source in addition to those usually considered. This energy may also set off or increase the intensity of convection.

The effect of wind shear on the occurrence and development of thunderstorms also is of great importance. Unfortunately, the results of studies in this area often seem contradictory. Fulks (1951) stated that organized convection systems such as squall lines are generally associated with strong winds aloft. As a result of experiments conducted in southern France, Dessens (1960) claimed that strong wind at upper levels was the important factor which determined whether or not a thunderstorm would become a destructive hailstorm. While he did not state the necessity of strong wind shear explicitly, its presence was implied by the suggested wind structure favorable for severe storm development. Das (1962) investigated the influence of wind shear on the growth of hail in a model cloud and found a higher probability of hail in thunderstorms with strong vertical shear than those without. More recently, Erbes and Grant (1976) studied the kinematic structure of some Colorado thunderstorms and found that the longest lived multicell systems required an environment of moderately strong low- and upper-level winds.

On the other side, Byers and Battan (1949) stated that when strong wind shear exists, no thunderstorms can develop since the shear restricts the maximum height reached by the storms. They cited the tendency for the tops of cloud columns to be blown away from their bases in the presence of strong wind shear. Ratner (1961), by climatological analysis, showed that in the U. S. neither the speed of winds aloft nor

wind shear between 500 and 200 mb appeared to be the determining factor in the development of severe thunderstorms with hail. In a study by Endlich and Mancuso (1968), high wind speeds by themselves in the low or upper troposphere got poor ratings as objective indicators of severe storm activity. These conditions are generally present in severe storm areas but also cover extensive regions without severe storms. However, wind shear did get a good rating indirectly because it contributes to destabilization through differential temperature advection which related to severe storm development. Negative values of vorticity between the low and middle troposphere also was found to be a good indicator of severe storm activity. Recently, Lebedev (1976) used a numerical model of convection systems to show that the intensity of precipitation decreased as the vertical wind shear increased.

Newton and Newton (1959) attempted to explain these contradictions by making a distinction between the effect of strong wind shear on small and large convective systems. They stated that the hydrodynamic pressure field induced by relative motions near the boundaries of large convective systems resulted in vertical gradients of pressure which aid in the formation of new convection on the downshear side of large systems. While wind shear might stop the development of small clouds, they claimed the tendency for tops of cloud columns to be blown away from their bases was less pronounced in large systems.

A common approach used in the study of the wind is to make an approximation to the real wind and study its variability. Carlson (1973), following this approach, found that gradient wind changes were poor estimates of observed wind changes over 3- and 6-h time periods but improved over a 12-h period. He found that over 3- and 6-h time periods the correlation coefficients between local changes in the observed and gradient wind speeds were not statistically different from zero, but the correlation was significant over a 12-h interval. Scoggins and Phelps (1973) related changes in the measured wind at selected constant pressure surfaces to changes in the thermal wind within a layer below the constant pressure surface. They found that if the thickness fields (average temperature) in a layer are assumed to be quasi-conservative and the changes in the wind at the bottom of

the layer are relatively small, the variability of the wind over a period of 12 h and less at the top of a relatively thick layer was related to, and may be determined from, the variability of the thermal wind within the layer.

The present study considers changes in the wind at two levels and the resulting development of wind shear in the layer between these levels. The actual change in vertical wind shear is broken down into its geostrophic and ageostrophic components to help understand the factors which produce the changes and the relative contributions of each factor. Palmen and Newton (1969) reported vertical shears that may differ by a factor of 3 to 4 from the thermal wind were sometimes observed. Observed shears differing considerably from the thermal wind implies the existence of large deviations of the real wind from the geostrophic wind at the top, bottom, or throughout the layer. If accelerations vary appreciably in the vertical, then it is necessary to consider the shear of the acceleration also.

b. Objectives

The objectives of this study are to describe the development of wind shear in various layers as measured by rawinsonde data taken at 3- and 6-h intervals.

Specific objectives include:

1) Determine the relative importance of geostrophic and ageostrophic processes to the development of wind shear for 3-, 6- and 12-h time intervals.

2) Investigate the relationship between changes in vertical wind shear and radar-observed convective activity.

2. ANALYTICAL METHODS

a. Wind shear development equation

Above the friction level it is often assumed that the wind is geostrophic. Wind shear in this report is broken down into its geostrophic and ageostrophic components. Although the gradient wind is a better approximation to the real wind than the geostrophic wind, difficulty in accurately computing trajectory curvature, and especially its time rate-of-change, prohibited the investigation of the development of gradient wind shear. Carlson (1973) found that the curvature term was responsible for disagreement in the signs of the changes in the gradient and observed wind speeds 70% of the time in his study. Although the breakdown of the real wind into its geostrophic and ageostrophic components is evident, we will begin with the complete equation of motion in order to show the various parts of the geostrophic and ageostrophic motions.

Vectorially, the equation of motion on a constant pressure surface is given by

$$\frac{\partial \vec{V}}{\partial t} = - g\vec{\nabla}z - f(\vec{k}\cdot\vec{V}) - \vec{F}r \qquad (1)$$

where $\vec{V}$ is the vector wind, g is gravity, z is geopotential height of the pressure surface, f is the coriolis parameter, and $\vec{F}r$ is the friction force vector.

Taking the cross product with $\vec{k}$, dividing by f, and rearranging gives

$$\vec{V} = \frac{g}{f}\vec{k}\cdot\vec{\nabla}z + \frac{1}{f}\vec{k}\cdot\left(\frac{\partial \vec{V}}{\partial t}\right) + \frac{1}{f}\vec{k}\cdot\vec{F}r. \qquad (2)$$

The first term on the right-hand-side of the equation is defined as the geostrophic wind, $\vec{V}_g$, and is proportional to the gradient of geopotential height at a given location. The second term on the

right-hand-side is the acceleration. When expanded in a natural coordinate system, the acceleration contains a tangential component and a normal, or centripetal, component. The effects of the tangential acceleration, centripetal acceleration, and friction will be combined into the ageostrophic wind, $\vec{V}_{ag}$, so that (2) can be written

$$\vec{V} = \vec{V}_g + \vec{V}_{ag}.$$

In this study, the ageostrophic wind will not be computed analytically by the last two terms in (2) but will be determined at each grid point as the residual necessary to balance (3) when the actual wind, $\vec{V}$, is measured and the geostrophic wind, $\vec{V}_g$, is computed from geopotential height.

Also in this study, only the wind speeds will be used and not the vector winds. This approximation does not greatly limit the results of the study. Carlson (1973) found that the contributions to the vector wind change due to direction change was negligible for 3-, 6-, and 12-h time periods. Also, Kochanski (1958) found that the major part of the ageostrophic vector deviation was due to speed deviation and not direction. Neiberger and Angell (1956) found that at 300 mb, the speed shear accounts for at least 83% of the average velocity shear.

When speeds are substituted for vectors in (3) and the equation differentiated with respect to pressure and time with a sign change, one obtains

$$\frac{\partial}{\partial t}\left(-\frac{\partial V}{\partial p}\right) = \frac{\partial}{\partial t}\left(-\frac{\partial V_g}{\partial p}\right) + \frac{\partial}{\partial t}\left(-\frac{\partial V_{ag}}{\partial p}\right). \qquad (4)$$

The local development of actual vertical shear (left-hand-side of (4)) is given by the sum of the local time rate-of-change of the vertical shear of the geostrophic wind and of the ageostrophic wind. The development of geostrophic wind shear is due to changes in the thickness of a layer and may be viewed also as the development of thermal wind.

The development of geostrophic wind shear is due to changes in the vertical distribution of tangential and normal accelerations and friction.

b. Error analysis

An error analysis of the wind shear and its development was done to determine the reliability of the computed fields. A propagation of error method described by Deming (1943) was used to calculate the effect of random errors on the measured wind. RMS errors for the wind measured at an elevation angle of 20° were obtained from Fuelberg (1974). The resulting error estimates are given in Table 8 along with the average magnitudes and extremes for each quantity. Only the error estimates for the 6-h development of wind shear are shown in Table 8 but, the relationships between the errors, average magnitudes, and extremes in 3- and 12-h development are similar to those shown.

Table 8 shows that errors in the individual terms are generally the same order of magnitude as the absolute mean value of the terms, but usually an order of magnitude smaller than the extremes. Errors generally increase with height since the basic errors in the wind and height measurements also increase with height. Errors in the geostrophic development of wind shear above 700 mb are almost as large as the typical extreme values. These fields must be viewed with caution and only the general placement of centers of geostrophic wind shear development can be taken with confidence.

Errors in the ageostrophic wind shear and wind shear development are not shown in Table 8 since they are computed as a residual of the measured shear and the computed geostrophic shear. Therefore, ageostrophic wind shear development also represents data measurement errors and errors introduced by finite difference approximations in the partial derivatives in (4).

Two other factors will affect the values of individual fields of wind shear development. The first is the presence of processes with wavelengths too small to be detected by the synoptic-scale network, but which affect shear development and its measured value nonetheless. The second is the time lag between changes in the height field and subsequent

changes in the actual wind field. Haltiner (1971) computed that a 40-m change in height at a point requires 5 to 10 hr before geostrophic balance is achieved again in the acutal wind flow. In this study, changes in the height field will show immediately in the calculated geostrophic shear development, but there will be a lag in the subsequent measured wind shear development. The actual effect of these factors on the results reported in this report are not known, but are included in the ageostrophic shear development fields.

Table 8. Estimated rawinsonde RMS errors in wind shear and the 6-h development of wind shear. Average and extreme values represent these in AVE IV.

Term	SURFACE-850 mb			850-700 mb			700-500 mb			500-300 mb		
	AM [1]	EV [2]	RMSE [3]	AM	EV	RMSE	AM	EV	RMSE	AM	EV	RMSE
$-\frac{\partial V}{\partial p}$	3.3	17.	0.1	2.8	11.	0.7	3.4	9.0	1.1	5.6	12.	1.8
$-\frac{\partial V_g}{\partial p}$	5.0	14.	0.7	2.2	6.6	1.6	2.8	8.7	2.4	4.5	13.	4.9
$(10^{-2}ms^{-1}mb^{-1})$												
$\frac{\partial}{\partial t}(-\frac{\partial V}{\partial p})$	10.	39.	0.9	14.	47.	4.4	7.4	26.	7.5	12.	45.	11.8
$\frac{\partial}{\partial t}(-\frac{\partial V_g}{\partial p})$	12.	43.	4.6	6.3	20.	10.5	5.2	17.	15.7	7.1	35.	32.1
$(10^{-7}ms^{-2}mb^{-1})$												

[1] Average magnitude
[2] Extreme value
[3] RMS error

3. RESULTS

a. Relationships between terms in the wind shear development equation

The actual, geostrophic, and ageostrophic development of wind shear were computed using the procedures outlined above. The layers considered were surface-850, 850-700, 700-500, and 500-300 mb. Wind shear development was computed over a 3-h time interval starting at 1200, 1500, 1800, and 2100 GMT on 24 April 1975. Wind shear development was computed for 6-h periods centered at 1500, 1800, and 2100 GMT, and for a 12-h time interval centered at 0600, 1200, and 1800 GMT on 24 April, and 0000 and 0600 GMT on 25 April.

Figure 26 shows the average vertical profiles for the measured, geostrophic, and ageostrophic wind shear for 1800 GMT 24 April. In the surface-850-mb and 850-700-mb layers, geostrophic and ageostrophic components of the wind shear are almost equal in average magnitude. However, in the boundary layer the shear is predominately ageostrophic since the geostrophic wind shear was on the average of opposite sign from the measured wind shear. In the 700-500-mb and 500-300-mb layers, the average geostrophic component of the shear is greater than the average ageostrophic component. The wind shear in these layers is predominately geostrophic.

Although the shear at any one time may be predominately geostrophic, the development of shear is predominately ageostrophic. Table 9 gives the mean and average magnitudes of the actual, geostrophic, and ageostrophic wind shear development for 3- , 6-, and 12-h time intervals starting or centered at 1800 GMT 24 April. For all the layers and time periods considered, the average absolute magnitude of the ageostrophic shear development was greater than the average absolute magnitude of the corresponding geostrophic value. The ageostrophic development also showed a greater tendency to have the same sign as the measured shear development than did the geostrophic development. Also, the average magnitude of wind shear development (measured, geostrophic, and ageostrophic) increased with decreasing time interval over which the development was calculated. This indicates that the rate-of-change in shear over 3 and 6 h are likely to be as large or larger than changes over

12 h, and that there is extreme variability in the development of wind shear not measured in the conventional 12-h rawinsonde data. Most of the development of shear takes place over 6- or 3-h periods.

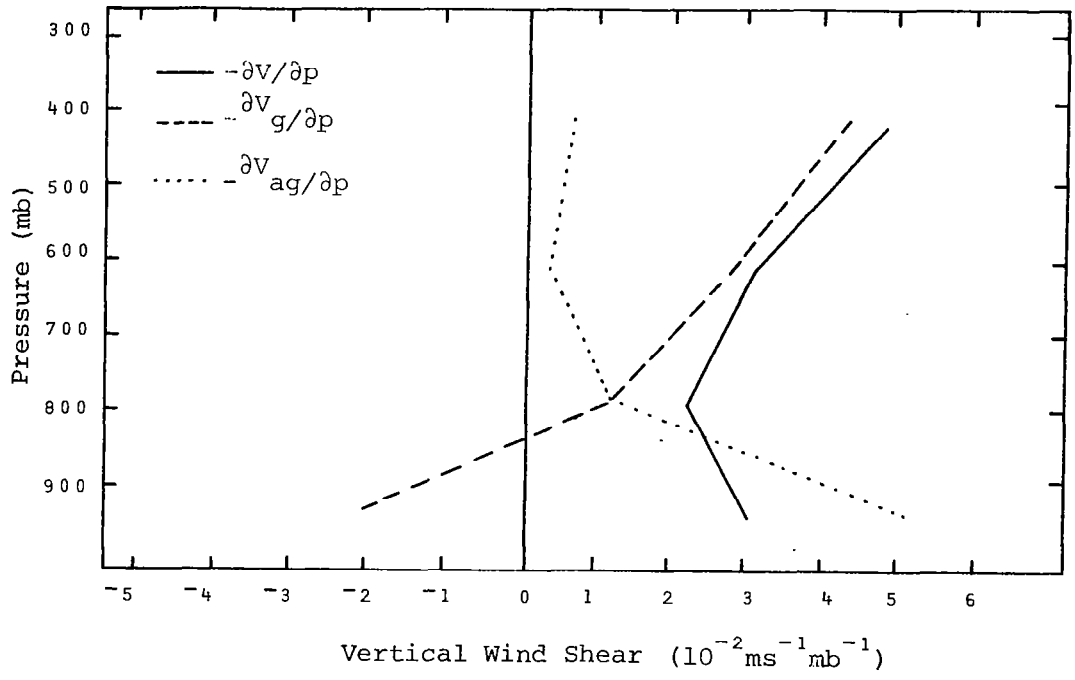

Fig. 26. Average vertical profiles of the measured, geostrophic, and ageostrophic vertical wind shears for 1800 GMT 24 April.

The frequency that either the geostrophic or ageostrophic wind made the largest contribution to changes in the shear was determined and the results are shown in Table 10 for 1800 GMT. Other observation times showed similar results. The dominance of the ageostrophic contribution to the development of wind shear is again evident in all layers and for all time intervals for which the computations were made. In most cases, the ageostrophic component was dominant for at least 60% of the grid points. However, in most cases ageostrophic dominance decreased as the time interval got longer with the geostrophic contribution showing a greater frequency of being as large or larger than the ageostrophic contribution. The only exception was the 500-300-mb layer where the frequencies were almost constant for all time intervals considered. Near jet streams, the ageostrophic

wind speed may be a large fraction of the actual wind speed, especially when wind speed and curvature are large. This fact may account for the persistent dominance of the ageostrophic component in the 500-300-mb layer where the jet stream was located. In the lower layers, the improvement of the geostrophic contribution is probably due to the fact that changes in trajectory curvature are not as important to wind speed changes over longer time periods as are changes in the height gradient (Carlson, 1973). Carlson found that over 3- and 6-h intervals, changes in the height gradient and trajectory curvature were the largest contributors to changes in the gradient wind speed in approximately the same number of cases. However, over a 12-h interval, changes in the height gradient made the largest contribution in approximately 80% of the cases.

Table 9. Means and average magnitudes of the development of shear ($10^{-7}ms^{-2}mb^{-1}$) for 3-, 6-, and 12-h time intervals starting or centered at 1800 GMT 24 April.

Time interval	Layer	$\frac{\partial}{\partial t}(-\frac{\partial V}{\partial p})$ Mean	AAM*	$\frac{\partial}{\partial t}(-\frac{\partial V_g}{\partial p})$ Mean	AAM*	$\frac{\partial}{\partial t}(-\frac{\partial V_{ag}}{\partial p})$ Mean	AAM*
3 h	sfc-850 mb	0.8	14.	-2.4	14.	3.2	20.
	850-700 mb	11.	19.	-1.0	9.4	12.	23.
	700-500 mb	-3.5	12.	2.7	9.9	-6.3	16.
	500-300 mb	-4.5	17.	4.2	13.	-8.7	19.
6 h	sfc-850 mb	-4.0	10.	-0.5	11.	-3.5	16.
	850-700 mb	12.	14.	0.4	6.3	12.	14.
	700-500 mb	-2.7	7.4	1.0	5.2	-3.7	8.2
	500-300 mb	-4.2	12.	0.6	7.1	-4.8	12.
12 h	sfc-850 mb	-5.0	7.2	0.1	8.4	-5.2	9.1
	850-700 mb	4.5	6.6	1.0	3.4	3.6	6.7
	700-500 mb	-0.5	5.3	1.2	3.7	-1.7	5.4
	500-300 mb	-1.8	9.5	1.2	4.9	-3.0	8.5

*Average Absolute Magnitude

Table 10. Percentage of time that the largest contribution to shear development was geostrophic, ageostrophic, or of the same magnitude for 1800 GMT 24 April.

Layer	Time interval	GD[1]	AD[2]	G & A[3]
sfc-850 mb	3 h	35%	61%	4%
	6 h	35%	61%	4%
	12 h	47%	46%	7%
850-700 mb	3 h	24%	72%	4%
	6 h	20%	77%	3%
	12 h	25%	67%	8%
700-500mb	3 h	32%	65%	3%
	6 h	30%	63%	7%
	12 h	32%	59%	9%
500-300mb	3 h	35%	60%	5%
	6 h	32%	63%	5%
	12 h	35%	61%	4%

[1] Geostrophic dominant [3] Geostrophic & Ageostrophic same
[2] Ageostrophic dominant

Although on the average, the ageostrophic component of wind shear development was dominant, individual fields of the measured, geostrophic, and ageostrophic development of wind shear show the geostrophic component to depict the centers and signs of the measured shear development relatively well. Figures 27, 28, and 29 show measured, geostrophic, and ageostrophic shear development in the 500-300-mb layer for 12-, 6-, and 3-h time intervals, respectively. The fields show consistency between the 12-, 6- and 3-h centers and signs with negative values in the south, along the Atlantic coast, throughout the midwestern states, and a small center in northern Arkansas. Positive centers of stability development, indicating an increase in wind shear, were located in east Texas, Oklahoma, and eastern Kansas with a tongue of positive values extending up the Ohio Valley. The

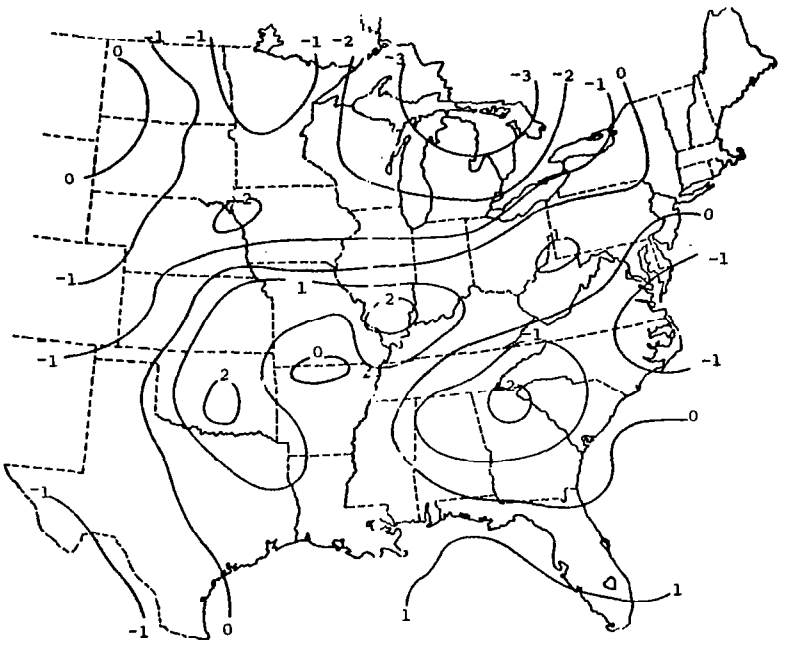

(a) $\frac{\partial}{\partial t}\left(-\frac{\partial V}{\partial p}\right)$

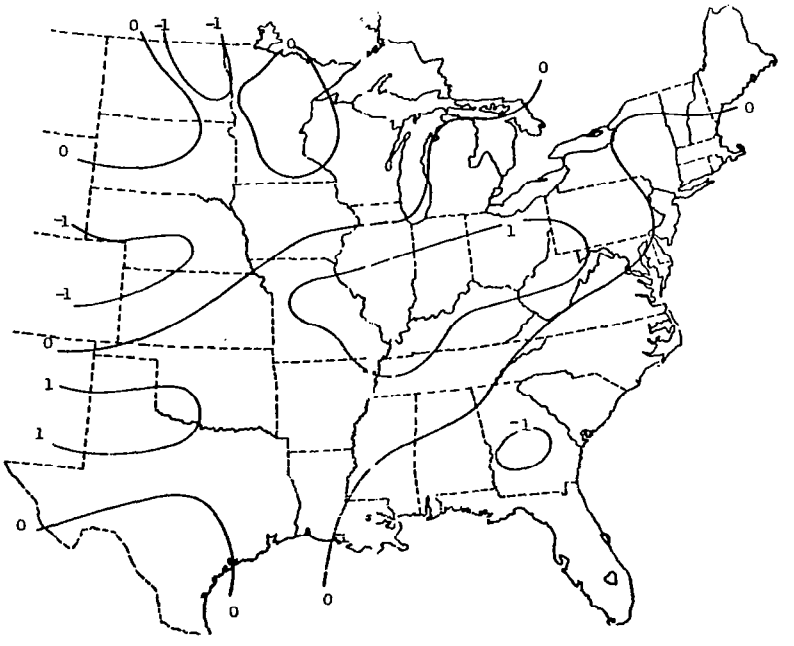

(a) $\frac{\partial}{\partial t}\left(-\frac{\partial V_g}{\partial p}\right)$

Fig. 27. Analysis of the development of wind shear ($10^{-7}s^{-2}mb^{-1}$) in the layer from 500-300 mb over a 12-h period centered at 1800 GMT 24 April.

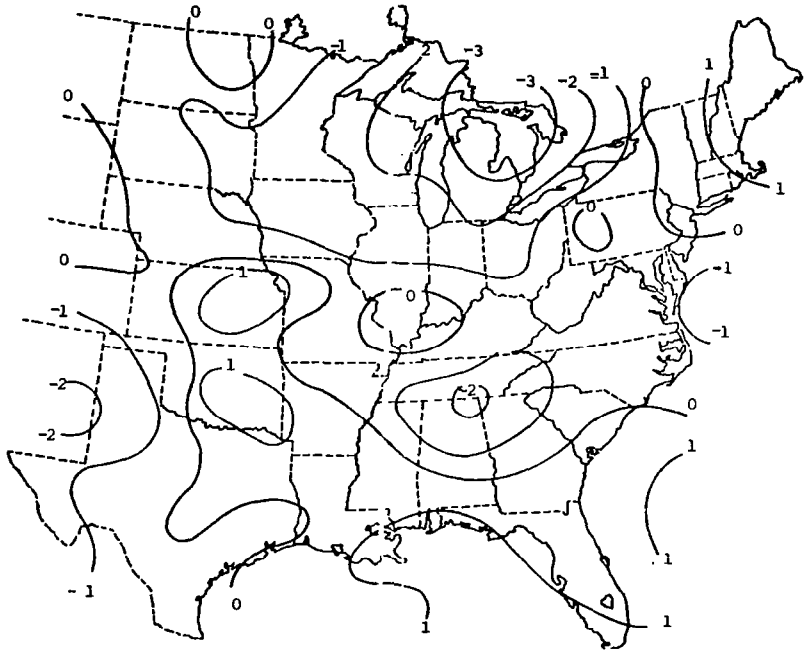

(c) $\frac{\partial}{\partial t}(-\frac{\partial V_{ag}}{\partial p})$

Fig. 27. (Continued)

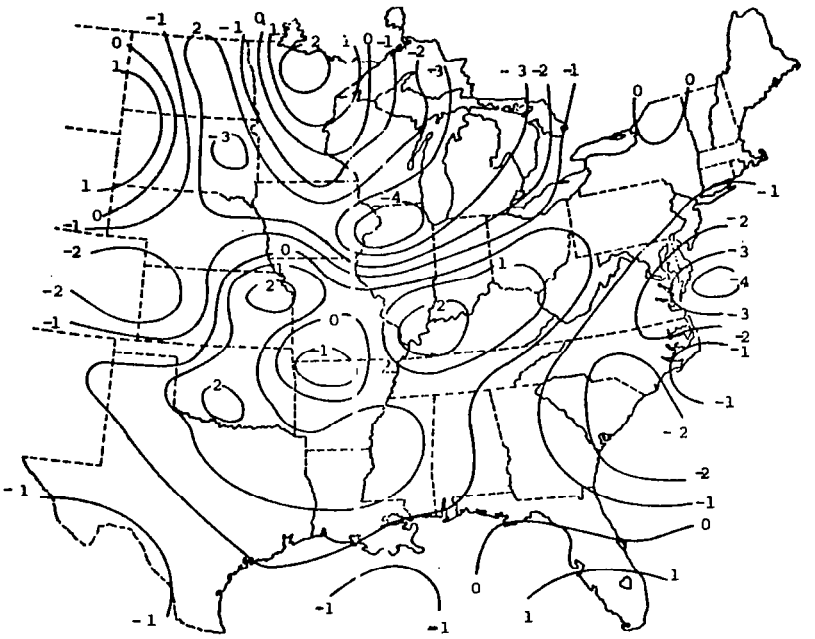

(a) $\frac{\partial}{\partial t}(-\frac{\partial v}{\partial p})$

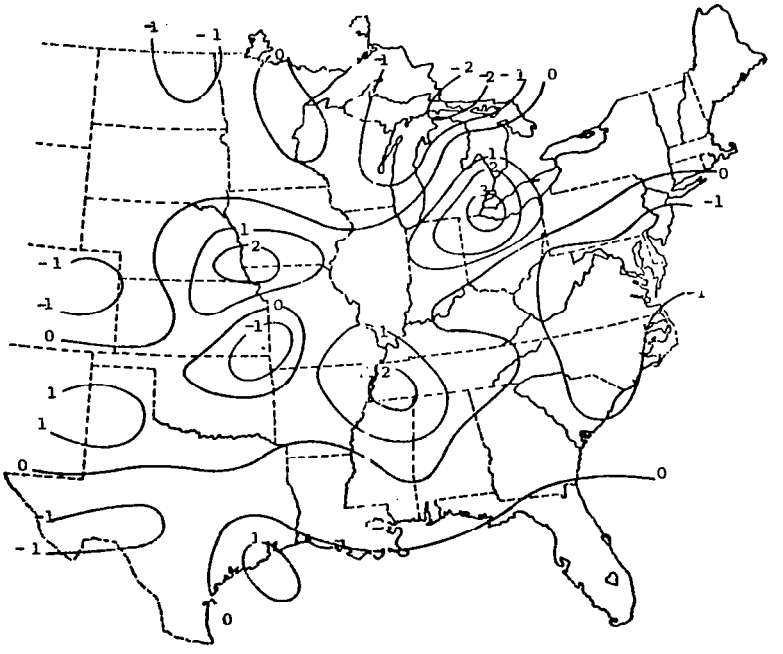

(b) $\frac{\partial}{\partial t}(-\frac{\partial v_g}{\partial p})$

Fig. 28. Analysis of the development of wind shear ($10^{-7}ms^{-2}mb^{-1}$) in the layer from 500-300 mb over a 6-h period centered at 1800 GMT 24 April.

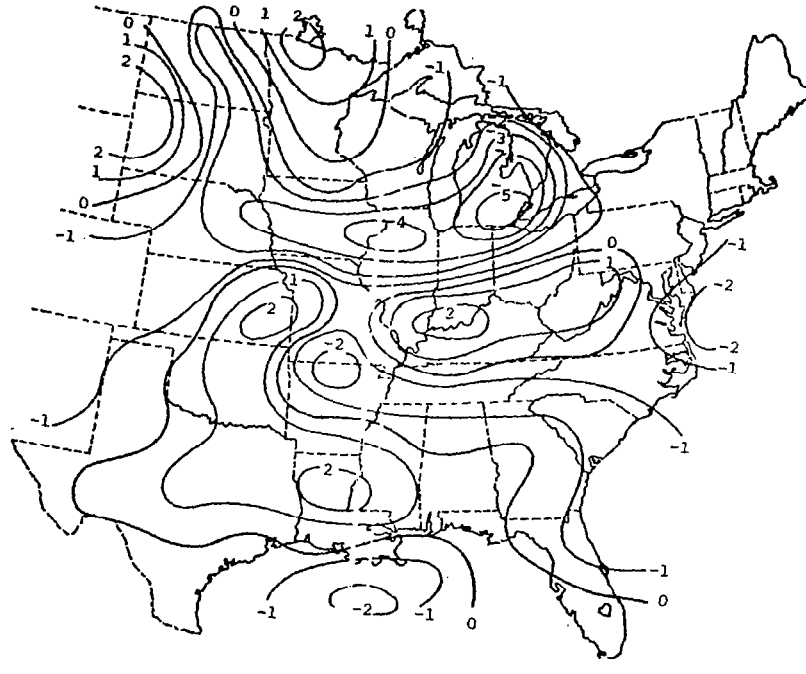

(c) $\frac{\partial}{\partial t}(-\frac{\partial V_{ag}}{\partial p})$

Fig. 28. (Continued)

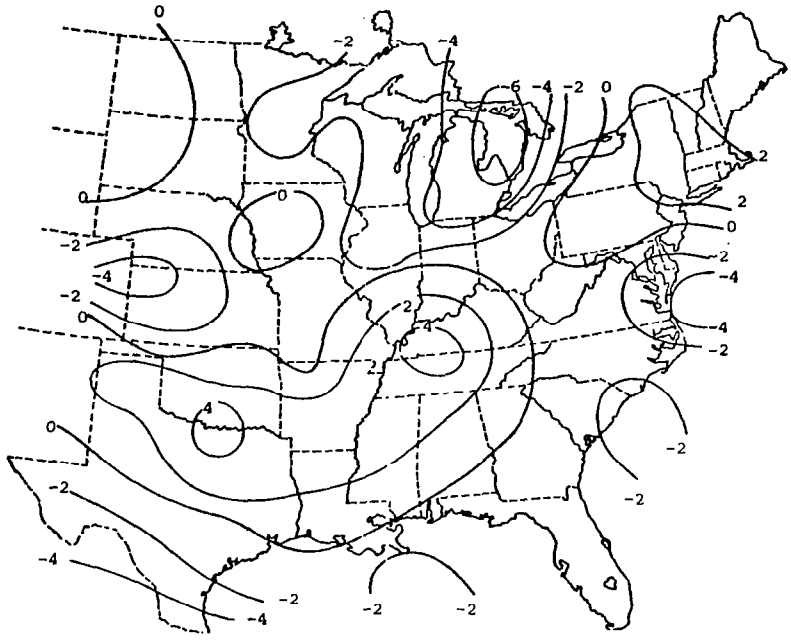

(a) $\frac{\partial}{\partial t}(-\frac{\partial V}{\partial p})$

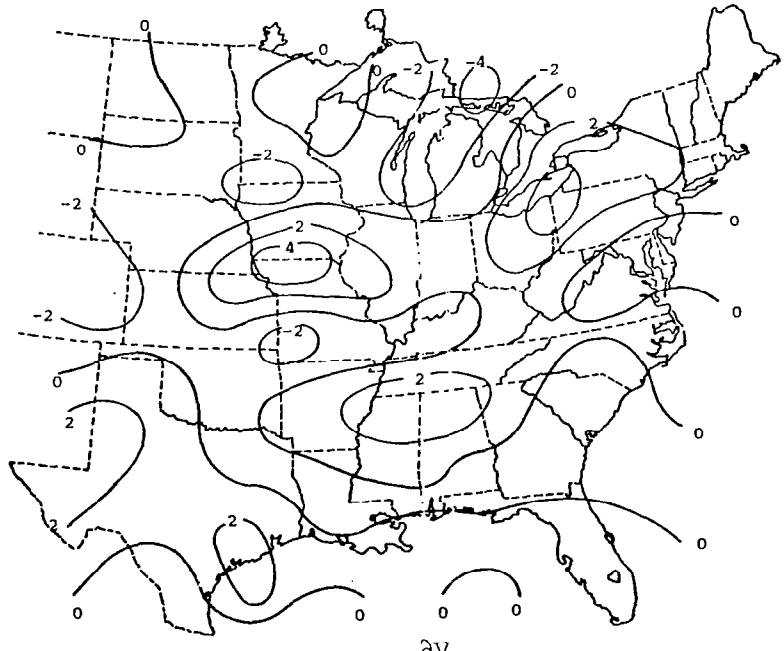

(b) $\frac{\partial}{\partial t}(-\frac{\partial V_g}{\partial p})$

Fig. 29. Analysis of the development of wind shear ($10^{-7} ms^{-2} mb^{-1}$) in the layer from 500-300 mb over a 3-h period starting at 1800 GMT 24 April.

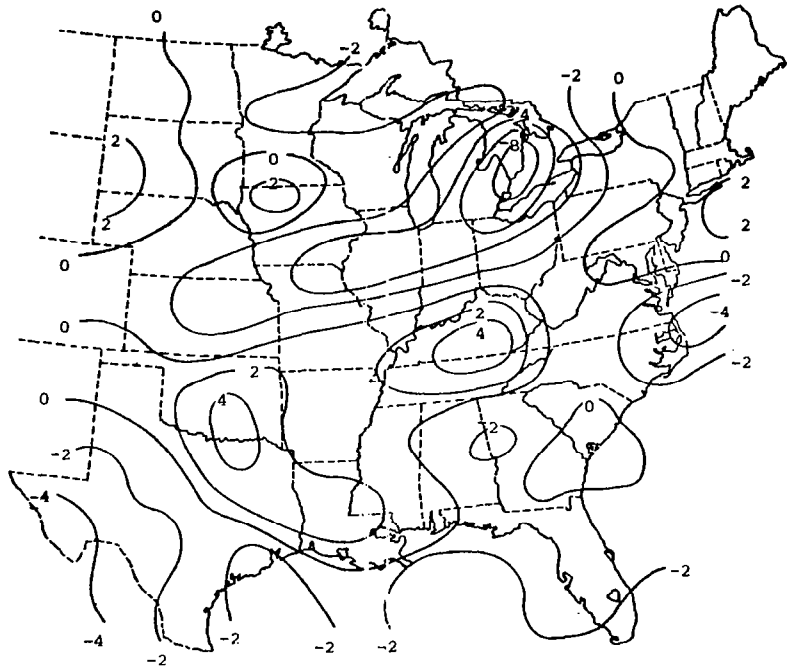

(c) $\frac{\partial}{\partial t}(-\frac{\partial v_{ag}}{\partial p})$

Fig. 29. (Continued)

fields of geostrophic development of wind shear also showed these general trends.

Linear correlation coefficients were computed between changes in the measured shear and changes in the shear of the geostrophic wind for the 500-300-mb layer at 1800 GMT 24 April. The coefficient for the 12-h interval was found to be 0.79, better than the correlation for 6- and 3-h intervals which had coefficients of 0.53 and 0.64, respectively.

Values in the centers of shear development became larger as the time interval over which the calculations were made became smaller. This again demonstrates that there exist long term trends in the development of wind shear but the majority of the change takes place in a 3- or 6-h period. The consistencies in time described for the 500-300-mb layer also were present in the other layers, but there was also a greater dominance of the ageostrophic shear development in those layers with the measured shear

development not corresponding as well with the computed geostrophic shear development. There was no evidence of a vertical consistency in shear development.

b. Relationship between the development of wind shear and synoptic systems and convection

The variability of wind shear in the 500-300-mb layer and its resolution in upper-air measurements taken over time intervals of 3, 6, and 12 h are compared in Fig. 30. A 12-h period was selected starting at 1200 GMT 24 April and ending at 0000 GMT 25 April. Figures 30(a), (b), (c) and (d) show fields of measured wind shear development for the four 3-h intervals making up the 12-h period with starting times of 1200, 1500, 1800, and 2100 GMT, respectively. These figures show the greatest time resolution possible using the AVE IV data. Time continuity in the development of wind shear can be observed. For example, centers of increasing wind shear, $\frac{\partial}{\partial t}(-\frac{\partial V}{\partial p}) > 0$, in the first 3-h time interval (Fig. 30 (a)) in western Kansas and southern Illinois moved slightly eastward and were located in eastern Kansas and southern Ohio during the second 3 h (Fig. 30 (b)). Decreasing wind shear, $\frac{\partial}{\partial t}(-\frac{\partial V}{\partial p}) < 0$, was persistent in the southern states during this time. Large variability in the fields of wind shear development can also be observed, such as the centers of positive wind shear development along the Atlantic coast of South Carolina and in northern Minnesota in Fig. 30 (a), which were replaced by centers of negative wind shear development in the same areas in Fig. 30 (b). Similar trends were present in the other 3-h charts of wind shear development with positive values becoming especially predominate in an area stretching northeastward from Texas to Illinois and then eastward to the Atlantic coast. Negative centers of wind shear development replaced the earlier positive values in Kansas and the surrounding area. Negative centers in the Great Lakes area were consistent throughout all four of the 3-h development fields.

Figures 30 (e) and (f) show fields of measured wind shear development for the two 6-h intervals covering the same 12-h period shown in Fig. 30 (a) - (d). Figure 30 (e) represents the development over the first 6 h and covers the same time interval as in Figs. (a) and (b). Likewise, Fig. 30 (f) covers the development of wind shear in the last 6 h and is also represented by the two 3-h development fields presented in Figs. 30 (c) and

(d). The consistent positive values of wind shear development centered in Kansas and Illinois observed in the 3-h representations in Figs. 30 (a) and (b), and the consistent negative values in the southern states and the Great Lakes area, also are strong centers of wind shear development in the 6-h representation of Fig. 30 (e). Areas in which the wind shear development changed sign between the 3-h time intervals, such as in South Carolina and northern Minnesota, are areas of small 6-h wind shear development. Similarly, Fig. 30 (f) shows the tendency in the last 6 h for positive values to form a band from Texas to Pennsylvania, and negative values to be centered in Kansas, the Carolinas, and the Great Lakes Area.

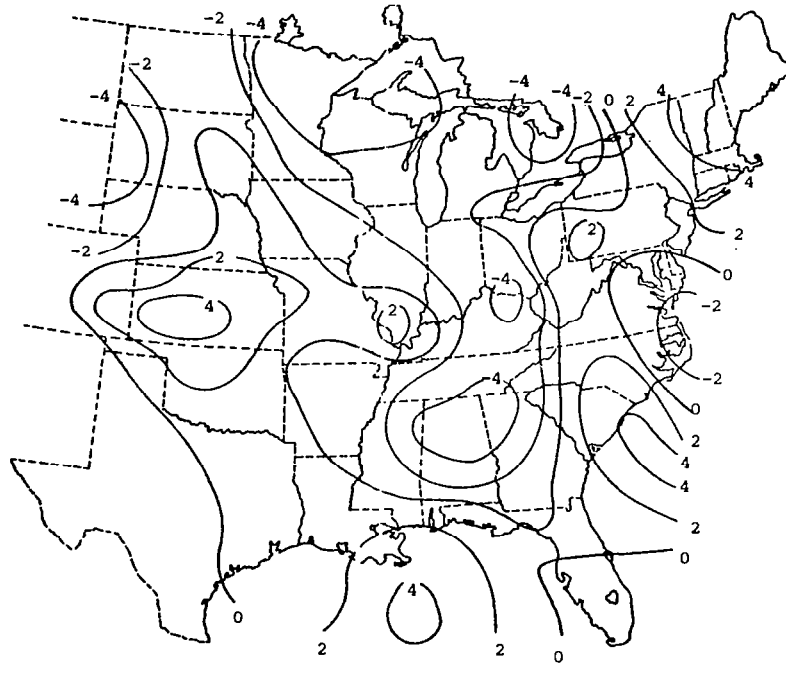

(a) 3-h wind shear development starting at 1200 GMT.

Fig. 30. Measured wind shear development ($10^{-7}ms^{-2}mb^{-1}$) in the 500-300-mb layer for various time intervals within the 12-h period from 1200 GMT 24 April to 0000 GMT 25 April (surface frontal position and thunderstorm areas at 1800 GMT shown for reference in 30 (g)).

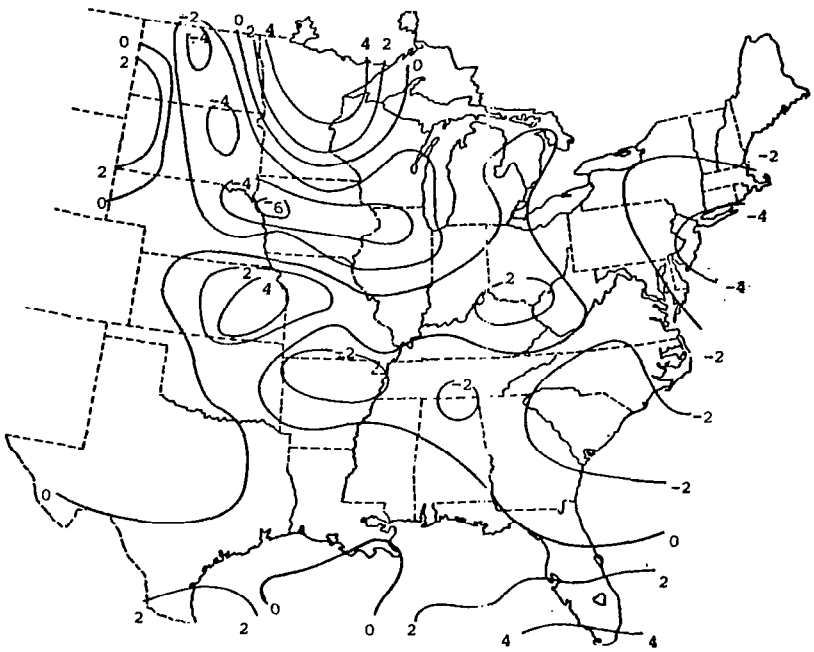

(b) 3-h wind shear development starting at 1500 GMT.

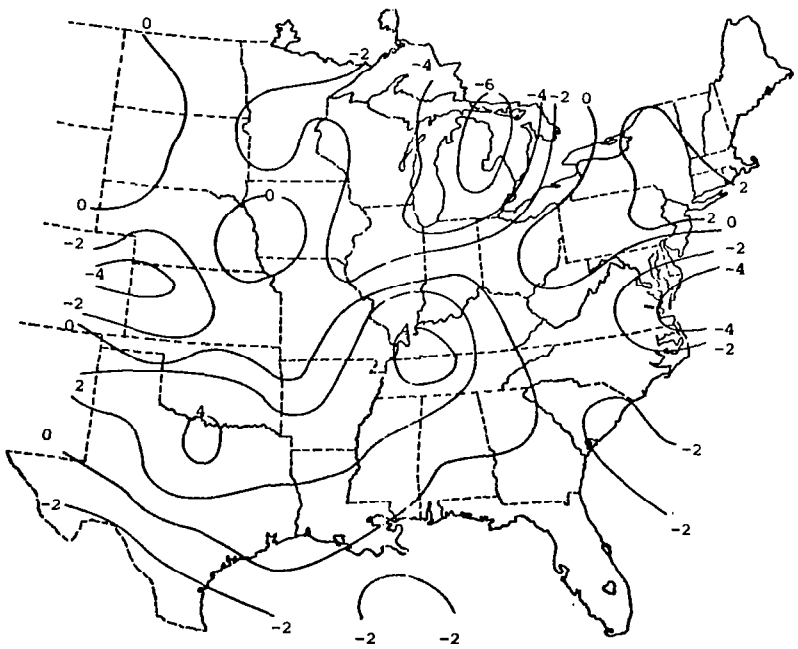

(c) 3-h wind shear development starting at 1800 GMT.

Fig. 30. (Continued)

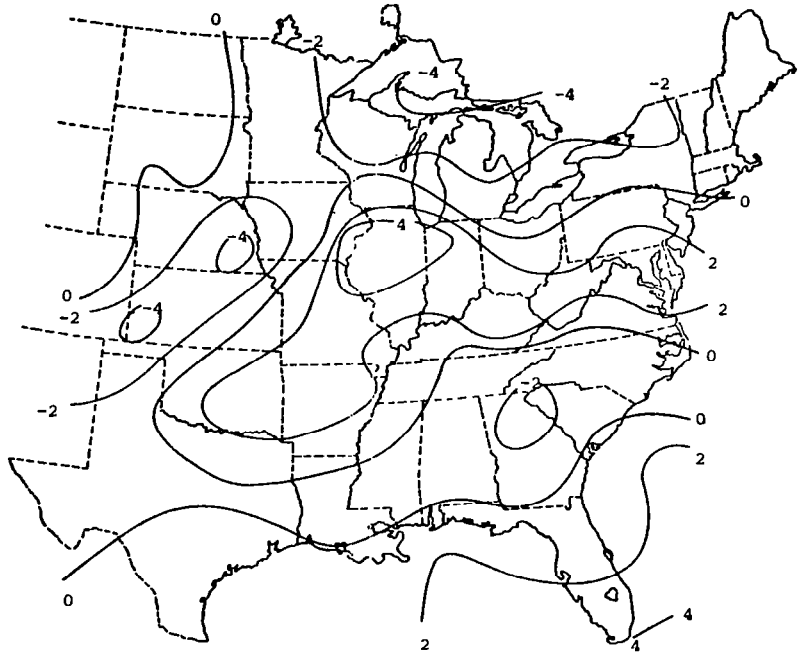

(d) 3-h wind shear development starting at 2100 GMT.

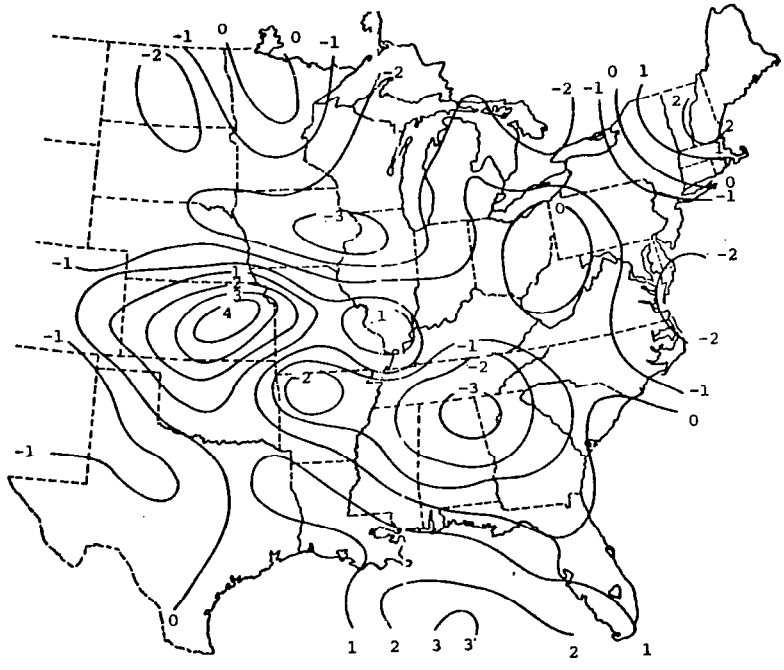

(e) 6-h wind shear development starting at 1200 GMT.

Fig. 30. (Continued)

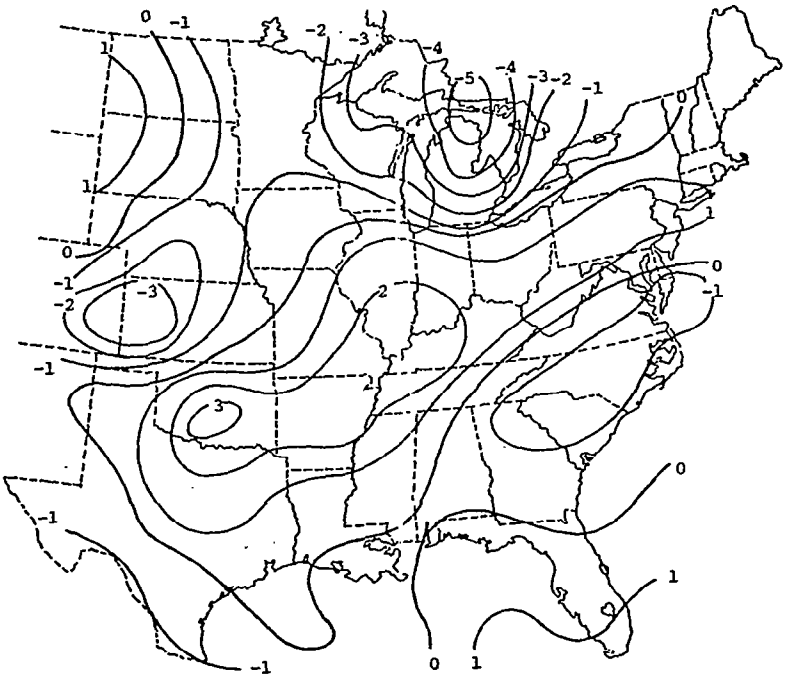

(f) 6-h wind shear development starting at 1800 GMT.

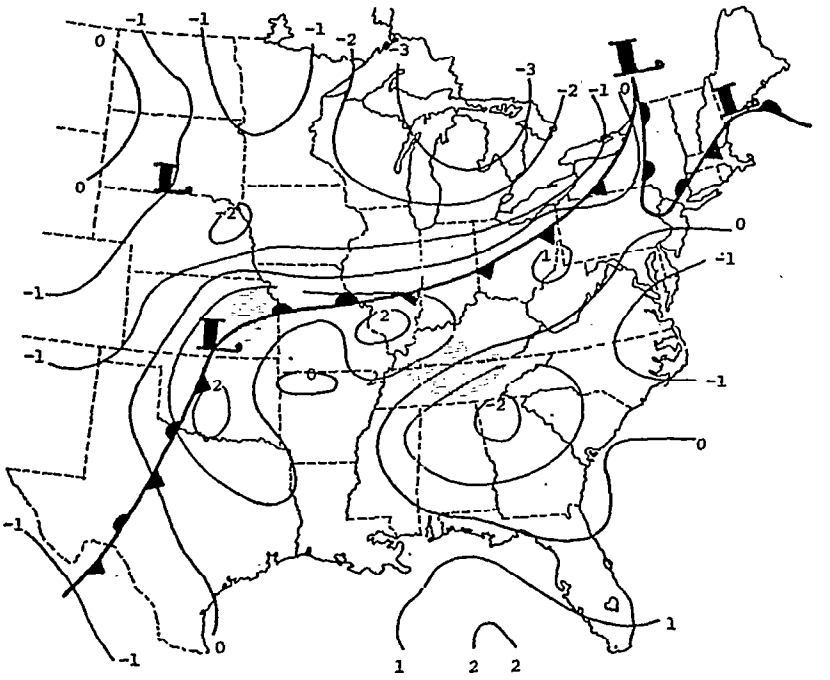

(g) 12-h wind shear development starting at 1200 GMT.

Fig. 30. (Continued)

Figure 30 (g) shows the field of measured wind shear development in the 500-300-mb layer for the entire 12-h period. The surface frontal position at the center of the 12-h interval, 1800 GMT 24 April, is shown for reference. Centers of increasing wind shear are located in Oklahoma, southern Illinois, and eastern Ohio. These are areas that most consistently had positive values of wind shear development during the two 6-h intervals, or equally, during the four 3-h intervals. Consistent negative values in the southern states are indicated by negative 12-h wind shear development values in the same area. The consistency of the decrease in wind shear in the Great Lakes area also is observed in the 12-h representation of wind shear development. However, the variability of the wind shear development indicated in the 3- or 6-h development fields can not be seen in Fig. 30 (g). The development of wind shear in the 500-300-mb layer is usually positive above the surface position of the front with centers of increasing wind shear development slightly ahead of the front. Negative wind shear development is found immediately behind the front and some distance ahead of it.

The variability or continuity of geostrophic and ageostrophic wind shear development was also studied in relation to synoptic systems. Figure 31 shows the 6-h development of geostrophic wind shear in the 500-300-mb layer for 3 overlapping time periods centered at 1500, 1800, and 2100 GMT 24 April, respectively. Surface frontal positions and the location of thunderstorms are indicated for each time. The other layers studied in this research showed much greater variability than did the 500-300-mb layer. The fields of geostrophic wind shear development are generally continuous in time with the development in the 500-300-mb layer usually positive above the surface position of the front. Centers of maximum positive change existed on both sides of the surface frontal position either above or ahead of the 850-mb frontal position. This position often coincides with the most probable area of strongest winds or jet stream in the upper atmosphere associated with the front. Areas of negative geostrophic wind shear development were located behind the surface and 850-mb frontal positions. These retreated in the southern states from 1500 to 2100 GMT before the advancing centers of positive geostrophic shear development. Thunderstorms were usually located in areas of positive geostrophic shear development in the 500-300-mb layer.

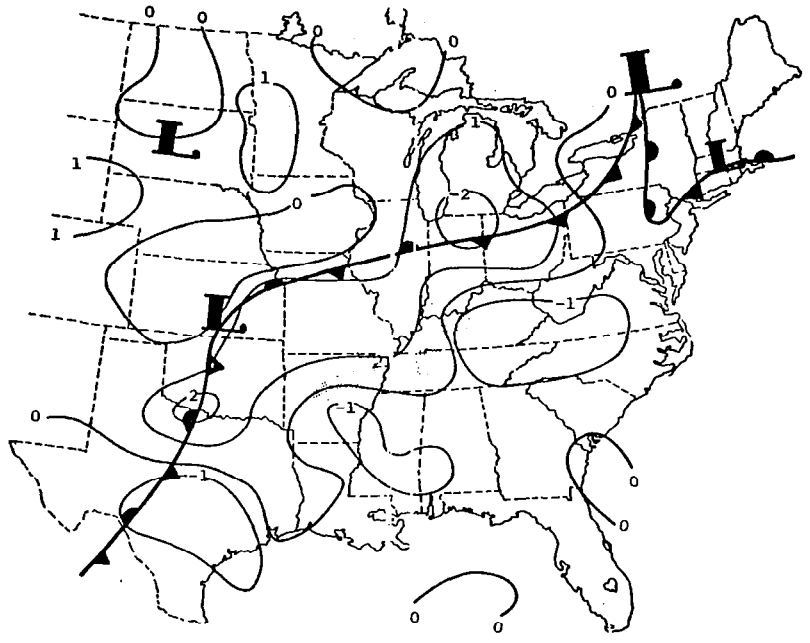

(a) 1500 GMT.

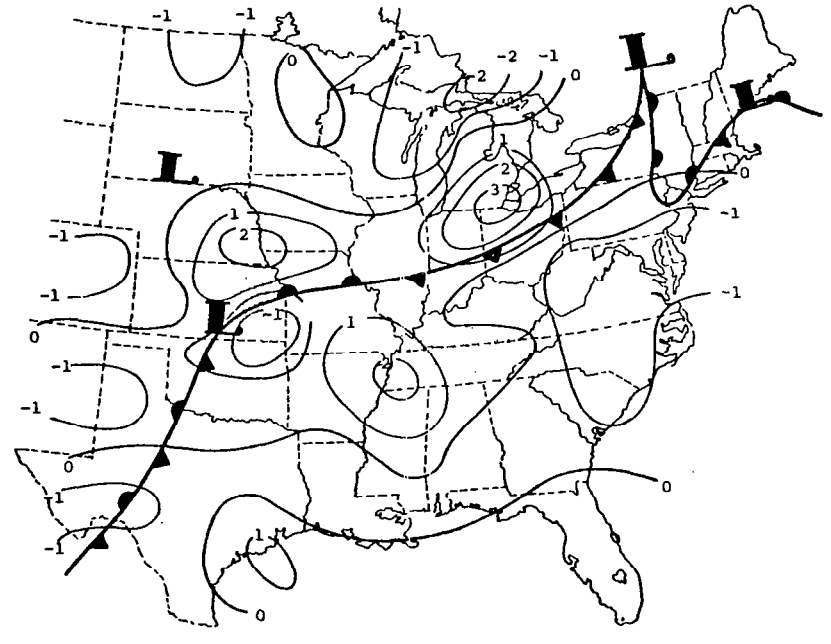

(b) 1800 GMT.

Fig. 31. Geostrophic 6-h wind shear development ($10^{-7}ms^{-2}mb^{-1}$) in the 500-300-mb layer for 3 overlapping time periods centered at the indicated times (surface frontal positions and thunderstorm areas for each time are for reference).

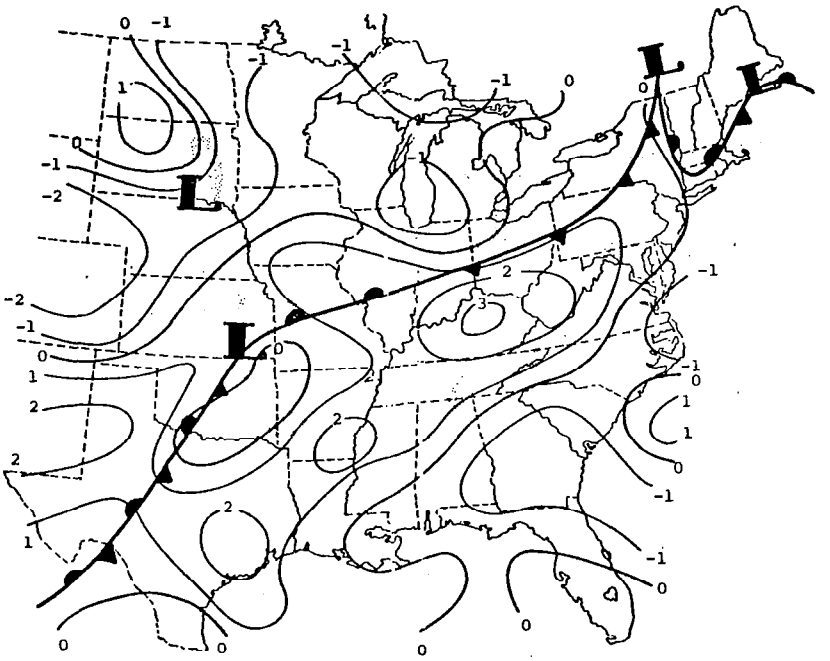

(c) 2100 GMT.

Fig. 31. (Continued)

Figure 32 shows the 6-h development of ageostrophic wind shear in the 500-300-mb layer for 3 overlapping time periods centered at 1500, 1800, and 2100 GMT, the same time periods of geostrophic development in Fig. 31. The centers are stronger than those found in the geostrophic development fields. Although the fields of ageostrophic wind shear development are generally continuous in time, the front and thunderstorms do not consistently lie within areas of positive or negative ageostrophic shear development. The most continuous area of increasing ageostrophic wind shear is in Kansas near the low pressure center. The variation of curvature with height may have a dominant effect in this case. Figure 32 also shows that the actual wind shear development in the Great Lakes region noted in Fig. 30 is predominately ageostrophic. The geostrophic and ageostrophic development are often of opposite sign. It is interesting to note that several centers of ageostrophic wind shear development were also areas of maximum upward or downward vertical motion.

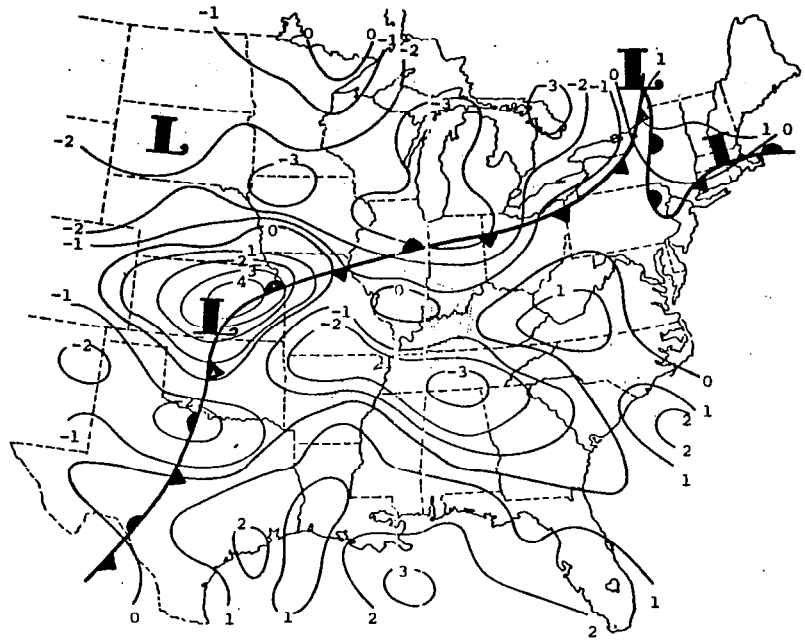

(a) 1500 GMT.

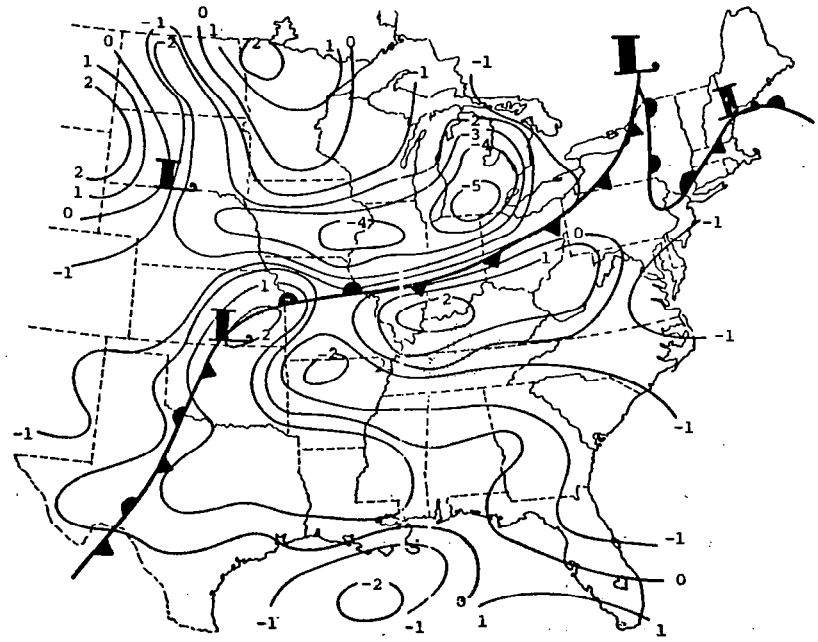

(b) 1800 GMT.

Fig. 32. Ageostrophic 6-h wind shear development (10^{-7}ms^{-2}mb^{-1}) in the 500-300-mb layer for 3 overlapping time periods centered at the indicated times (surface frontal positions and thunderstorm areas for each time are shown for reference).

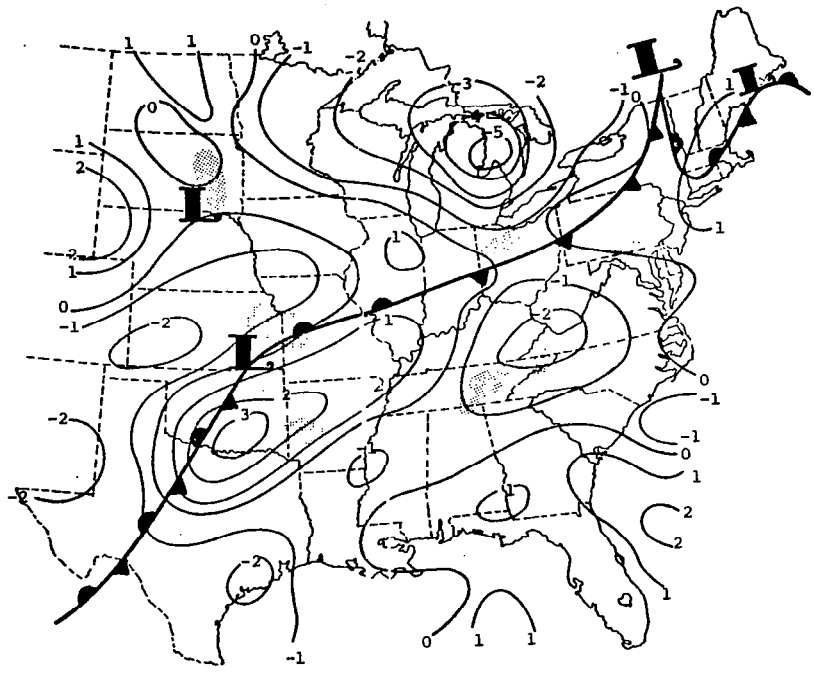

(c) 2100 GMT).

Fig. 32. (Continued)

Characteristics of measured, geostrophic, and ageostrophic wind shear development in layers other than 500-300-mb will be described next in the discussion of the computed average vertical profiles of shear development. The other layers generally showed greater variability in time than did the 500-300-mb layer. The frontal position and wind shear development pattern were not as strongly related in the other layers as they were in the 500-300-mb layer.

Average vertical profiles of the development of wind shear based on categories of convective severity were determined in order to reduce the effect of random errors and show general relationships between the development of wind shear and convection. The sign or magnitude of the wind shear seldom corresponded consistently on individually analyzed fields with the intensity of the convection present. The profiles were calculated by taking an average of each term computed for each category of convection determined from the gridded MDR data. Four categories of MDR values showing an increasing severity of convection were selected for the purpose of making comparisons. They were MDR $\leq$ 1 representing no convection, MDR $\geq$ 2

representing all convection, MDR $\geq$ 4 representing thunderstorms, and MDR $\geq$ 8 representing severe thunderstorms.

Figure 33 shows the average vertical profiles for wind shear. In the lower and middle layers the average profiles show the shear in convective areas to be generally greater than that in nonconvective areas. The shear consistently became stronger with increasing severity of convection in the 850-700-mb layer and 700-500-mb layer. However, in the upper layer, 500-300-mb, the shear in nonconvective areas was as large or larger than the wind shear in areas with convection. It is interesting to note with reference to the distinction of Newton and Newton (1959) between the effect of wind shear on small and large convective systems, that the shear is strongest in non-convective regions. Systems of lesser intensity were found in this study to exist in regions of more moderate wind shear.

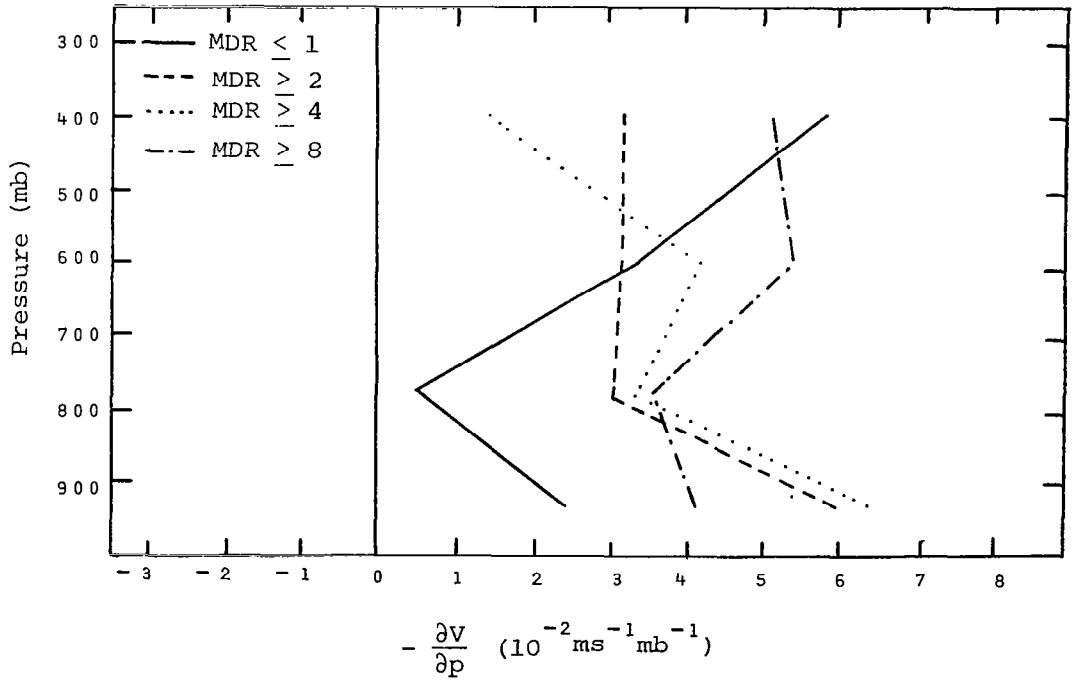

Fig. 33. Average vertical profiles of vertical wind shear.

The vertical profiles of the development of shear for 3-, 6- and 12-h time intervals were similar. Therefore, only the 6-h profiles are shown. However, the values obtained in each layer for each time interval are given

in Table 11 which shows that values of shear development for 3- and 6-h periods were very nearly the same. Values of shear development over 12 h showed the same trends usually as the calculations made over the other time intervals but were smaller. This was especially evident for the development of shear in areas containing severe thunderstorms (MDR $\geq$ 8) where the 3- and 6-h values are often an order of magnitude larger than the average values determined over a 12-h period. This demonstrates the existence of long term trends in the development of shear with respect to convection throughout the 12-h period, but which are largest around the immediate time of the thunderstorm activity. Most of the change in shear takes place in 3 or 6 h. Table 11 also shows that in the 850-700-mb and 700-500-mb layers over a 12-h time interval, and in all layers for 3- and 6-h time intervals, the ageostrophic development of shear in areas containing severe thunderstorms was much greater in average magnitude than the development of shear in areas of lesser convective intensity or no convection. The greater vertical transport of momentum in severe thunderstorms may account for this observed trend. The same pattern occurred in the values of the development of measured shear.

Table 11. Averages of measured, geostrophic, and ageostrophic wind shear development ($10^{-7}ms^{-2}mb^{-1}$) over 3-, 6-, and 12-h time intervals for various intensities of convective activity.

Layer	surface-850mb			850-700mb			700-500mb			500-300mb		
Time Interval	3h	6h	12h	3h	6h	12h	3h	6h	12h	3h	6h	12h
MDR $\leq$ 1	-5.1	-4.7	-1.5	5.0	7.8	0.3	-0.8	-1.7	0.2	-2.4	-3.2	0.5
MDR $\geq$ 2	-4.9	-4.5	-3.7	2.9	4.6	2.4	0.7	0.6	0.5	0.6	-0.4	1.6
MDR $\geq$ 4	-5.3	-1.1	-3.2	3.3	3.2	2.7	-1.9	-2.2	0.2	7.6	6.5	3.5
MDR $\geq$ 8	-19.	-18.	-1.1	24.	27.	5.0	-16.	-15.	-3.6	-1.7	-4.5	0.1
MDR $\leq$ 1	-0.9	-1.3	-0.4	0.3	0.2	0.5	0.2	0.2	-0.1	0.0	0.2	-0.2
MDR $\geq$ 2	3.6	4.3	0.1	3.3	2.7	2.1	5.1	4.5	2.4	5.8	4.1	1.9
MDR $\geq$ 4	3.0	1.3	0.6	3.2	1.5	3.2	4.2	3.3	0.9	9.4	5.9	1.7
MDR $\geq$ 8	1.2	2.5	0.8	-22.	-4.1	2.5	-0.9	-3.5	-0.5	14.	5.5	1.0
MDR $\leq$ 1	-4.2	-3.4	-1.2	4.7	7.6	-0.2	-0.9	-1.9	0.2	-2.4	-3.4	0.7
MDR $\geq$ 2	-8.6	-8.8	-3.7	-0.4	1.9	0.3	-4.4	-3.9	-1.9	-5.2	-4.5	-0.3
MDR $\geq$ 4	-8.3	-2.4	-3.8	0.2	1.7	-0.4	-6.1	-5.5	-0.7	-1.7	0.6	1.8
MDR $\geq$ 8	-20.	-20.	-1.9	45.	31.	2.5	-15.	-11.	-3.1	-16.	-10.	-0.8

Figure 34 shows the average vertical profiles for the measured 6-h development of wind shear. The shear development was negative (on the average) indicating a decrease in shear in the boundary layer in all areas, and in the upper levels in areas containing severe thunderstorms. The most consistent trend took place in the 850-700-mb layer where shear increased with time, especially in areas containing severe thunderstorms. The shear also increased in the upper levels in areas containing convection that was not necessarily severe. The shear development here was larger in magnitude for areas containing thunderstorms than areas of just general convection, but after the thunderstorms became severe the shear showed a tendency to decrease slightly.

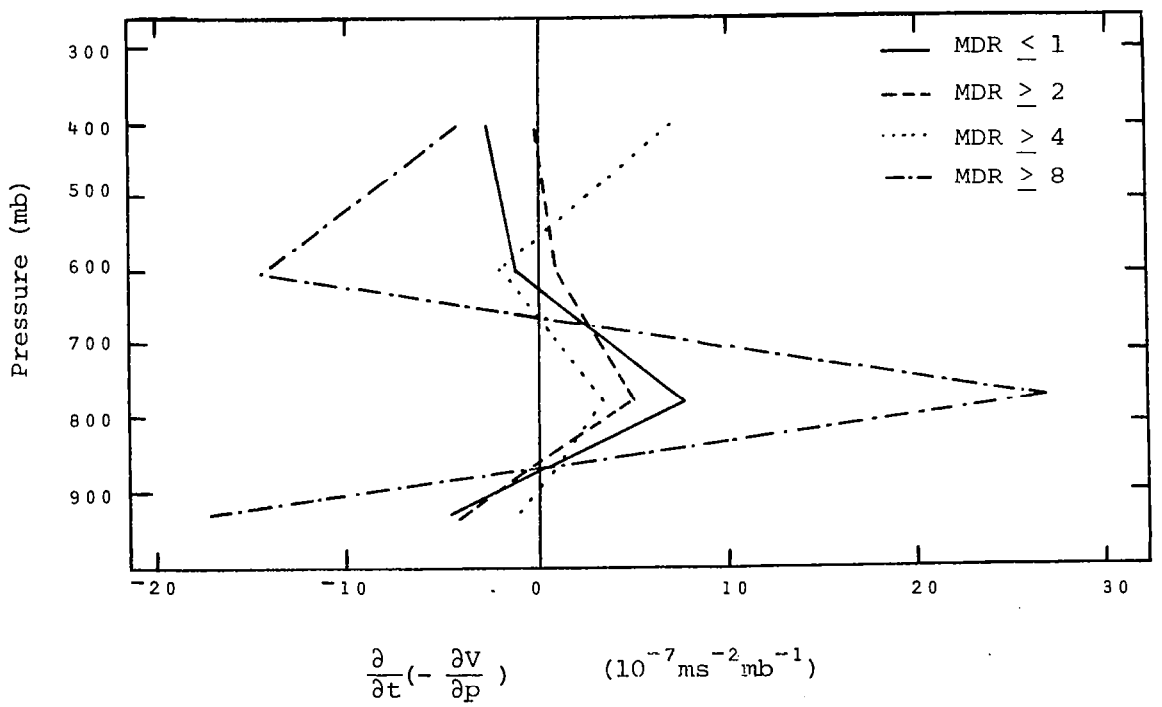

Fig. 34. Average vertical profiles of the development of measured vertical wind shear.

Figure 35 shows the average vertical profiles of the development of geostrophic wind shear over a 6-h interval. The values are very small (in all layers) for areas containing no convection. However, the trends were not consistent with increasing severity of convective activity. Moderate convective activity was associated with an increase in geostrophic wind shear in the middle troposphere, while severe thunderstorms were

associated with a decrease in geostrophic wind shear for the same layers. All levels of convective intensity showed increasing geostrophic wind shear in the upper levels and in the boundary layer. This was also noted in the discussion of individually analyzed fields in Fig. 31.

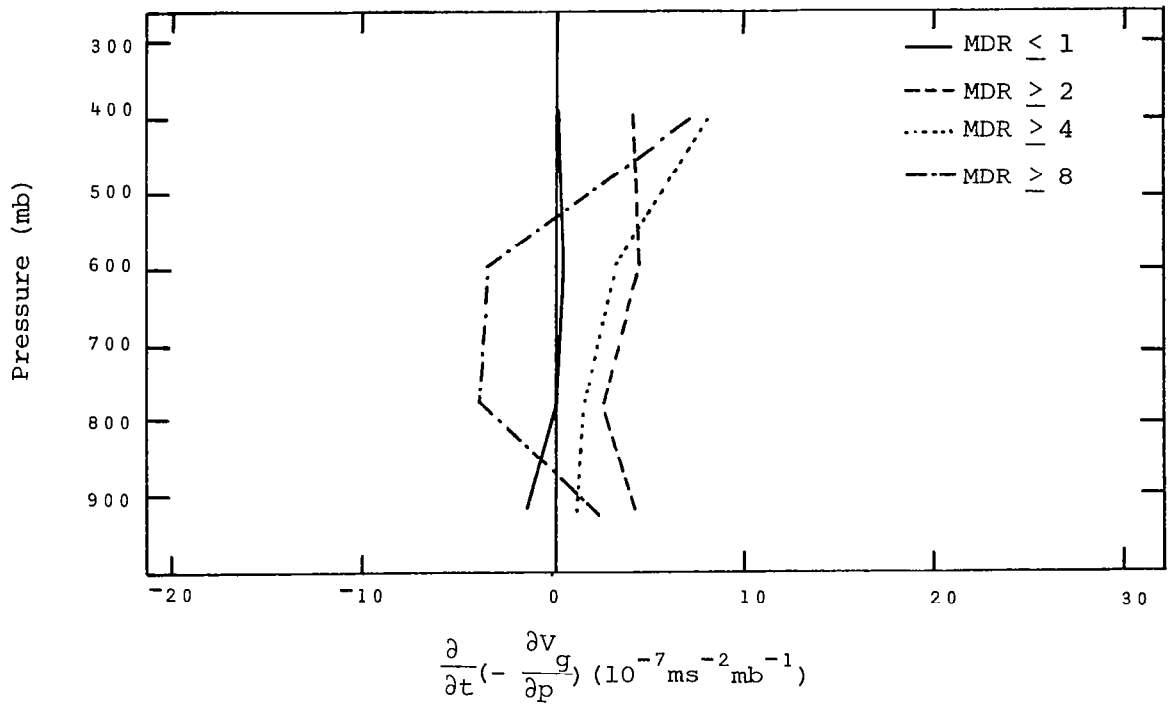

Fig. 35. Average vertical profiles of the geostrophic development of vertical wind shear.

Figure 36 shows the average vertical profiles for the 6-h development of ageostrophic wind shear. They are similar to the measured shear development profiles in Fig. 34. This again shows that the development of wind shear was predominately due to ageostrophic motions. Palmen and Newton (1969) stated that vertical wind shear is generated mainly by variations of the cross stream circulation with height which, of course, is ageostrophic flow. The interaction of convective-scale processes with synoptic-scale processes might be one source of ageostrophic motions, especially since the ageostrophic development of shear has maximum effect in areas containing severe thunderstorms.

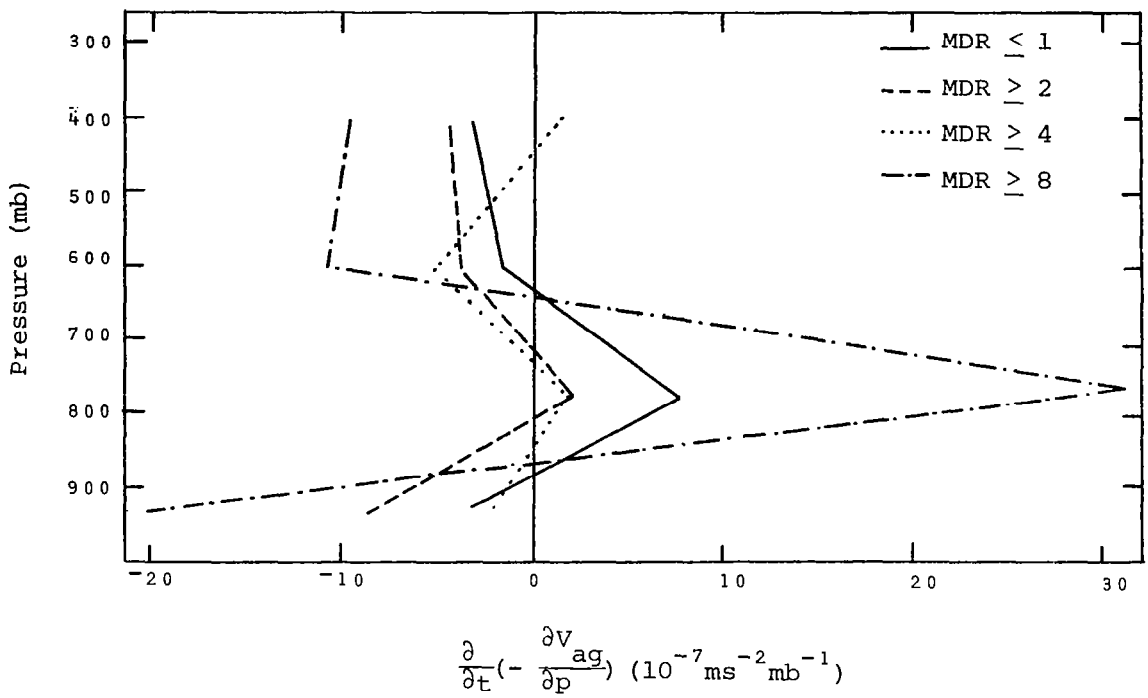

Fig. 36. Average vertical profiles of the ageostrophic development of vertical wind shear.

4. SUMMARY AND CONCLUSIONS

The development of wind shear has been studied over 3-, 6- and 12-h periods using the AVE IV rawinsonde data. The wind shear was divided into its geostrophic and ageostrophic components and the development (local time change) of each was studied over 3-, 6-, and 12-h time intervals. Analyzed fields of the measured, geostrophic, and ageostrophic shear development were studied along with their average values to establish which factors were predominate. Average vertical profiles based on categories of convective intensity also were used to relate shear development to convective systems.

It was found that although the shear at any one time predominately results from the shear of the geostrophic wind, the development of wind shear was mainly ageostrophic. However, the dominance of ageostrophic motions in the development process was diminished when longer time intervals were used to calculate the change in the shear. Patterns of measured shear development and geostrophic shear development compared best for the 500-300-mb layer. Also, long term trends were found to exist in the development of wind shear, but the majority of the change in shear took place over a 3- to 6-h period. The strength or development of the wind shear seldom corresponded consistently to the intensity of the convection present on individually analyzed fields. However, average vertical profiles showed the measured wind shear to be greater in the lower and middle troposphere in convective areas than in nonconvective areas. In the upper troposphere strong shear existed on the average in areas of no convection and areas of severe thunderstorms. The development of shear in the 500-300-mb layer was usually positive ahead of the front.

PART III: VERTICAL MOTION

1. INTRODUCTION

a. Statement of problem

In an objective analysis of environmental conditions associated with severe thunderstorms, Endlich and Mancuso (1968) found that the regions with the largest upward motion generally included the areas where severe storms formed. Boundary layer quantities were found to be most directly related to convection with boundary layer upward motion a very good indicator of thunderstorm development. As we would expect, convergence in the lower troposphere and divergence in the upper troposphere also were related to thunderstorm activity. Paegle and McLawhorn (1973) computed the vertically integrated boundary layer convergence and found good agreement between the resulting vertical velocities and the time and spacing of thunderstorm activity. However, the fact that some areas with strong positive vertical velocities had no thunderstorms indicated that there were other atmospheric conditions which also must be considered in the prediction of convective activity.

House (1968) speculated that there were possible reversals of vertical motion occurring closely in space and time. The 3- and 6-h sounding intervals of the AVE IV data provide an opportunity to better determine the temporal changes in vertical motion and relate these changes to stages of thunderstorm development.

b. Objectives

The main objective of this study is to describe the development of vertical motion at various atmospheric levels computed from rawisonde data taken at 3-h intervals.

Specific objectives include:

1) Describe a process that would lead to the development of vertical motion.
2) Relate the observed changes in vertical motion to convective activity.

2. ANALYTICAL METHODS

a. Vertical motion development equation

The vertical velocities used in this study were calculated using the kinematic method and the adjustment scheme developed by O'Brien (1970). This method has been shown to produce realistic magnitudes and patterns of vertical motion (Smith, 1971; Chien and Smith, 1973). It will also be used to describe the development of vertical motion.

The continuity equation in pressure coordinates is

$$\frac{\partial \omega}{\partial p} + \overline{(\vec{\nabla}_p \cdot \vec{V})} = 0 \qquad (1)$$

where the overbar represents average divergence for a given pressure layer. By integrating this equation with respect to pressure from the surface upward gives the vertical motion at the top of any layer k as

$$\omega_k = \omega_0 + \sum^{k} \overline{(\vec{\nabla}_p \cdot \vec{V})} \Delta p \qquad (2)$$

where Δp is the pressure interval, and ω_0 is the vertical motion at the bottom of the first layer, which in this case is the terrain-induced vertical motion. Taking the local derivative of (2) gives

$$\frac{\partial \omega_k}{\partial t} = \frac{\partial \omega_0}{\partial t} + \sum^{k} \frac{\partial}{\partial t} \overline{(\vec{\nabla}_p \cdot \vec{V})} \Delta p. \qquad (3)$$

The local rate-of-change of terrain-induced vertical motion was small for the time periods considered and was neglected. The pressure interval is also constant with time in all layers except the bottom layer due to the changing pressure pattern at the surface. However, the percentage of this change over the 6-h time period used to calculate the tendencies is small and the error in assuming a constant pressure interval is not appreciable. Therefore, the development of vertical motion at a given level is given by the summation of the average local change of the divergence multiplied by the pressure interval in the layers between the surface and that level. Layers of 50-mb thickness were used for the computations in this study with the divergence being measured at the top of the layer, and local tendencies computed by 6-h centered differences.

b. Error Analysis

An error analysis of the development of vertical motion as indicated by the local rate-of-change of divergence was accomplished for the computed fields and vertical profiles. A propagation of error method described by Deming (1943) was used to calculate the effect of random errors in the measured wind. Following the procedures in Parts I and II, RMS errors for the wind measured at an elevation angle of 20° were obtained from Fuelberg (1974). The resulting error estimates along with the average magnitude and extreme value for each quantity are given in Table 12.

Table 12. Estimated RMS errors determined for rawinsonde data for the development of vertical motion.

Level (mb)	$\frac{\partial}{\partial t}(\vec{\nabla}_p \cdot \vec{V})$ AM[1]	$(10^{-10}s^{-2})$ EV[2]	RMS error	$\frac{\partial \omega}{\partial t}$ AM	$(10^{-5}\mu bars\ s^{-2})$ EV	RMS error
900	4.8	20.	0.8	2.5	10.0	0.4
850	4.9	17.	1.7	4.3	16.	1.0
800	4.8	16.	2.5	5.7	20.	2.1
750	5.1	21.	3.3	6.0	21.	3.5
700	6.0	26.	4.2	6.9	24.	5.4
650	5.4	24.	5.4	8.0	29.	7.8
600	5.9	20.	6.2	9.1	30.	10.7
550	6.5	23.	7.5	9.9	31.	14.1
500	5.9	24.	8.3	10.0	36.	18.0

[1]Average magnitude

[2]Extreme value

Errors were generally the same order of magnitude as typical values of the development of vertical motion and divergence during AVE IV. Both the average magnitude and the error in the local rate-of-change of vertical motion increased with height due to the integration method used in calculating vertical velocity. Average magnitudes of the local rate-of-change in divergence were nearly constant with height. Table 12 shows that

above approximately 650 mb, the average magnitudes of the measured changes in both vertical motion and divergence are less than the RMS errors determined from 6-h centered differences. Most of the observations made in this report will, therefore, be limited to conditions below this level.

3. RESULTS

a. Profiles of the development of divergence and vertical motion in relation to convective activity.

Average vertical profiles based on categories of the severity of convective activity were determined in order to reduce the effect of random errors and to show general relationships between the development of vertical motion and convection. The profiles were calculated by taking an average of each term computed for each category of convection determined from the gridded MDR data. Four categories of MDR values representing increased severity of convection were selected for the purpose of making comparisons. They were MDR $\leq$ 1 representing no convection, MDR $\geq$ 2 representing all convection, MDR $\geq$ 4 representing thunderstorms, and MDR $\geq$ 8 representing severe thunderstorms. The unique 3-h data of AVE IV also allowed average vertical profiles to be computed with the MDR data lagged by 3 and 6 h, thereby showing the conditions existing prior to the convective activity.

Figures 37 a-c show average vertical profiles of divergence at the time of convective activity, 3 h prior to the convective activity, and 6 h prior to the activity, respectively. Positive values indicate divergence while negative values indicate convergence. The average vertical profiles of divergence for areas containing no convection are similar for all 3 times and show small convergence below and small divergence above about 700 mb. The low-level convergence increased with increasing severity of the convection at all 3 times as did the mid-level divergence, except at the time of the activity when areas with MDR $\geq$ 2 (all convection) and MDR $\geq$ 4 (thunderstorms) experienced convergence throughout the layer considered. The average magnitude of the low-level convergence and mid-level divergence in areas containing severe thunderstorms increased as the time of thunderstorm occurrence approached.

Figure 38 shows the average vertical profiles of vertical motion corresponding to the profiles of divergence at the time of the activity, and 3 and 6 h prior to it. Positive values indicate downward motion ($\omega > 0$), while upward motion is shown by negative values ($\omega < 0$). The low-level convergence topped by mid-level divergence resulted in upward motion, as we would expect, with convective areas generally showing greater magnitudes of upward motion than nonconvective areas. However, the increasing magnitude of divergence in the mid levels for areas containing severe thunderstorms

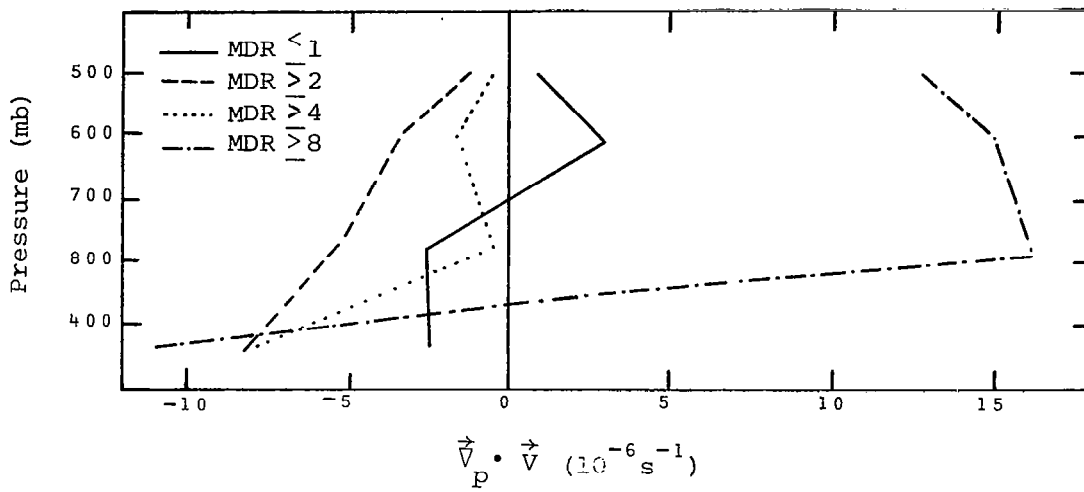

(a) No lag in MDR data

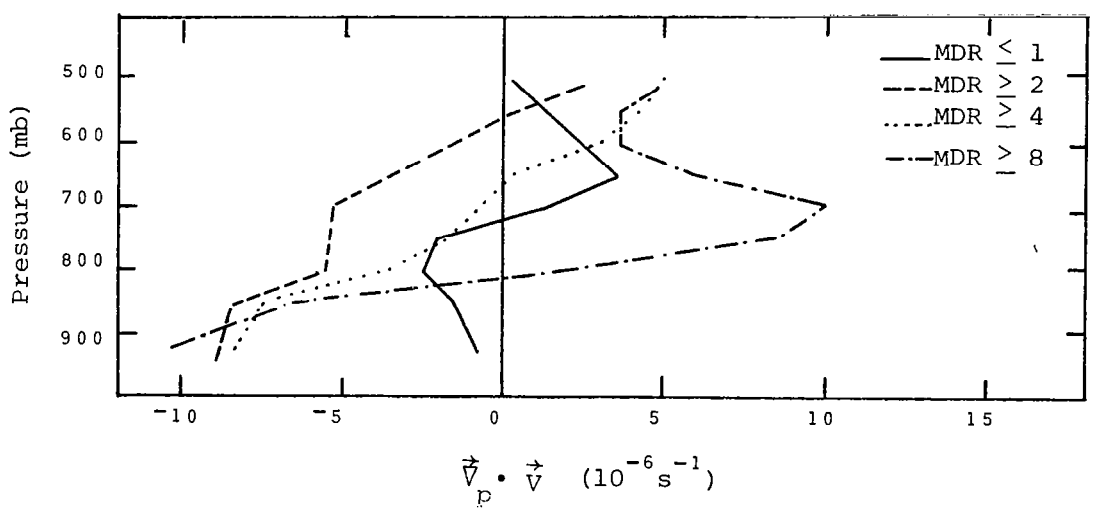

(b) MDR data lagged 3h

Fig. 37. Average vertical profiles of divergence.

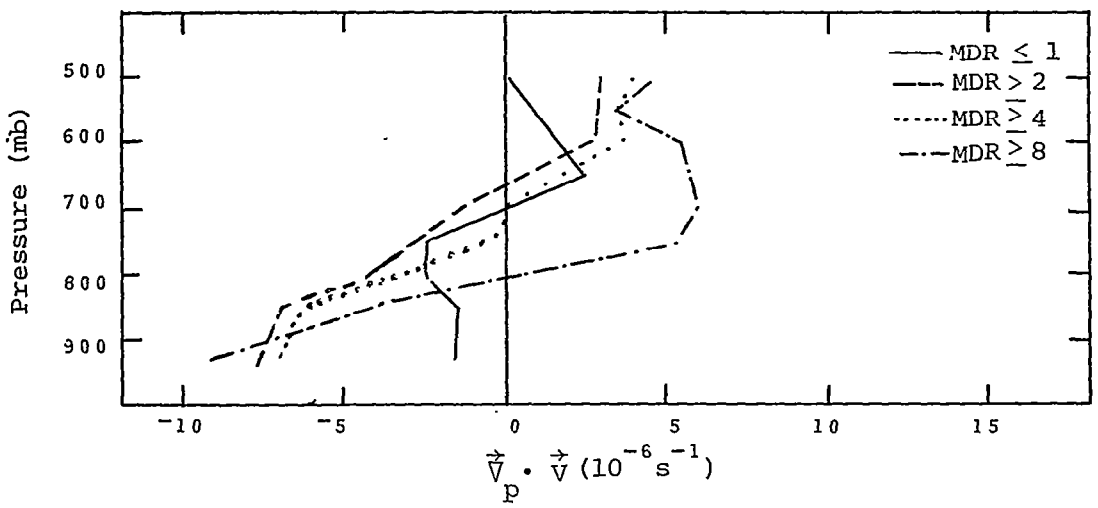

(c) MDR data lagged 6h

Fig. 37. (Continued)

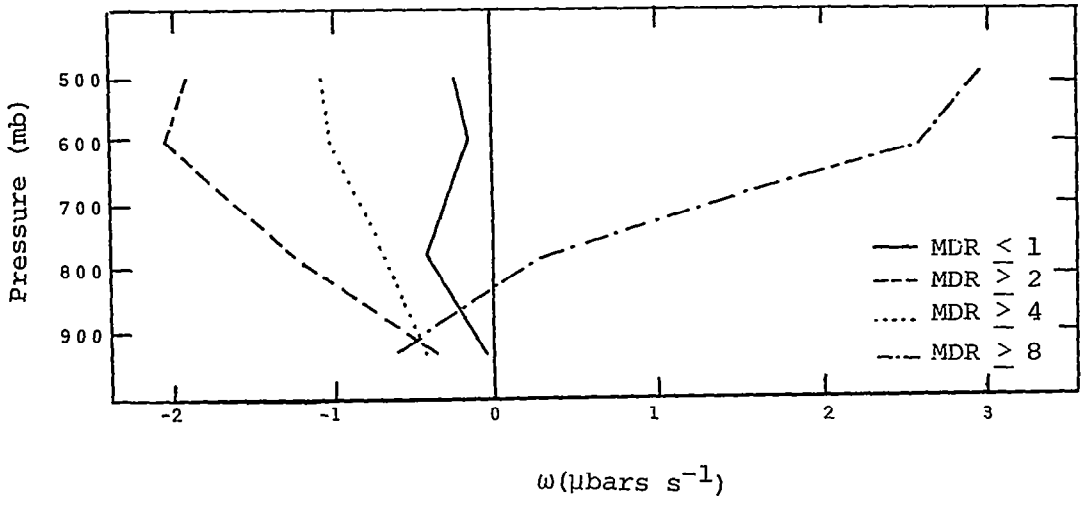

(a) No lag in MDR data

Fig. 38. Average vertical profiles of vertical motion.

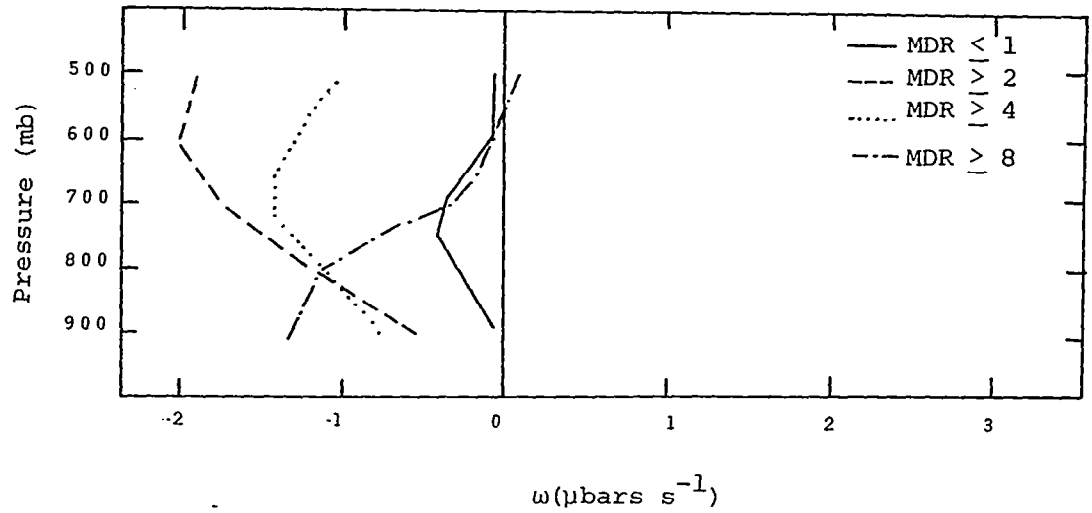

(b) MDR data lagged 3h

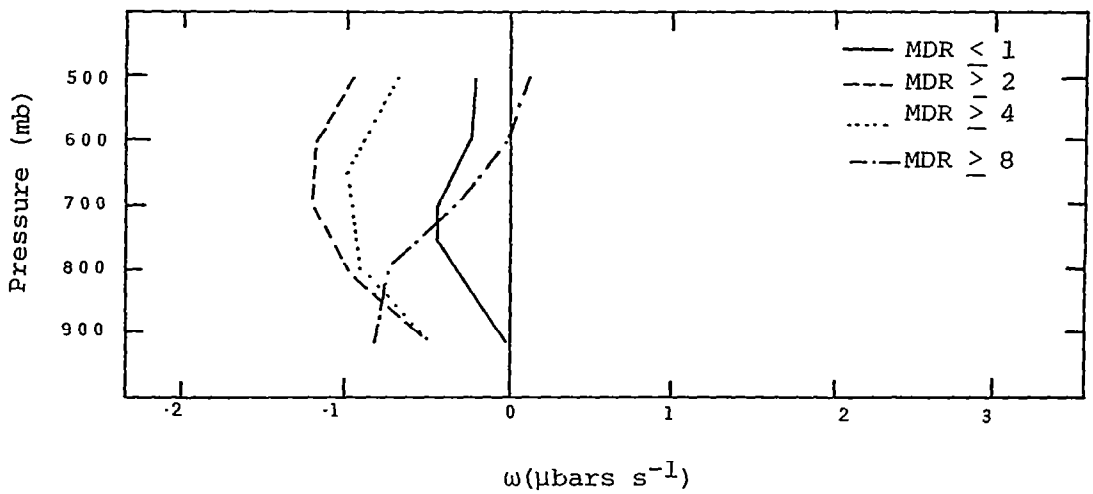

(c) MDR data lagged 6h

Fig. 38. (Continued)

resulted in a similar layer of increasing downward motion in the vertical motion profile. Since the AVE IV network was on the synoptic scale, this downward motion in the area of severe thunderstorms might represent the large-scale subsidence thought to compensate for the strong small-scale upward motion in the thunderstorm cells. However, in general, convective areas (MDR $\geq$ 2) showed upward motion throughout the layer considered.

Figure 39 shows average vertical profiles of the actual development of divergence. Positive values indicate increasing divergence or decreasing convergence, while negative values indicate increasing convergence or decreasing divergence. At 6 h prior to the convective activity, the convergence in the lower levels was increasing for all categories of convective activity as was the mid-level divergence. This would be favorable for the continued development of positive vertical motion within that layer. Nonconvective areas generally showed the development of divergence throughout the layer. However, at 3 h prior to the time at which the convective activity was classified, the low-level convergence began to decrease for all categories of convection and there was a similar tendency for the magnitude of the mid-level divergence to decrease also. At the time of the convective activity, the average vertical profile for the development of divergence in areas of severe thunderstorms had reversed its shape from 6 h prior to the activity. Now the convergence in the lower levels and the divergence in the mid levels were both decreasing. Areas of MDR $\geq$ 2 and MDR $\geq$ 4 also showed a decrease of convergence throughout the layer considered. These tendencies would act to destroy the vertical motion present at that time.

Average vertical profiles of the local development of vertical motion are shown in Fig. 40. As the vertical profiles of the local change in divergence would have implied, at 6 h prior to the activity positive vertical motion was increasing in areas of convective activity except at the very top of the layer for severe thunderstorms where the developing divergence resulted in downward motion. The small upward motion in nonconvective areas was decreasing as it also did 3 h prior to and at the time of activity. At 3 h prior to the time of activity, positive vertical motion was decreasing in areas containing convective activity. It was also decreasing at the time of the convective activity for areas with MDR $\geq$ 2 (all convection) and

MDR $\geq$ 4 (thunderstorms), and in the lowest levels for areas with MDR $\geq$ 8 (severe thunderstorms). The mid-level downward motion in areas of severe thunderstorms was increasing.

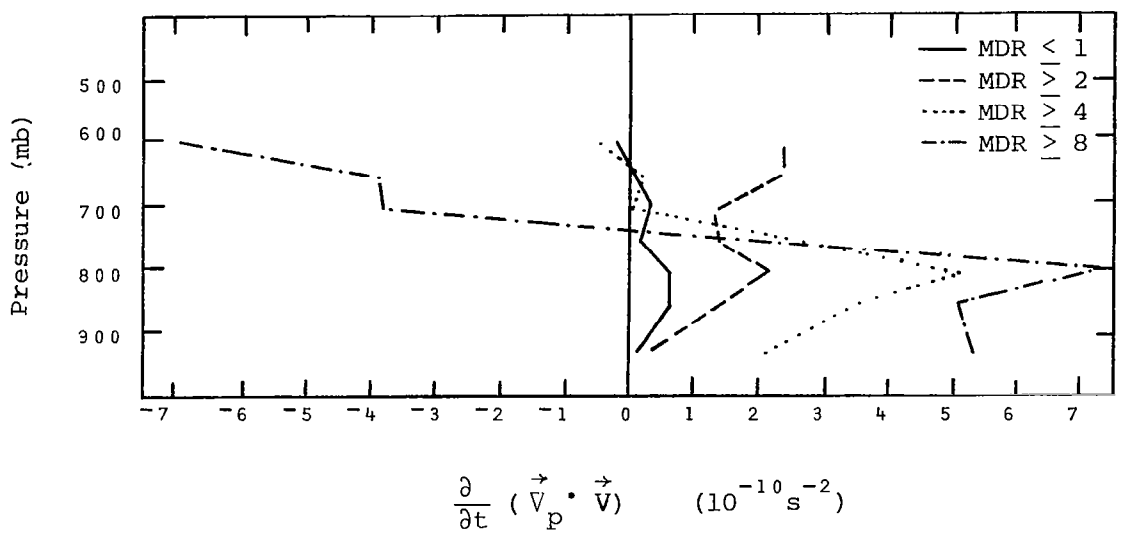

(a) No lag in MDR data

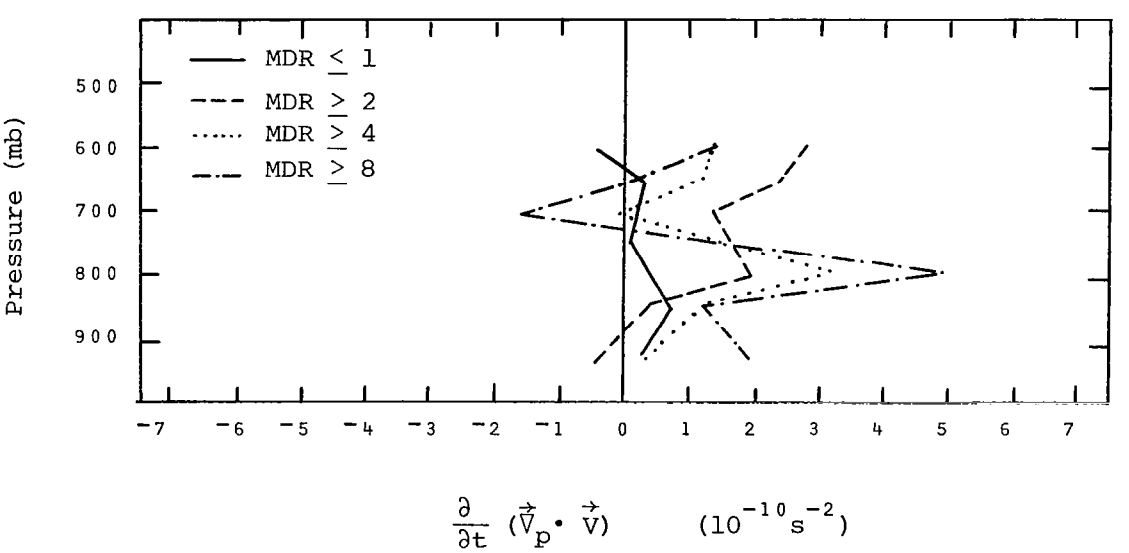

(b) MDR data lagged 3h

Fig. 39. Average vertical profiles of the development of divergence.

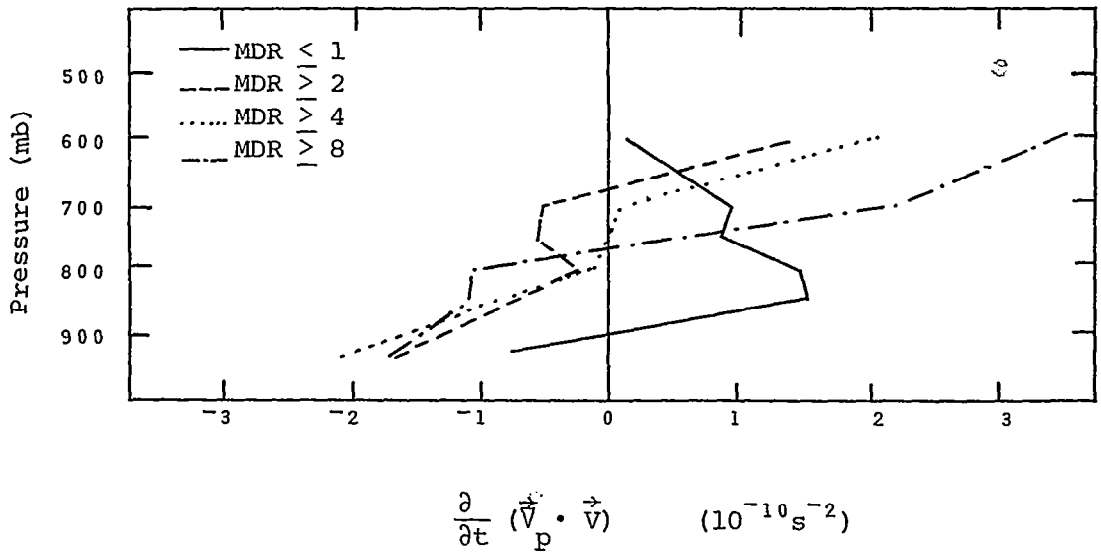

(c) MDR data lagged 6h

Fig. 39. (Continued)

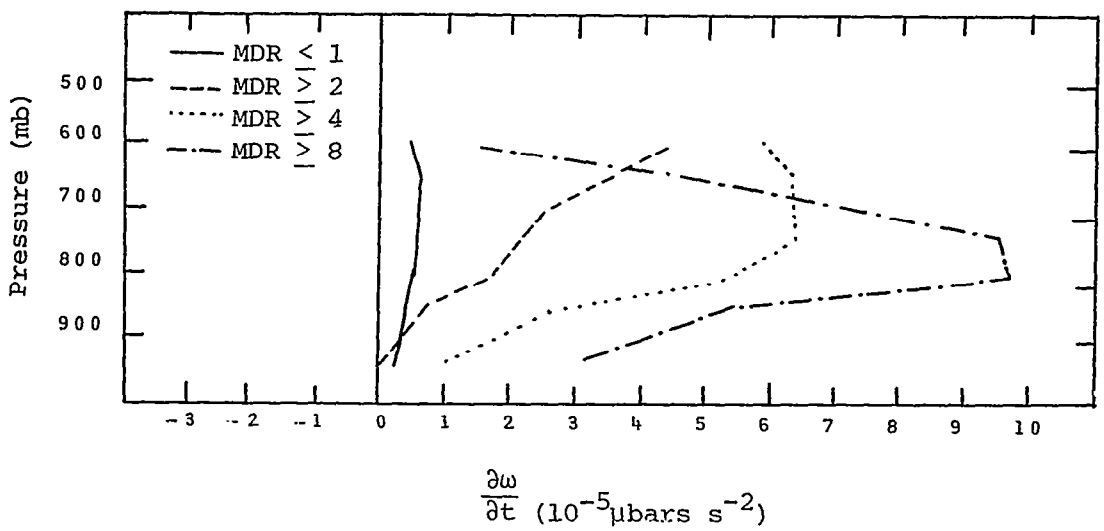

(a) No lag in MDR data

Fig. 40. Average vertical profiles of the development of vertical motion.

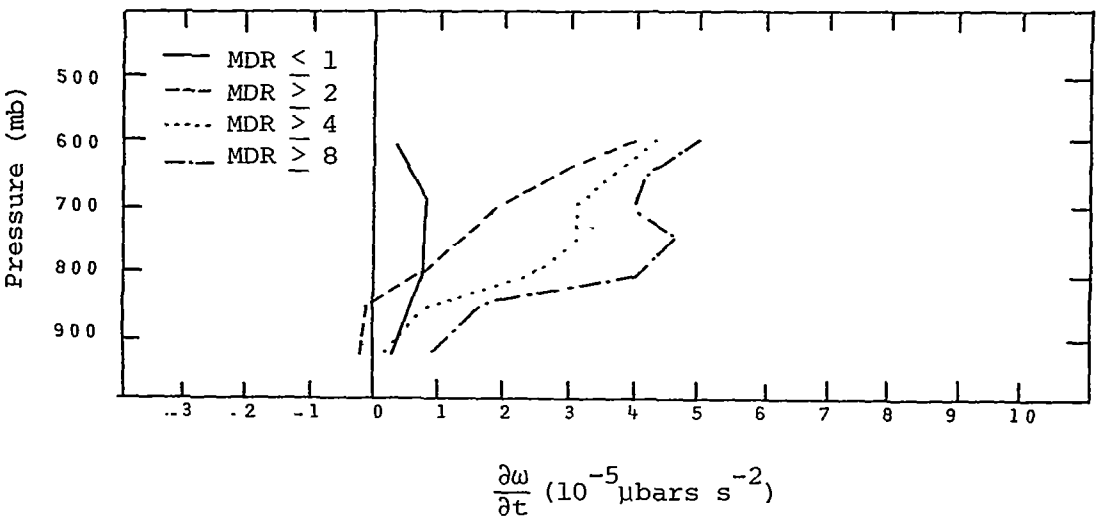

(b) MDR data lagged 3h

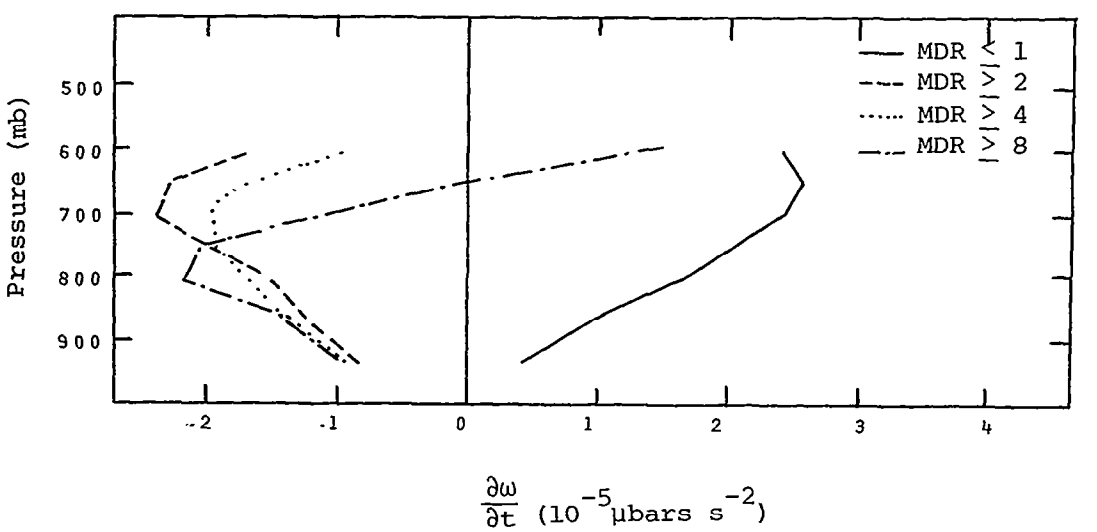

(c) MDR data lagged 6h

Fig. 40. (Continued)

b. Fields of development of vertical motion in relation to convective activity.

Figure 41 shows analyzed fields of the local tendency of vertical motion at the 850-mb level measured over a 6-h period with MDR $\geq$ 4 (thunderstorms) stippled in for 1500, 1800, and 2100 GMT 24 April 1975. General observations made from the average vertical profiles can also be seen in these charts. Again, positive values indicate downward development and negative values indicate upward development. Thunderstorm areas are often in regions of downward development especially when the convective activity was dissipating. For example, in Fig. 41a the convective area in northern Arkansas was within a region of downward vertical motion development, and Fig. 41b shows these thunderstorms to have dissipated. Thunderstorms in Kentucky were within a region of upward vertical motion development, and Fig. 41b shows these thunderstorms to have persisted. However, downward tendencies in Kentucky at 1800 GMT resulted in these storms dissipating by 2100 GMT as indicted in Fig. 41a. Positive vertical motion development was present in South Dakota at 1500 and 1800 GMT with thunderstorms occuring at 2100 GMT. The thunderstorms in Kansas, Missouri, Oklahoma, and Arkansas at 2100 GMT were located in an area of upward motion development and these storms greatly intensified within the next 3 h. The correlation between vertical motion tendencies and the intensification or dissipation of thunderstorms is not perfect, however. Some areas of upward development never contain convective activity, such as Illinois at 1500 GMT, or east and central Texas at all times. Similarly, some areas of general downward vertical motion development had thunderstorms form within them, such as eastern Kansas at 1800 GMT. Of course, there are factors controlling thunderstorm development other than the large-scale tendencies of vertical motion. The stability in Illinois and Texas was positive throughout the time period considered thereby suppressing convective development, and the thunderstorm that developed in eastern Kansas was within an area becoming increasingly unstable at 1500 GMT. By comparing the fields of convective stability tendencies and vertical motion tendencies provided a much more reliable method of predicting convective activity than did considering either of the fields separately. Areas in which the atmosphere was both becoming convectively unstable and in which positive vertical motion was developing

usually had convective activity present within the next 3 to 6 h. The front existed in areas of both increasing upward motion and increasing downward motion.

The fields of vertical motion development are generally continuous with height so that the centers of local vertical motion change at 700 mb, shown in Fig. 42, correspond well with the centers seen at 850 mb in Fig. 41. The average magnitude of the vertical motion change is larger at 700 mb than at 850 mb since the development of divergence is integrated from the surface to 700 mb. The same observations made for Fig. 41 apply to Fig. 42 with thunderstorm development or intensification in areas of upward vertical motion development and dissipating in areas of downward motion development.

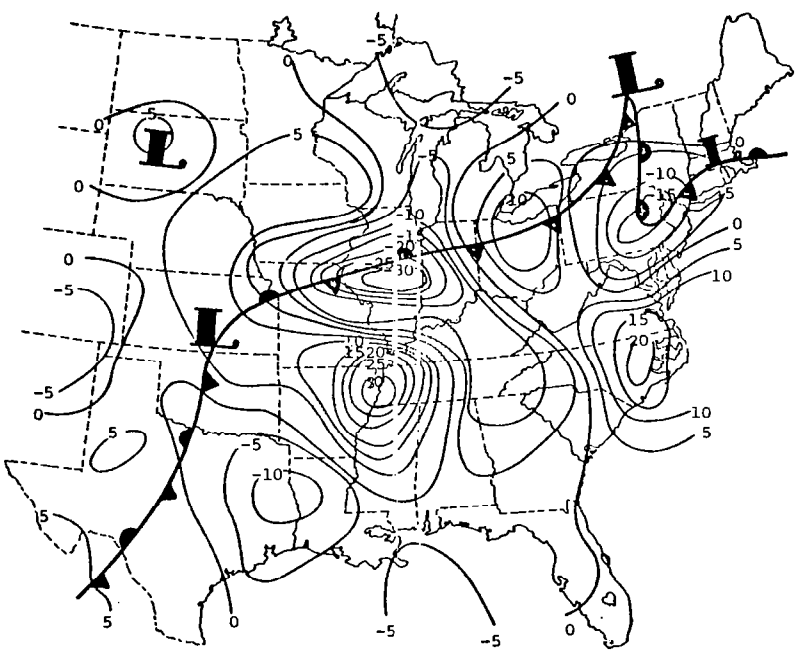

(a) 1500 GMT.

Fig. 41. Analysis of the development of vertical motion at 850 mb (10^{-5} µbars s^{-2})

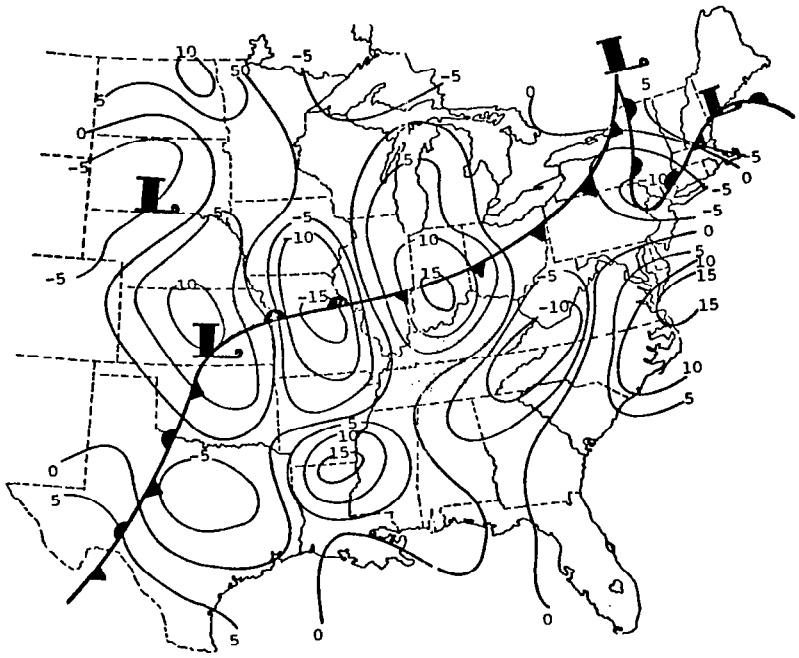

(b) 1800 GMT.

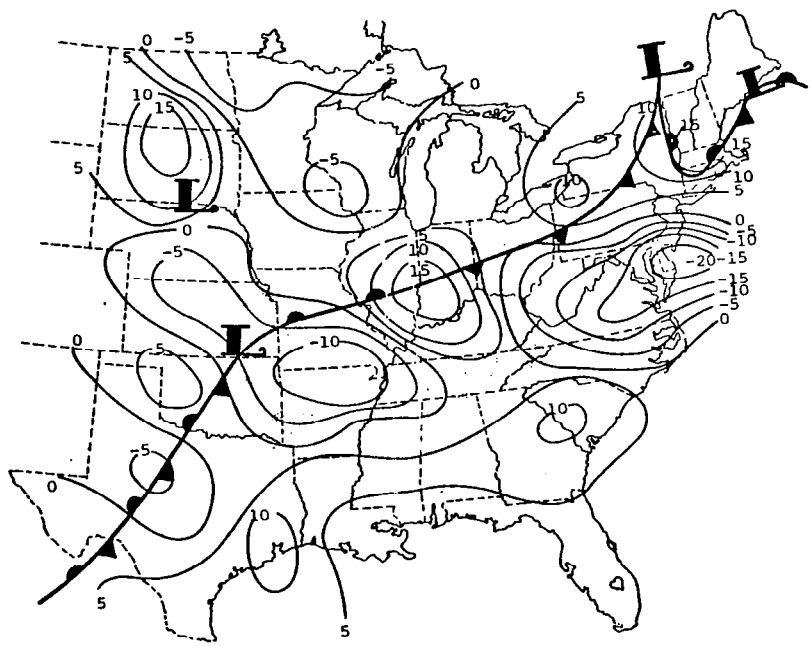

(c) 2100 GMT.

Fig. 41. (Continued)

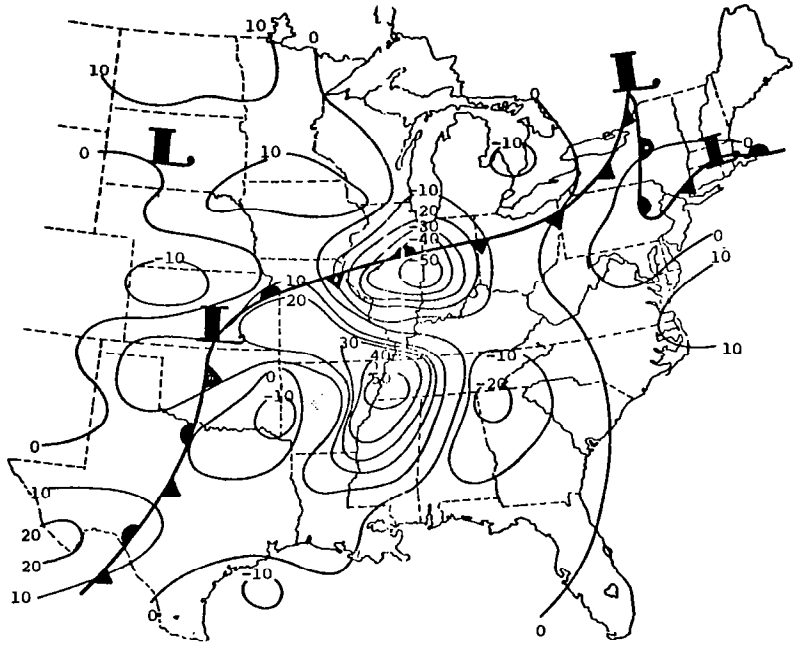

(a) 1500 GMT.

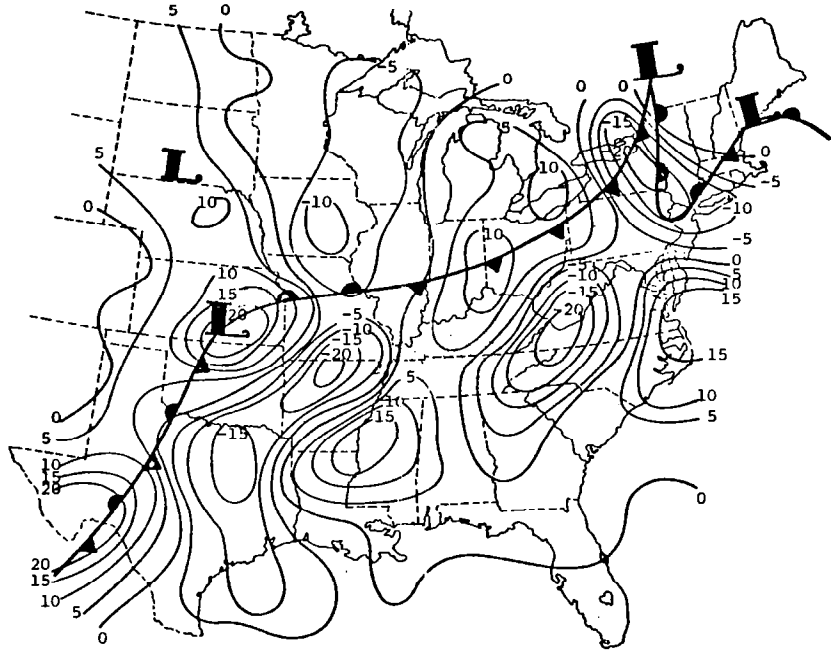

(b) 1800 GMT.

Fig. 42. Analysis of the development of vertical motion at 700 mb (10^{-5} µbars s^{-2}).

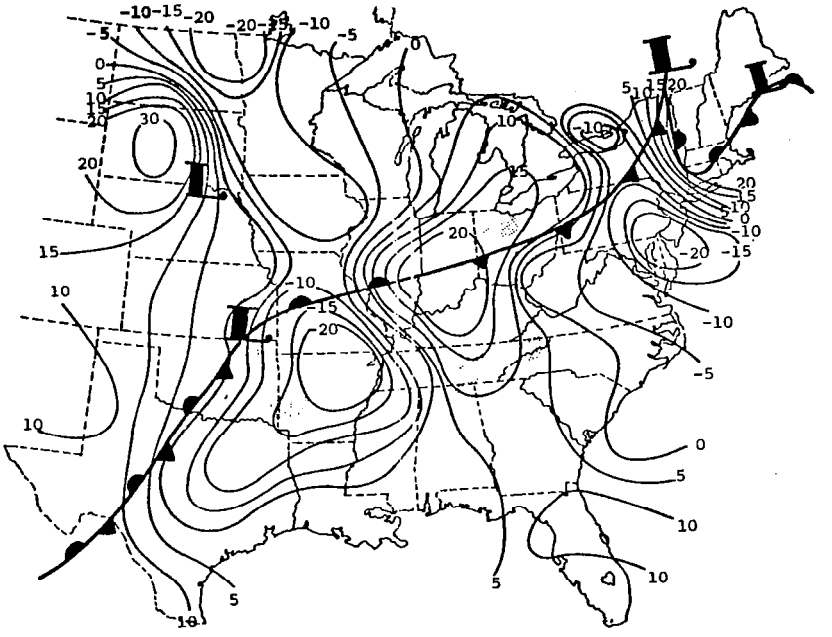

(c) 2100 GMT.

Fig. 42. (Continued)

Table 13, showing the means and average absolute magnitudes for the development of divergence and vertical motion, summarizes the results for the various levels. At 1500 and 1800 GMT, the lowest layer had increasing convergence, on the average, which resulted in the negative mean change in vertical motion at 900 mb ($\frac{\partial \omega}{\partial t} < 0$), or, upward motion was increasing. Above that level, the development of divergence was usually positive, indicating increasing divergence or decreasing convergence, and the development of vertical motion was correspondingly downward. The development of convergence on the average at 750 mb at 1800 GMT, and at 650 and 600 mb at 2100 GMT, did not result in upward motion development because of the large average amount of divergence below those levels.

The average absolute magnitude of the development of divergence, which represents a typical value one could expect the development of divergence to have at a given level, was approximately constant throughout the layers considered. The average absolute magnitude of the development of vertical

motion, however, increased with height due to the integration method used in the computation of vertical velocity.

Table 13. Means and average absolute magnitudes of the development of divergence and vertical motion.

Time	Level	$\frac{\partial}{\partial t}(\text{div } \vec{V})$ $(10^{-10} s^{-2})$ mean	AAM*	$\frac{\partial \omega}{\partial t}$ $(10^{-10}$ μbars $s^{-2})$ mean	AAM
	900	-0.8	6.7	-0.5	3.6
	850	0.7	6.5	-0.2	6.3
	800	1.2	5.8	0.4	8.0
1500 GMT	750	0.7	5.4	0.7	8.4
	700	0.8	6.1	1.0	8.3
	650	1.2	6.9	1.6	8.6
	600	1.0	6.9	2.0	9.4
	900	-0.6	4.8	-0.2	2.5
	850	0.7	4.9	0.1	4.3
	800	0.8	4.8	0.4	5.7
1800 GMT	750	-0.2	5.1	0.2	6.0
	700	0.1	6.0	0.2	6.9
	650	0.9	5.4	0.5	8.0
	600	0.8	5.9	0.7	9.1
	900	1.8	5.9	1.1	3.1
	850	1.0	4.6	1.5	5.0
	800	0.8	5.1	1.8	6.3
2100 GMT	750	0.8	6.0	2.1	7.4
	700	0.7	6.2	2.2	8.8
	650	-0.2	5.6	1.9	9.8
	600	-0.8	5.8	1.3	11.0

*Average Absolute Magnitude

4. SUMMARY AND CONCLUSIONS

The development of vertical motion was studied for four categories of convective activity. The categories were: MDR $\leq$ 1 representing no convection; MDR $\geq$ 2 representing all convection; MDR $\geq$ 4 representing thunderstorms; and MDR $\geq$ 8 representing severe thunderstorms. Conditions preceeding the convective activity by 3 and 6 h and at the time of the convective activity were investigated. Low level convergence and mid-level divergence increased with increasing severity of the convection at all three times except for MDR $\geq$ 2 and MDR $\geq$ 4 when convergence existed at all levels. Low-level convergence and mid-level divergence increased in magnitude as the time of thunderstorm occurrence approached. Vertical motion computed by the kinematic method indicated upward motion generally in convection areas, however some upward motion of smaller magnitude occurred in nonconvective areas. Upward vertical motion generally occurred at all levels in convective areas (MDR $\geq$ 2).

Six hours prior to convective activity, low-level convergence and mid-level divergence was increasing, i.e., development was occurring. At 3 h prior to the convective activity, there was a tendency for both the low-level convergence and mid-level divergence to decrease. By the time the convective activity occurred, the vertical profile of the development of divergence had reversed its shape in areas of severe thunderstorms compared with its shape 6 h prior to the activity.

As expected, the development of vertical motion paralleled the development of divergence. At 6 h prior to convective activity, positive vertical motion was increasing except at high levels near severe thunderstorms where downward motion developed. At 3 h prior to the convective activity, positive vertical motion was decreasing as well as at the time of convective activity in areas with MDR $\geq$ 2 and MDR $\geq$ 4, and in the lowest levels in areas with MDR $\geq$ 8.

Convective activity usually occurrs in regions of the development of positive vertical motion at 850 mb except when the activity has reached maturity and begins dissipating. Usually, the development of upward vertical motion occurs 3 to 6 h in advance of the formation of convective activity. Vertical continuity in the development of vertical motion is indicated at 850 and 700 mb with the 700-mb fields being more pronounced than the 850-mb fields.

REFERENCES

Appleby, J.F., 1954: Trajectory method of making short range forecast of differential temperature advection, instability and moisture, Mon. Wea. Rev., 82, 320-324.

Barnes, S. L., 1964: A technique for maximizing detail in numerical weather map analysis. J. Appl. Meteorol., 3, 396-409.

Barr, S., W. K. Widger, Jr., I. A. Miller, and R. Stantin, 1971: Objective subsynoptic upper level analysis. J. Appl. Meteorol., 10, 410-417.

Beebe, R. G., and F. C. Bates, 1955: A mechanism for assisting in the release of convective instability. Mon. Wea. Rev., 83, 1-10.

Bonner, W. D., 1966: Case study of thunderstorm activity in relation to the low-level jet. Mon. Wea. Rev., 94, 167-178.

Byers, H. R., and J. Batton, 1949: Some effects of vertical wind shear on thunderstorm structure. Bull. Amer. Meteor. Soc., 30, 168-175.

Carlson, R. D., 1973: Time changes in gradient and observed winds. A Compilation of Studies from Atmospheric Variability Experiment (AVE). NASA Contractor Report CR-2304, NASA Marshall Space Flight Center, Alabama, 59-121

Chien, H., and P. J. Smith, 1973: On the estimation of kinematic parameters in the atmosphere from radiosonde wind data. Mon. Wea. Rev., 101, 252-261.

Crawford, M.E., 1950: A synoptic study of instability lines. Bull. Amer. Meteor. Soc., 31, 351-357.

Das, P., 1962: Influence of wind shear on the growth of hail. J. Atmos. Sci., 19, 407-414.

Deming, W. E., 1943: Statistical Adjustment of Data. New York, Dover Publications, Inc., 37-40.

Dessens, H., 1960: The severe hailstorms are associated with very strong winds between 6,000m and 12,000m. Physics of precipitation (Geophysical Monograph No. 5), Washington, D. C., Amer. Geophys. Union, 333-338.

Doswell III, C. A., 1977: Subsynoptic scale dynamics of severe local storms: A case study. Preprints Conference on Weather Forecasting and Analysis and Aviation Meteorology, Silver Spring, 511-514.

Endlich, R. M., and R. L. Mancuso, 1968: Objective analysis of environmental conditions associated with severe thunderstorms and tornadoes. Mon. Wea. Rev., 96, 324-350.

Erbes, R. E., and L. O. Grant, 1976: A kinematic description of some Colorado thunderstorms. Preprints of Papers, International Conf. on Cloud Physics, Boulder, 446-451.

Feteris, P. J., 1977: Interactions between mesoscale flow and cumulus convective systems - forecasting problem. Preprints Conference on Weather Forecasting and Analysis and Aviation Meteorology, Silver Springs, 102-105.

Foster, D. S., and R. M. Reap, 1975: Thunderstorm and severe local storm frequency distributions for 1974 derived from manually digitized radar data and severe local storms reports. Preprints of Papers, Ninth Conf. on Severe Local Storms, Norman, 64-67.

Fritsch, J. M., C. F. Chappell, and L. R. Hoxit, 1976: The use of large scale budgets for convective parameterization. Mon. Wea. Rev., 104, 1408-1418.

Fucik, N. F. and R. E. Turner, 1975: Data for NASA's AVE IV experiment: 25-mb sounding data and synoptic charts. NASA TM X-64952, NASA Marshall Space Flight Center, Alabama, 140 pp.

Fuelberg, H. E., 1974: Reduction and error analysis of the AVE II pilot experiment data. NASA Contractor Report CR-120496, NASA Marshall Space Flight Center, Alabama, 140 pp.

Fulks, J. R.: Compedium of Meteorology, American Meteorological Society, Boston, Mass., 1951.

Haltiner, G. J., 1971: Numerical Weather Prediction, New York, Wiley and Sons, Inc., 317 pp.

House, D. C., 1958: Air mass modification and upper-level divergence. Bull. Amer. Meteor. Soc., 39, 137-143.

_____, 1959: The mechanics of instability line formation. J. Meteor., 16, 108-120.

Kochanski, A., 1958: Ageostrophic deviations and wind prognoses. J. Meteor., 15, 84-90.

Kreitzberg, C. W., and D. J. Perkey, 1976: Release of potential instability: Part I. A sequential plume model within a hydrostatic premitive equation model. J. Atmos. Sci., 33, 456-475.

Lebedev, S. L., 1976: A numerical model of the system of convective clouds and showers for wind change with height. Preprints of Papers, International Conf. on Cloud Physics, Boulder, 364-367.

Lewis, J. M., 1975: Test of the Ogura-Cho model on a prefrontal squall line case. Mon. Wea. Rev., 103, 764-778.

_____, Y. Ogura, and L. Gidel, 1974: Large-scale influences upon generation of a mesoscale disturbance. Mon. Wea. Rev., 102, 545-560.

Lloyd, J. R., 1942: The development and trajectories of tornadoes. Mon. Wea. Rev., 70, 65-75.

Miller, R. C., 1967: Notes on analysis and severe storms forecasting procedures of the Air Force Flobal Weather Central. Air Weather Service Technical Report 200, 102 pp.

Moyer, V., J. R. Scoggins, N. M. Chou, and G. S. Wilson, 1978: Atmospheric structure deduced from routine Nimbus 6 satellite data. Mon. Wea. Rev., 106, 1340-1352.

Newton, C. W., 1963: Dynamics of severe convective storms. Meteorol. Monograph, 5, American Meteorological Society, Boston, 33-58.

Newton, C. W., and H. R. Newton, 1959: Dynamical interactions between large convective clouds and environment. J. Meteor., 16, 483-496.

Ninomiya, K., 1971: Mesoscale modification of synoptic situations from thunderstorm development as revealed by ATS III and aerological data. J. Appl. Meteorol., 9, 197-203.

O'Brien, J. J., 1970: Alternate solution to the calssical vertical velocity problem. J. Appl. Meteorol., 9, 197-203.

Paegle, J., and D. W. McLawhorn, 1973: Correlation of nocturnal thunderstorms and boundary layer convergence. Mon. Wea. Rev., 101, 877-883.

Palmen, E. , and C. W. Newton, 1969: Atmospheric Circulation Systems. New York, Academic Press, 603 pp.

Panofsky, H. A., 1958: Introduction to Dynamic Meteorology. University Park, Pa., The Pennsylvania State University, 106-107.

Ratner, B., 1961: Do high-speed winds aloft influence the occurrence of hail? Bull. Amer. Meteor. Soc., 42, 443-446.

Read, W. L., and J. R. Scoggins, 1977: Vorticity imbalance and stability in relation to convection. NASA Contractor Report CR-2819, NASA Marshall Flight Center, Alabama, 111 pp.

Sanders, F., and R. J. Paine, 1975: The structure and thermodynamics of an intense mesoscale convective storm in Oklahoma. J. Atmos. Sci., 32, 1563-1579.

Schuman, F. G., 1957: Numerical methods in weather prediction: II. Smoothing and Filtering. Mon. Wea. Rev., 85, 357-361.

Scoggins, J. R., and R. W. Phelps, 1973: An approach to the determination of the variability of wind through the use of quasi-conservative thickness fields. A Compilation of Studies from Atmospheric Variability Experiment (AVE). NASA Contractor Report CR-2304, NASA Marshall Space Flight Center, Alabama, 163-192.

Scoggins, J. R. and J. E. Wood, 1971: Factors in the formation and prediction of convective clouds and thunderstorms. Preprints of Papers, Seventh Conf. on Severe Local Storms, Kansas City, 110-117.

Scott, R. W., and J. R. Scoggins, 1977: The moisture budget in relation to convection. NASA Contractor Report CR-2817, NASA Marshall Flight Center, Alabama, 88 pp.

Smith, P. J., 1971: An analysis of kinematic vertical motions. Mon. Wea. Rev., 99, 715-723.

Vincent, D. G., and L. N. Chang, 1975: Kinetic energy bugets of moving systems: Case studies for an extratropical cyclone and hurricane Celia, 1970. Tellus, 27, 224-235.

Wilson, G. S., 1977: Relationships between convective storms and their environment in AVE IV determined from 3-dimensional subsynoptic-scale trajectory model. Preprints of Papers, Tenth Conf. on Severe Local Storms, 247-254.

_____, and J. R. Scoggins, 1976: Atmospheric structure and variability in areas of convective storms determined from 3-h rawinsonde data. NASA Contractor Report CR-2678, Marshall Flight Center, Alabama, 117 pp.

1. REPORT NO.	2. GOVERNMENT ACCESSION NO.	3. RECIPIENT'S CATALOG NO.
NASA CR-3386		

4. TITLE AND SUBTITLE	5. REPORT DATE
The Development of Convective Instability, Wind Shear, and Vertical Motion in Relation to Convective Activity and Synoptic Systems in AVE IV	February 1981
	6. PERFORMING ORGANIZATION CODE
7. AUTHOR(S)	8. PERFORMING ORGANIZATION REPORT #
James G. Davis and James R. Scoggins	
9. PERFORMING ORGANIZATION NAME AND ADDRESS	10. WORK UNIT NO.
Department of Meteorology Texas A&M University College Station, Texas 77843	M-342
	11. CONTRACT OR GRANT NO. NAS8-31773
12. SPONSORING AGENCY NAME AND ADDRESS	13. TYPE OF REPORT & PERIOD COVERED
National Aeronautics and Space Administration Washington, D.C. 20546	Contractor Report
	14. SPONSORING AGENCY CODE

15. SUPPLEMENTARY NOTES

Marshall Technical Monitor: Robert Turner

16. ABSTRACT

Data from the fourth Atmospheric Variability Experiment (AVE IV) conducted by NASA on 24-25 April 1975 were used to investigate conditions/factors responsible for the development (local time rate-of-change) of convective instability, wind shear, and vertical motion in areas with varying degrees of convective activity (none to MDR Code 9). AVE IV sounding data were taken at 3- or 6-h intervals during a 36-h period on 24-25 April 1975 over approximately the eastern half of the United States. An error analysis was performed for each variable studied.

17. KEY WORDS	18. DISTRIBUTION STATEMENT
Atmospheric Variability Experiment Convective instability Wind shear Vertical motion	Unclassified - Unlimited Subject Category 47

19. SECURITY CLASSIF. (of this report)	20. SECURITY CLASSIF. (of this page)	21. NO. OF PAGES	22. PRICE
Unclassified	Unclassified	145	A07

For sale by National Technical Information Service, Springfield, Virginia 22161

NASA-Langley, 1981